2021-01-07

On the Spectral Efficiency and Energy Efficiency Analysis of Cache-Enabled Heterogeneous Networks with Device-to-Device Communication and Cooperative Transmission

Ochia, Okechukwu Emmanuel

UNIVERSITY OF CALGARY

On the Spectral Efficiency and Energy Efficiency Analysis of Cache-Enabled Heterogeneous Networks with Device-to-Device Communication and Cooperative Transmission

by

Okechukwu Emmanuel Ochia

A THESIS
SUBMITTED TO THE FACULTY OF GRADUATE STUDIES
IN PARTIAL FULFILLMENT OF THE REQUIREMENTS FOR THE
DEGREE OF DOCTOR OF PHILOSOPHY

GRADUATE PROGRAM IN ELECTRICAL AND COMPUTER ENGINEERING

CALGARY, ALBERTA
JANUARY, 2021

Abstract

The Heterogeneous network (HetNet) is a viable candidate for achieving high spectral efficiency (SE) and energy efficiency (EE) in fifth generation (5G) networks. Cache-enabled HetNets with device-to-device (D2D) communication can exploit the availability of cheap memory to improve file delivery and reduce file download latency. In HetNets with simultaneous requests for different file types, the design problems centered on what file to store and how to utilize limited caching capacity impact the SE and EE.

In this thesis, an association scheme that computes the D2D communication range based on out-of-cell interference is proposed for establishing cellular and D2D links in a HetNet. The proposed interference-aware, D2D distance threshold-based association scheme achieves up to 67% gain in the SE and EE compared to the state-of-the-art minimum path loss-based association scheme. Further, a popularity and size-aware (PSA) caching scheme is proposed in a hybrid microwave/millimeter wave HetNet. The PSA caching scheme allocates memory blocks for caching according to Pareto, lognormal, and Gamma file size distributions based on empirical measurements and is different than the state-of-the-art probabilistic, size-weighted-popularity (SWP)-based, and most-popular-content (MPC) caching schemes that assume equal file size. Numerical results show that the proposed PSA caching scheme provides up to 33% increase in the cache hit probability compared to the probabilistic and MPC caching schemes. Besides, the PSA scheme achieves up to 17% gain in the file transmission success probability compared to the state of the art. Also, cooperative transmission among transmitters under the PSA caching scheme realizes up to 70% gain in the file transmission success probability compared to a non-cooperative transmission scheme.

Lastly, the integration of large scale antenna arrays is proposed to enhance the transmission capacity of a cache-enabled HetNet with D2D communication. The results reveal that the transmission capacity of the HetNet scales linearly with the number of antenna elements per transmitter, provided that the number of antenna elements is not so large. The results in this thesis prove the usefulness of adopting content-aware caching and multiple transmission schemes to improve the performance of a HetNet with unlimited file requests and limited caching capacity.

Acknowledgements

I would like to express my utmost gratitude to my supervisor, Dr. Abraham Fapojuwo who provided me with the opportunity to undertake this research project that has culminated in a thesis. I have been fortunate to work under his supervision which has enabled me to develop my research and communication skills. I am equally thankful for his mentorship and the numerous feedback he provided that have greatly improved the quality of my scholarly works.

I would equally like to thank the members of my examination committee, including Dr. Abu-Bakarr Sesay, Dr. Geoffrey Messier, Dr. Vassil Dimitrov, and Dr. Carey Williamson. I would like to thank Dr. Ekram Hossain of the University of Manitoba who was the external examiner for my thesis.

I would also like to thank my past and present colleagues at the Wireless Networking Research Lab, including Dr. Kasun Hemachandra, Dr. Kazi Ashrafuzzaman, Dr. Fatemeh Ghods, Dr. Ismail Kamal, Dr. Xiaobin Yang, Dr. Isaac Osunkunle, Dr. Jonathan Kwan, Dr. Hai Wang, Simon Windmuller, Akash Melethil, Dr. Ahmed Darwesh, Manobendu Sarker, Vatsala Sharma, Lisa Zhao- I am most grateful for your companionship. I would especially like to thank Dr. Ahmed Darwesh whom I worked with on multiple projects. His insightful feedback on my work were invaluable to the completion of this thesis.

Last but not the least, I would like to thank my father, mother, and siblings for their moral and spiritual support throughout my doctoral program. I would not have been able to complete the program without their support.

Table of Contents

List of Tables

List of Figures

List of Abbreviations

Abbreviation	Definition
3GPP	Third Generation Partnership Project
5G	Fifth Generation
BS	Base Station
CoMP	Coordinated MultiPoint
D2D	Device-to-Device
EE	Energy Efficiency
FD	Full Duplex
FHPPP	Finite Homogeneous Poisson Point Process
GB	Gigabytes
HD	Half Duplex
HetNet	Heterogeneous Network
HPPP	Homogeneous Poisson Point Process
i.i.d	independent and identically distributed
IP	Internet Protocol
KP	Knapsack Problem
LOS	Line-of-Sight
LTE	Long Term Evolution
MIMO	Multiple-Input Multiple-Output
mmWave	millimeter wave
MPC	Most-Popular-Content
MRT	Maximum-Ratio-Transmission
NLOS	Non-Line-of-Sight
OFDMA	Orthogonal Frequency Division Multiple Access

PCP	Poisson Cluster Process
pdf	probability density function
PPP	Poisson Point Process
PSA	Popularity and Size-Aware
RB	Resource Block
SE	Spectral Efficiency
SINR	Signal-to-Interference-Plus-Noise Ratio
SIR	Signal-to-Interference Ratio
SNR	Signal-to-Noise Ratio
SWP	Size-Weighted Popularity
UT	User Terminal
VNI	Visual Networking Index

List of Symbols

Symbol	Definition
Φ_1	Macro BS PPP
Φ_2	Pico BS PPP
Φ_3	User PPP
Φ_c	CH PPP
λ_1	Macro BS density
λ_2	Pico BS density
λ_3	User density
λ_c	CH density
σ_c	Variance of PCP
P_1	Macro BS transmit power
P_2	Pico BS transmit power
P_3	User transmit power
P_t	CH transmit power
α	Path loss exponent
α_L	LOS path loss exponent
α_N	NLOS path loss exponent
ϵ_L	LOS path loss intercept
ϵ_N	NLOS path loss intercept
η	Nakagami shape parameter
η_L	LOS Nakagami shape parameter
$\mathbf{U}(.)$	Unit step function
$\mathbf{1}(.)$	Indicator function
β	Shape parameter of Pareto file size distribution

ξ	Scale parameter of Pareto file size distribution
ϖ	Shape parameter of Gamma file size distribution
$\varkappa$	Scale parameter of Gamma file size distribution
μ	Location parameter of lognormal file size distribution
σ	Scale parameter of lognormal file size distribution
$PL(x)$	Path loss experienced by a link of length x
$P_L(x)$	LOS probability for a link of length x
C	LOS range under blockage model-A
R_L	LOS range under blockage model-B
R	Network radius
r_d	D2D range
G_k	Maximum array gain of a node type k ($k = 1 =$ macro BS, $k = 2 =$ pico BS)
G_i	Random array gain of an interfering BS
θ_k	main lobe signal beamwidth of a node type k
M_k	Cache capacity of a node type k
γ	SINR coverage threshold
ψ	rate threshold for successfully decoding a received file
Ψ_c	Cellular association probability
Ψ_d	D2D association probability
Ψ_{tx}	D2D transmit mode probability
$\Psi_{rx,d2d}$	D2D receive mode probability
Ψ_{HD}	HD-only mode probability
Ψ_{FD}	FD-only mode probability
$\Psi_{FD/HD}$	Mixed FD/HD mode probability
$\Upsilon_{cov,cell}$	Cellular coverage probability
$\Upsilon_{cov,FD/HD}$	Mixed FD/HD coverage probability
$\Gamma_c(r)$	Cellular received SINR for a link of length r
$\Gamma_d(r)$	D2D received SINR for a link of length r
$\overline{\Gamma}_d$	D2D average received SINR
$\Upsilon_{cov,k}(\gamma, f)$	SINR coverage probability of a file f in a tier of node type k
$S_{k,f}(\gamma, f)$	Transmission success probability of file f in a tier of node type k
S_k	Average success probability in the k-th tier

q_{kf}	Caching probability of a file f in a node type k
c_{kf}	Cache hit probability of a file f in a node type k
c_k	Cache hit probability in the k-th tier
SE_{avg}	Cluster average SE
$\mathcal{S}_c$	Cellular SE
$\mathcal{S}_d$	D2D SE
$\bar{\mathcal{S}}$	Area SE
$\mathcal{R}_c$	Cellular rate
$\mathcal{R}_d$	D2D rate
$\bar{\mathcal{R}}$	Network rate
$\mathcal{R}_k(\psi, f)$	Rate coverage probability of a file f in a node type k
$\mathcal{E}_c$	Cellular EE
$\mathcal{E}_d$	D2D EE
$\bar{\mathcal{E}}$	Network EE
$DL_{avg,\delta}$	Content average download latency for δ-communication mode (cellular or D2D)
$\mathcal{H}(\psi)$	Successful content delivery probability

Chapter 1

Introduction

1.1 Background

The demand for data-centric services and the scale of content generation has seen unprecedented growth in recent years. For example, the Cisco Visual Networking Index (VNI) reports that the amount of global Internet Protocol (IP) traffic will reach 400 exabytes per month by 2022, representing a 3-fold increase from 2017 [1] as illustrated in Fig. 1.1. Moreover, Fig. 1.2 shows that more than 8 billion mobile smartphones and tablets will be able to connect to the Internet by 2022. Thus, the huge demand for bandwidth and data requires innovative technologies that can extend the spectral efficiency (SE) and energy efficiency (EE) of the fifth generation (5G) and beyond networks.

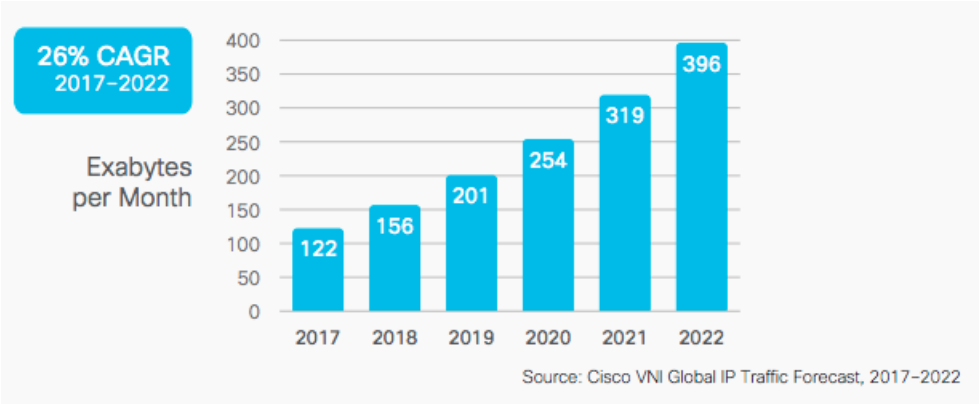

Figure 1.1: Global IP traffic growth [1]

The heterogeneous network (HetNet) architecture is currently a promising solution for supporting the massive density of wireless communications and the ubiquitous device connections [2, 3, 4]. In general, a

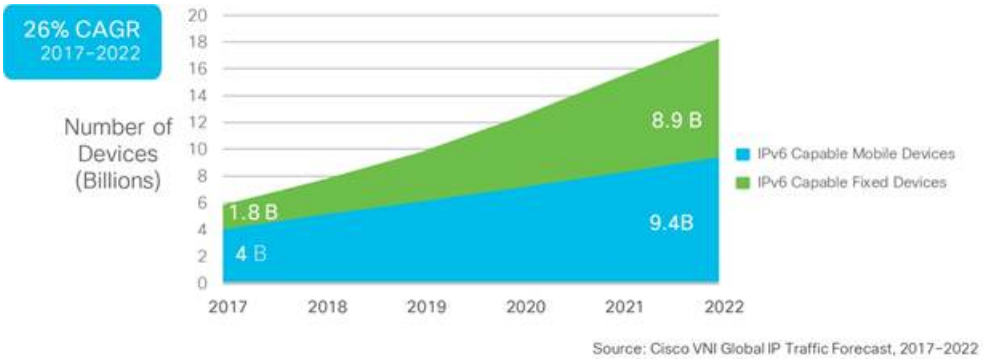

Figure 1.2: Global device connection growth [1]

HetNet comprises multiple tiers of base stations (BSs), such as macro BSs, pico BSs, and femto BSs. The macro BS tier provides wide area coverage within a cell, whereas the pico and femto BSs provide broadband coverage at cell edges and in hotspots [5]. Besides, cooperative transmission schemes can enable multiple BSs within a tier or in different tiers to serve user requests and enhance the aggregate cellular capacity [6, 7].

The millimeter wave (mmWave) spectrum, which extends from $30 - 300$ GHz [8, 9], has attracted current research efforts because of the availability of wide bandwidth, which is necessary for high data rate applications. Notably, the $28 - 86$ GHz range of mmWave bands have favorable propagation conditions [10] and are incorporated in 5G HetNets to address the spectrum crunch. However, the mmWave peculiarities such as the highly directional nature of the signals and the significant blockage require antenna beamforming techniques [11, 12]. Nonetheless, Device-to-device (D2D) communications can operate in mmWave bands to enhance the reliability of cellular systems. In this regard, some studies have focused on the integration of D2D communications into hybrid microwave/mmWave HetNets where the D2D tier can be deployed either in underlay or overlay modes [13, 14, 15]. Additionally, analytical methods such as point process theory and the tools of stochastic geometry are adopted to model the spatial randomness of nodes and to evaluate the achievable performance of D2D-enabled HetNets [16, 17, 18, 19].

The offloading of content from the core network for caching at the edge and in user terminals (UTs) can alleviate the pressure on the backhaul of the HetNet. In a cache-enabled HetNet, a UT that requests for content can be serviced through D2D communication by a neighboring UT that has the content in its local cache. The performance analysis of cache-enabled D2D HetNets has revealed performance gains such as the maximization of the cache hit probability and successful transmission probability using most-popular-content caching [20], enhancement in throughput via frequency reuse [21], and the use of a distributed caching policy to minimize the interference in dense HetNets [22]. Lastly, large scale antenna arrays or massive multiple-input multiple-output (MIMO) provide multiple degrees of freedom that allow a high degree of spatial multiplexing and diversity. Thus, cache-enabled HetNets with massive MIMO can achieve higher coverage

probability and average rate compared to conventional MIMO systems without caching, provided appropriate caching algorithms and precoding schemes are employed [23, 24].

1.2 System Modeling Using Stochastic Geometry

A rigorous evaluation of the performance of wireless networks requires exhaustive simulations that are time-consuming and which do not provide insights on the achievable performance bounds. In this regard, the tools of stochastic geometry have been applied to the analysis of cellular networks and HetNets [25, 26, 27]. Notably, point process theory is used as a tool for modeling the spatio-temporal randomness in the locations of the nodes of a network. However, the choice of the appropriate point process model for a specific network deployment presents a tradeoff between analytical tractability and the accuracy in capturing the network settings.

The Poisson point process (PPP) has been widely used to model cellular networks because of its simplicity and tractability [28]. However, the uniform distribution of points over an infinite area of a PPP realization does not apply to many real network configurations. Wireless networks are characterized by deployments over a finite area, device clustering, attraction/repulsion between nodes, and correlation in content requests. Hence, more sophisticated point processes such as the Binomial point process (BPP), Poisson Hole Process (PHP), Thomas cluster process (TCP), Poisson cluster process (PCP), and the Ginibre point process (GPP) are required to account for the aforementioned peculiarities. The BPP is suitable for modeling a finite wireless network area with a uniform distribution of nodes [19]. The PHP is suitable for cellular deployments with exclusive regions of communication such as HetNets with D2D communications, while the TCP and PCP are suited for HetNets with device clustering and correlation between device requests [29, 30, 31]. Lastly, the GPP is a good model for networks when the nodes exhibit repulsion [28].

The main factor that mitigates the performance of HetNets is interference between the multiple BS tiers and the multiple access schemes. Thus, the tools of stochastic geometry are used to characterize the interference distribution which can be used to compute the coverage probability performance of the HetNet. However, many of the more accurate point process models do not lend tractability to the characterization of the interference distribution in the general case. Hence, approximations for special cases and numerical techniques are required to provide useful insights.

The mmWave frequency bands are distinct from the microwave frequency bands because of the adverse blockage effects experienced by mmWave links. The blockage effects can be modeled using random distributions, exponential models, and line-of-sight (LOS) ball models [32, 33, 34]. The locations of potential blockers of a target receiver link can be modeled by a uniform distribution based on a PPP or BPP [34, 35].

Besides, the exponential model can be combined with large-scale path loss whereby a multiplicative term that decays exponentially with the link length is added to the path loss function. The LOS radius model assumes a fixed radius within which a mmWave link is LOS with respect to a BS or transmitter, while a link is non-line-of-sight (NLOS) outside the LOS radius, which results in significant blockage. The choice of the appropriate blockage model depends on the deployment environment. Intuitively, an urban network deployment has a high density of potential blockers within a small area, hence, the LOS radius model with a pre-selected radius measured by experiments is suitable to capture the blockage effects. In contrast, the blockage effects in rural or suburban deployments with a low density of potential blockers can be modeled by a slowly-decaying exponential profile as a function of the mmWave link length.

In summary, the choice of the tools of stochastic geometry and the selection of point process models rely on an understanding of the deployment parameters of the HetNet, and appropriate approximations are required to simplify the subsequent performance analysis.

1.3 Problem Statement and Objectives

The open problems that form the research topics in this thesis are divided into four areas listed as follows:

- How does the performance of a mixed full duplex (FD)/half duplex (HD) scheme compare with an FD-only or HD-only scheme [36, 37, 38] in a D2D-enabled HetNet? The analysis and discussions of Chapter 3 address this problem.

- How can D2D communications be managed to extend the coverage of a HetNet and what protocols will govern the association of UTs to BSs or D2D UT transmitters? Further, what propagation models are needed to leverage the strong directional characteristics of mmWave frequencies and how can the system parameters be tuned to achieve a desired SE-EE goal? How can mmWave propagation characteristics and directional beamforming techniques be exploited to enhance the existing minimum path loss-based and maximum average received power-based association schemes [15, 39, 40, 41, 42, 43, 33, 44, 45]? The content in Chapter 4 focuses on the stated problems.

- Given backhaul capacity constraints, how can caching and cooperative transmission schemes exploit knowledge of the available content to improve the performance of a hybrid microwave/mmWave HetNet? Notably, how does a caching scheme that maximizes the aggregate popularity of the cached files impact the system performance, and what are the tradeoffs compared to caching schemes that are not content-aware [46, 47, 17, 48, 49]? These problems form the topic of Chapter 5.

- How does a content-aware caching scheme affect the average achievable rate and successful content delivery probability of a HetNet with D2D communication and large scale antenna arrays? This problem is addressed in Chapter 6.

The following thesis objectives, which are aimed at solving the aforementioned open problems, are outlined in the following:

- *Enhance the SE and average download latency of a cache-enabled HetNet with D2D communications.* Chapter 3 focuses on this objective and introduces a mixed FD/HD D2D mode selection scheme where a device is capable of operating in both FD and HD D2D communication modes.

- *Formulate and solve an optimization problem to jointly maximize the SE and EE of a D2D-enabled HetNet operating in mmWave frequencies.* In Chapter 4, this objective is realized through an association scheme that accounts for mmWave propagation effects and the antenna design parameters. Besides, a goal attainment algorithm is introduced as a solution to the SE-EE optimization problem.

- *Design a caching scheme that exploits knowledge of the available content to improve the successful transmission of files in a cache-enabled HetNet operating in microwave and mmWave frequencies.* Based on this objective, Chapter 5 proposes a file popularity and size-aware (PSA) caching scheme that exploits the knowledge of the file popularity and non-uniform file size of the available content to improve the average cache hit probability and average file transmission success probability in the HetNet.

- *Study the achievable performance of a cache-enabled HetNet with D2D communications and large scale antenna arrays.* Chapter 6 addresses this objective by investigating the impact of linear precoding and large scale antenna arrays on the performance of the HetNet.

1.4 Contributions and Outline

The objectives in Section 1.3 reveal the need to couple the caching design and the physical layer design to optimize the SE and EE in a cache-enabled HetNet with D2D communications. In this regard, the main contributions of the thesis are listed in the following:

- Chapter 3 assesses the performance of a HetNet that can serve content requests via cellular or D2D links. Specifically, the analytical expressions for the key performance metrics of device communication probability, coverage probability, average SE, and content average download latency are derived. Further, the average download latency of the D2D-enabled HetNet is studied and compared under

FD-only, HD-only, and mixed FD/HD communication modes. Lastly, insights are provided on the optimal communication mode subject to the content popularity distribution.

- Chapter 4 introduces the peculiar characteristics of mmWave propagation and investigates the performance of a D2D-enabled network operating in mmWave frequencies. Moreover, an association scheme that is parameterized by an interference-aware distance threshold is proposed. The interference-aware association scheme also accounts for the antenna radiation and the random blockage pattern experienced by the mmWave signals. Using the tools of stochastic geometry, the analytical expressions for the association probability, coverage probability, SE, and EE are derived. Finally, a goal attainment algorithm for the joint optimization of the SE and EE is proposed. The goal attainment algorithm incorporates a dynamic transmit power and bandwidth allocation scheme and is compared with a baseline scheme that assumes constant transmit power and bandwidth allocation.

- Chapter 5 proposes a PSA caching scheme for a hybrid microwave/mmWave HetNet that comprises macro BSs and pico BSs. The available files are assumed to have sizes that are drawn from independent Pareto and lognormal distributions according to studies on the statistics of content in servers. Second, the caching strategy is aimed at maximizing the aggregate popularity of the stored files of a BS, which is modeled as a zero-one knapsack problem (0-1 KP). The 0-1 KP is solved using dynamic programming and branch and bound algorithms. Finally, the downlink performance of the cache-enabled HetNet is analyzed under the PSA caching scheme, and the results are compared with the conventional caching schemes.

- Chapter 6 extends the study of the PSA caching scheme to a HetNet with large scale antenna arrays. The main contribution of this chapter is the downlink performance analysis of a mmWave HetNet with D2D communications and maximum-ratio-transmission precoding. The expressions for the cache hit probability, average achievable rate, and successful content delivery probability are derived and the impact of the large-scale antenna arrays on the system performance is investigated.

Besides Chapters 3-6, Chapter 2 reviews the related literature and Chapter 7 presents the thesis conclusions, the significance of the findings, and suggestions for future work.

Table 1.1: Summary of Main Contributions of Thesis

S/N	Contributions	Chapter/Section	Publication
1	Analysis of the device communication probability, coverage probability, average SE, and content average download latency in a D2D-enabled HetNet	3	[50]
2	Presentation and analysis of an interference-aware distance threshold-based association scheme that accounts for the propagation characteristics in a D2D-enabled mmWave cellular network	4.3	[51]
3	Analysis of cellular and D2D association probabilities, SE, and EE in a D2D-enabled mmWave cellular network	4.4, 4.5.1	[51]
4	Presentation of a goal attainment algorithm as a solution to the SE-EE joint optimization problem	4.5.2, 4.5.3	[51]
5	Presentation and analysis of a PSA caching scheme under random file size distributions in a cache-enabled HetNet	5.4	A journal paper, currently undergoing peer review in IEEE Transactions on Communications
6	Formulation and solution to a 0-1 KP based on the PSA caching scheme	5.5	A journal paper, currently undergoing peer review in IEEE Transactions on Communications
7	Performance analysis of the average achievable rate and successful content delivery probability under the PSA caching scheme in a cache-enabled HetNet with D2D communications and large scale antenna arrays	6	A manuscript, currently being finalized for submission to the IEEE Transactions on Communications

Chapter 2

Literature Review

This chapter reviews the body of related works and casts the research undertaken in this thesis within the context of the state of the art. Specifically, the related works are divided into three research areas relevant to the scope of this thesis. The first research area focuses on D2D communications in HetNets and surveys association schemes for D2D communications, which are aimed at improving the SE and EE of HetNets. The second research area deals with content-aware caching in HetNets, and reviews the caching schemes that account for the content popularity distribution and system parameters of HetNets. The last research area is concerned with the performance assessment of cooperative transmission techniques in cache-enabled HetNets with D2D communications and large scale antenna arrays. A comparison between the work in this thesis and the state of the art is also presented in this chapter.

2.1 Device-to-Device Communication in Heterogeneous Networks

D2D communication involves the direct exchange of content between user devices without routing the content through the access or core network. In terms of standardization, the Third Generation Partnership Project (3GPP) incorporated D2D communication under the Proximity Services feature in the LTE Release 12 and identified its use cases including network offloading, commercial/social-centric communication, third party application development that leverages 3GPP Proximity Services, and public safety communications during disaster recovery periods [52]. In [13], an outline of the D2D taxonomy is presented where D2D is categorized under inband D2D (underlay or overlay) on licensed 3GPP spectrum or outband (network controlled or autonomous) on unlicensed spectrum. Mathematical techniques have also been proposed to optimize resource allocation and power consumption in D2D-enabled cellular systems. These techniques include convex optimization approaches [53] and stochastic geometry [54].

The current literature on D2D-enabled HetNets focuses on resource allocation, power control, and interference management schemes as techniques to improve the network SE and EE. The authors of [55] propose a heuristic algorithm for resource allocation to enhance the total system rate in a heterogeneous cellular network comprising multiple microwave and mmWave bands. The idea of the heuristic algorithm is to make full use of the advantages of cellular network and mmWave network, while minimizing interference and maximizing the system transmission rate. Moreover, a multicasting service that uses software-defined networking is proposed in [56] to facilitate D2D communication in HetNets. As noted in [56], the advantage of the software-defined networking paradigm is the centralized management of the network, which stems from the separation of the control plane from the data plane. A three-tier HetNet that comprises D2D users, small cell users, and macro BSs is studied in [57] and a resource selection and scheduling algorithm is proposed to reasonably allocate the resources in the HetNet. Moreover, the studies account for the caching strategy, user density, and D2D radius in activating the links and scheduling resources.

Interference is a major drawback in HetNets where D2D links can access licensed cellular bands. Interference alignment is a promising solution aimed at reducing the impact of interfering signals by aligning them in orthogonal subspaces relative to desired signal subspace. In this regard, a D2D-assisted interference alignment framework in a multi-tier HetNet is investigated by the authors of [58] and they study the use of precoders and optimal receive filters at the small BSs as a means of enhancing the interference mitigation. The backhaul is also a major constraint that limits the traffic capacity of a HetNet with multiple node tiers, thus, the work in [16] proposes a non-uniform deployment of D2D communications to offload the backhaul traffic and reduce the average traffic delay in a HetNet with cloud computing capabilities. A D2D underlay with a relay selection mechanism is adopted in [59] to improve the resource utilization and mitigate interference from resource reuse in a HetNet with macrocells and femtocells. Moreover, the work in [60] formulates a joint power allocation and user scheduling problem to maximize the ergodic sum rate of users in a HetNet with D2D communications and non-orthogonal multiple access. The tools of stochastic geometry and the Poisson cluster process (PCP) are used in [61] to analyze the uplink of a D2D-enabled HetNet and the results show that the D2D tier enhances the coverage probability of the HetNet when compared to a HetNet without D2D. Additionally, [62] considers a channel assignment and power control optimization problem for a HetNet with D2D. Specifically, a resource allocation algorithm is proposed for the power control optimization problem while the results show an improvement in the throughput of cellular users and an improvement in the EE of D2D users.

Other works have considered mode selection algorithms for optimizing the performance of D2D communications in HetNets. For example, the work in [63] proposes a mode selection algorithm for interference mitigation in D2D-enabled HetNets and a power consumption minimization algorithm for mode selection and

EE in a D2D-enabled HetNet is studied in [64]. The use of multi-level codebooks with multicast scheduling is proposed in [65] to improve the EE and network throughput in a D2D-enabled HetNet.

None of the reviewed literature has studied network-aware association schemes for activating the communication links in a mmWave-based HetNet with D2D communications. In this regard, this thesis proposes an association scheme for establishing cellular and D2D links that is parameterized by a distance threshold and accounts for the system parameters including the out-of-cell interference, the antenna radiation pattern, and the blockage effects. Additionally, the proposed association scheme is compared with the existing minimum path loss-based and maximum average received power-based schemes adopted in [15, 39, 66]. Moreover, the analytical expressions of the coverage probability under noise and interference-limited assumptions of the mmWave HetNet are derived and insights are provided on the impact of the system parameters. The SE and EE performance metrics present competing tradeoffs in terms of resource allocation and power consumption, hence, a goal attainment algorithm is proposed to jointly maximize the network area SE and EE metrics. The algorithm incorporates the system design parameters including transmit power and bandwidth allocation. The performance of the interference-aware association scheme and the goal attainment algorithm is investigated under typical system conditions and compared with the existing works that adopt the minimum path loss-based and maximum average received power-based association schemes, which are not interference-aware. User clustering in a cache-enabled HetNet is modeled using the PCP, which is different than the lattice and Poisson point process (PPP) models that are adopted in the existing literature [16, 36, 37, 57]. Different than the work of [61], which equally adopts the PCP for modeling spatial interactions between users, the effect of activating full-duplex, half-duplex, and hybrid full-duplex/half-duplex D2D communications is investigated.

2.2 Content-Aware Caching in Heterogeneous Networks

The availability of cheap memory and storage capabilities on edge nodes and user devices has motivated research efforts in content caching schemes that aim to offload traffic from the access and core networks and minimize the content retrieval delay. Various caching schemes that are content-aware have been proposed in recent works, such as proactive caching schemes that rely on predictions of content demand and reactive caching schemes that optimize the delivery of content by observing previous content requests. In [67], a proactive caching technique that exploits the social and spatial structure of the network is investigated and shown to achieve some savings in the backhaul utilization. The authors in [17] propose an optimal geographic content placement scheme that makes use of spatial point models such as the Gibbs or Isings model to capture the interaction between D2D nodes in a wireless network. The spatially correlated content caching model

of [17] specifies exclusion regions where users that cache the same files do not reside, thus, exploiting the spatial diversity to improve the cache hit probability. The results of the analysis demonstrate higher cache hit probabilities compared to a baseline independent content placement scheme with no spatial interaction. Some other works such as [19] have proposed optimal cluster-centric caching to maximize the collective performance of D2D users within a cluster. Using stochastic geometry, the results in [68] investigate the impact of the density of cache-enabled nodes on the SE of a small cell network.

Caching schemes have equally been extended to HetNets with multiple tiers of BSs that have different densities and caching capabilities. The combination of dense small cells, macro BSs with wide area coverage, and multiple frequency bands are promising solutions to enhance the performance of HetNets. Notably, a cache-enabled two-tier HetNet with mmWave small cells is studied in [49] and the performance of the successful transmission probability is shown to outperform the performance under traditional HetNet architecture with no caching ability. A proactive caching technique is adopted in [69] as a means of exploiting D2D communications in HetNets comprising users with different file popularity profiles. The caching scheme is optimized and shows significant performance gains compared to a static caching scheme. Moreover, the MPC caching scheme is optimal in single-cell networks but is sub-optimal in networks with overlapping coverage and multiple access schemes [70]. The social relationships between users and user mobility are considered in [71] where an optimal caching strategy for a HetNet with D2D underlay is studied. The results in [71] show that the optimal caching scheme outperforms both MPC and random caching schemes. Similarly, user mobility is considered in [72] and a collaborative hierarchical caching strategy is proposed to maximize the EE in a D2D-enabled HetNet. The authors in [73] adopt a cache refreshment strategy that strikes a balance between user satisfaction and infrastructure cost, whereas the economical efficiency of a cache-enabled HetNet is optimized in [74] with the aid of a scalable video coding framework. In [75], a hybrid caching strategy that combines probabilistic caching and deterministic caching is employed in a cache-enabled HetNet. The numerical results show that hybrid caching outperforms MPC caching in HetNets with limited backhaul. Further, the optimal geographic content placement problem is revisited in [76] where the content placement and activation densities in a HetNet are jointly maximized, subject to constraints on the cache size and BS energy consumption. Similarly, the average cache hit rate of a cache-enabled HetNet is maximized in [77], subject to the cache size constraint of the small BSs.

Joint optimization problems that involve the caching design and other system design aspects have also been studied. Notably, joint consideration of the caching phase and the transmission phase is aimed at maximizing the probability of finding requested files within caches and transmitting desired files with minimum path loss, favorable channel fading, and minimum interference effects. For example, the authors of [78] consider joint cache-partitioning, content placement, and user association in D2D-enabled HetNets. By

accounting for the system parameters, the study proposes a two-stair algorithm to optimize the cache space utilization. On the other hand, the work in [79] proposes a distributed content caching and delivery policy to maximize the EE in a HetNet with different user preferences. The results of the study demonstrate higher EE compared with the conventional caching schemes. Moreover, the authors of [80] employ a deep deterministic and policy gradient algorithm to manage the relationships between user clustering and content caching in a HetNet with no knowledge of the channel gains. On the other hand, a coded caching framework is adopted in [81] which accounts for user mobility and content popularity and minimizes the amount of downloaded data from the macro BSs of a HetNet.

In HetNets with no prior knowledge of the content popularity distribution, learning algorithms have been proposed to track the content popularity profiles of the users. For example, the work in [82] proposes an online learning algorithm to predict the file popularity profile of a HetNet comprising dense small cells in order to maximize the SE. Further, a Bayes-based learning algorithm is proposed in [83] to estimate the popularity distribution of small cell HetNets with unknown content popularity. However, the cost that arises due to the extra delay from the learning phase is the main drawback. Moreover, a queue-aware cache update scheduling algorithm is proposed in [84] for the timely update of cached content and to maximize the content delivery in a HetNet.

The assumption of equal-sized content is adopted in the previous works on cache-enabled HetNets [68, 85, 86, 87, 88]. Different from the literature, this thesis focuses on the joint design of content/file popularity and content/file size as a means to enhance the success probability of cache-enabled HetNets operating in mmWave bands. Besides, the Pareto, lognormal, and Gamma distributions are adopted to model the statistics of the file size. The choice of the aforementioned probability distributions is based on existing works on file size statistics in content servers [89, 90]. Moreover, the cache capacity of the BSs and users are provisioned in terms of raw byte-size, different than the existing works that model the cache capacity in terms of the maximum number of files that can be stored. The optimal file caching problem is modeled as a 0-1 KP and a class of polynomial-time algorithms is proposed to reduce the exponential complexity of the problem formulation. Lastly, the performance under the proposed PSA caching scheme is benchmarked with the conventional MPC, probabilistic, and size-weighted popularity (SWP)-based caching schemes in the literature [46, 47, 49].

2.3 Cooperative Transmission and Multiple-Input Multiple-Output in Heterogeneous Networks

Cooperative transmission schemes are considered an attractive solution to enhance the performance of multi-cellular wireless networks. The 3GPP has standardized cooperative transmission techniques under the Co-ordinated MultiPoint (CoMP) framework, which was introduced in LTE-Advanced and has been adopted in fifth generation networks [91]. The CoMP framework makes provision for the synchronous or asynchronous joint transmission of data from multiple BSs in a HetNet [6, 92] and coordinated beamforming of signals of multiple BSs within a cluster [93, 94] to improve the SE and ergodic rate. In this regard, D2D communications in cache-enabled HetNets can exploit the aforementioned cooperative transmission techniques to maximize the system performance.

The studies in [95, 96] propose small BS cooperative transmission under a random caching scheme with the caching distribution as the design parameter. A random caching scheme stores files whose indices are selected from a caching distribution, as opposed to a deterministic caching scheme where the probability of storing a file is either zero or unity. The studies in [95, 96] show that the successful transmission probability is maximized and exhibits better performance compared to deterministic caching schemes including MPC and independent caching. In [97], a random caching-based cooperative transmission scheme is equally studied in a HetNet with popularity prediction errors. The ensuing results also demonstrate the robustness of the caching scheme when compared with the MPC caching scheme and the uniform caching scheme where all files are cached with equal probabilities. Hybrid caching with base station cooperation is adopted in [98] where popular files are fully cached and less popular files are partially cached in helper nodes. Moreover, cooperative strategies are designed to deliver the cached content to users and the results indicate significant gains in the performance of the system. Besides, the performance of a cooperative content delivery scheme in a D2D-enabled HetNet with BSs and small cells is analyzed in [57].

A cluster-centric small cell network is considered in [99] where cooperative joint transmission and parallel transmission are exploited to deliver the most popular and least popular content to requesting users. The results demonstrate performance gains when compared to a similar system without cooperative transmission. The authors in [100] study the impact of BS heights, transmission distance, cached contents, and cell load on the cooperative transmission mechanism of a HetNet. On the other hand, an optimal cooperative content caching and delivery policy for a HetNet is derived in [101]. The content delivery performance under the optimal cooperative content delivery policy is shown to outperform the performance obtained under a greedy caching scheme and a scheme without caching. In [102], a joint resource allocation and power control problem is formulated for a cooperative D2D HetNet. A quantum coral reef algorithm is subsequently proposed to

maximize the total throughput of the network and the results demonstrate excellent performance.

In parallel, cache-enabled HetNets with D2D communications in mmWave bands can exploit large scale antenna arrays or massive MIMO due to the extremely small wavelengths of the mmWave carrier frequencies which enable the design of antennas with very small apertures. In this regard, the benefits of massive MIMO are demonstrated in the uplink of a cache-enabled HetNet where users and small BSs can upload their content to other users and the core network, respectively. The outage probability and the average delivery rate are derived using the tools of stochastic geometry and the numerical results investigate the performance gains of the proposed framework in terms of the operating network parameters.

The work in [24] investigates a cache-aided massive MIMO framework that exploits linear precoding and interference cancellation. The results highlight the benefit of a joint linear precoding design with caching and massive MIMO in achieving a gain in the system ergodic rate compared to a conventional MIMO design. The analysis in [103] examines the joint caching design with massive MIMO for the downlink of a MIMO channel with Rayleigh fading and the results demonstrate performance gains with an increase in the number of antennas.

The effects of cell load and cache hit probability on the successful content delivery probability of an edge-caching network with massive MIMO-aided self-backhaul is studied in [104]. The analysis reveals the need to appropriately select the caching distribution to successfully deliver content. Moreover, massive MIMO-aided backhauling is shown to achieve a similar delay in retrieving cached content compared to non-cached content. The authors in [105] propose a non-linear programming model to optimize the EE and successful content delivery probability of a cache-enabled mmWave cellular network with massive MIMO. The results demonstrate performance gains compared to single-input single-output mmWave links. In [106], a hybrid microwave and mmWave HetNet with massive MIMO is studied while content-based and location-based user association schemes are proposed. The results demonstrate a positive correlation between the cache capacity and the network performance but require trade-offs in the user association strategies, the caching placement schemes, cache size, content popularity, blockages in the mmWave tier, and pilot contamination due to channel estimation in the massive MIMO tier.

Similar to the literature on cache-enabled HetNets with D2D communications, the body of literature that incorporate large scale antenna arrays into cache-enabled HetNets with D2D communications [24, 103, 104, 105, 107, 108, 109, 110, 111, 112, 113] do not account for the non-homogeneous content size. Thus, a chapter of this thesis is dedicated to the downlink performance analysis of a mmWave cellular HetNet with D2D communication and large scale antenna arrays under the PSA caching scheme. Also, mathematical expressions are derived for the cache hit probability, average achievable rate, and the successful content delivery probability of the system and the results are compared with the state-of-the-art SWP-based,

probabilistic, and MPC caching schemes.

Table 2.1: Comparison of the Proposed Schemes/Algorithms with Existing Schemes/Algorithms in the Literature

Proposed Scheme/Algorithm	**Features of Proposed Scheme/Algorithm**	**Features of Existing Schemes/Algorithms**
Mixed D2D FD/HD mode selection scheme	A device is capable of operating in both FD and HD modes with a non-zero probability	A device is capable of operating in either FD mode or HD mode but not both [36, 37, 38]
Interference-aware D2D distance-threshold based association scheme	Considers path loss, channel fading effects, blockage environment, and antenna design parameters	Consider only path loss and channel fading effects [15, 39, 40, 41, 42, 43, 33, 44, 45]
Goal attainment algorithm	SE and EE are coupled into a multi-objective optimization problem	SE and EE are decoupled into single-objective optimization problems [114]
PSA caching scheme with random file size distribution	Considers Pareto, Gamma, and lognormal distributions based on experimental studies	Assumes deterministic and equal file sizes [86, 88, 68, 87, 85]
PSA caching scheme with dynamic programming and branch and bound algorithms	Accounts for popularity, size, and cache capacity in bytes	SWP-based caching account for only popularity and size [46], Probabilistic and MPC/Popularity-based caching schemes account for only popularity [47, 17, 48, 49]

Chapter 3

Device-to-Device Communication in Heterogeneous Networks[1]

3.1 Introduction

This chapter presents the performance analysis of a HetNet operating in the microwave band that is capable of servicing requests for content using cellular and D2D communications. The main contribution of this chapter is the derivation of analytical expressions for the device communication probability, coverage probability, cluster average SE, and content average download latency of a HetNet when user devices in the HetNet are capable of operating in multiple communication modes. Moreover, the results highlight the importance of configuring user devices to operate in a particular mode of communication according to a target network design objective.

The conventional cellular architecture, where a user's request is serviced by retrieving the requested content from a content server in the core network, poses the drawback of excessive download latency and increased energy consumption at the network infrastructure nodes. To address the latency and energy consumption drawbacks, it has been proposed to offload popular content from the core network for caching at the edge and in user devices [115]. Popularity-based content placement schemes have been proposed for D2D-enabled networks, including *device-centric* placement where content is placed at a neighboring device relative to a requesting device and *cluster-centric* placement, which focuses on optimizing the combined performance of a group of devices with similar content preferences [19].

[1]The content of this chapter has generated a conference paper publication [50], K. T. Hemachandra, O. Ochia and A. O. Fapojuwo, "Performance study on cache enabled full-duplex device-to-device networks," in 2018 IEEE Wireless Communications and Networking Conference (IEEE 2018 WCNC), Barcelona, Spain, June 2018.

Spectrum sharing techniques in D2D-enabled HetNets have also been studied as a means of providing a better quality of service and meeting increasing user demands [116]. In a D2D underlaid HetNet, D2D transmissions reuse the cellular spectrum to maximize the network SE while access control techniques are employed to limit the interference that is experienced by cellular transmissions [116, 117]. On the other hand, in D2D overlaid HetNets, resource allocation for D2D communication is orthogonal with respect to cellular communication which simplifies the interference avoidance techniques at the cost of decreased SE gains [118, 119]. The performance analysis under a D2D overlaid HetNet with cluster-centric content placement is described in the following subsections.

3.2 System Model

3.2.1 Network Topology

The spatial distribution of devices within a HetNet is modeled according to a PCP [18, 120]. Under the PCP model, the HetNet is divided into two tiers where the first tier consists of BSs that are designated as cluster heads (CHs) and the second tier consists of user devices. The locations of the CHs, termed the *parent points*, are distributed according to a PPP Φ_c with density λ_c, and the locations of the user devices, termed the *offspring points*, are independently distributed around each CH, forming non-overlapping clusters that follow a symmetric Gaussian distribution with zero mean and variance $\sigma_c^2 \in \mathbb{R}^2$ [19, 121]. Each cluster represents a group of users with similar content preferences where the users are divided into cellular users that communicate with a CH and D2D users that communicate with other users within the cluster according to the content placement and delivery protocol that is described in Section 3.2.3.

The probability density function (pdf) of the location of a user device $x \in \mathbb{R}^2$ relative to its CH is given by [19, 120]:

$$f_X(x) = \frac{1}{2\pi\sigma_c^2} \exp\Big(- \frac{||x||^2}{2\sigma_c^2}\Big), \tag{3.1}$$

where $||x||$ represents the Euclidean distance between the user device and its CH. A D2D overlay model is assumed in the HetNet where the available system bandwidth is divided between D2D and cellular links to mitigate inter-tier interference. Additionally, communications within the same tier (cellular or D2D) occur in the same spectrum, resulting in intra-cluster and inter-cluster interference. However, due to the short-range nature of D2D links within a cluster, the D2D tier performance is limited by intra-cluster interference [18]. Hence, the D2D analysis focuses on a single representative cluster C_o with a CH located at the origin, and the cellular analysis considers inter-cluster interference from other transmitting CHs within the HetNet. Fig. 3.1 illustrates the topology of the HetNet where the number of user devices in a cluster is assumed to be a

constant N_c.

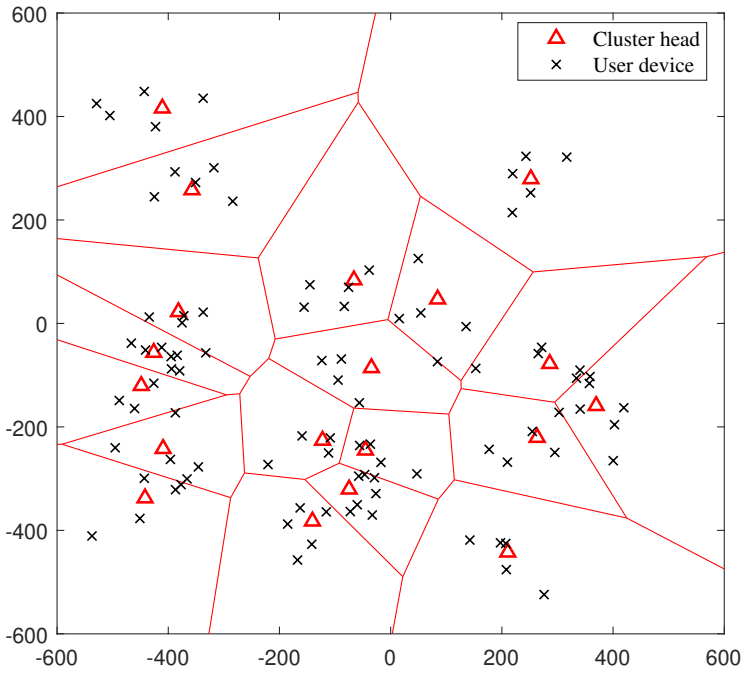

Figure 3.1: Topology of a HetNet divided into clusters where $\lambda_c = 10^{-5}\text{m}^{-2}$, $\sigma_c = 50$, and $N_c = 5$.

3.2.2 Propagation Model

All communications are assumed to occur in the microwave spectrum[2] and the propagation channel for a communication link is modeled using small-scale Rayleigh fading and large-scale path loss. The channel fading power gain is exponentially distributed with unit mean and the path loss is distance-dependent with a path loss exponent α [122, 123]. The CHs are assumed to transmit to the cellular user devices in the cluster with a constant power P_t and the user devices are assumed to transmit with a different constant power P_d.

3.2.3 Content Placement and Delivery

The users in C_o can request files from a library of M most popular files of equal size [3] denoted by $\mathcal{F} = \{f_1, f_2, \ldots, f_M\}$ where $\mathcal{F}$ is an ordered list such that the popularity of file f_i is inversely proportional to its index i [121]. In general, a user device can cache a subset of files in the set $\mathcal{F}$ according to its storage capacity, however, for simplicity, it is assumed that the storage capacity available for caching at a user device

[2]Millimeter wave-based communication is discussed in Chapter 4.
[3]File size distributions based on empirical studies are discussed in Chapters 5 and 6.

is limited to a single file[4] from the set $\mathcal{F}$ [19, 121]. In addition, the first N_c files in $\mathcal{F}$ are assumed to be cached at the N_c user devices in the cluster, such that user device i caches the i-th file without replicated caching of the i-th file at the other user devices referred to as deterministic caching [121]. The remaining $M - N_c$ files can be stored either at the CH or in a file server. For worst-case analysis, all the N_c users are assumed to simultaneously send requests to the CH for downloading a file from the file library set $\mathcal{F}$.

A Zipf distribution is adopted to model the user requests based on measurements of the popularity of files in user-generated systems [124]. Under the Zipf model, the probability that a user requests an arbitrary file f_i is given by [121, 125]

$$\Psi_{f_i} = \frac{\frac{1}{i^{\nu_r}}}{\sum_{j=1}^{M} \frac{1}{j^{\nu_r}}}, \qquad 1 \leq i \leq M, \tag{3.2}$$

where ν_r is the Zipf exponent which controls the skewness of the user requests. A large value of ν_r ($\nu_r > 1$) indicates that a high fraction of requests are dominated by few popular files and a small value of ν_r ($0 < \nu_r < 1$) means that the requests are spread out over the available files. In video streaming platforms like Netflix™ and Amazon™ Prime Video, a large value of ν_r can be likened to a timeline when a popular movie or series premieres and is seen by many subscribers over a short period. On the other hand, a small value of ν_r can be likened to normal periods of subscriber viewership. Moreover, the N_c users in a cluster are equally likely to request files in $\mathcal{F}$ and their respective requests are independent of each other. The CH is assumed to have complete knowledge of the cached file in each user device and determines the content delivery method for each user request as follows:

Consider the case when the i-th user u_i in C_o requests file f_j $(1 \leq j \leq M)$.

- If f_j is cached in u_i, u_i retrieves f_j from its own cache, i.e., self-request and self-delivery.
- If f_j is cached at user u_j $(j \neq i)$, the CH tags u_j as a D2D transmitter for u_i and u_j transmits f_j to u_i via a D2D link.
- if f_j is neither cached in u_i nor any device u_j in C_o, f_j is delivered via a cellular link.

With the described content delivery policy, a user retrieves its file from a single source while it may service the requests of multiple files via broadcast transmission.

3.2.4 Device Communication Modes

In order to analyze all the possible communication scenarios in the representative cluster C_o, six communication modes for user devices are considered, namely D2D receive mode, cellular receive mode, D2D transmit

[4]Caching of multiple files is assumed in Chapters 5 and 6.

mode, HD-only mode, FD-only mode, and mixed FD/HD mode.

- D2D/Cellular receive modes: A user device u_i operates in D2D receive mode when it requests a file that is not in its cache but is available in the cache of another user device u_j in the cluster where $j \neq i$. If the requested file is not found in the cache of any user device in the cluster, the device operates in cellular receive mode.

- D2D transmit mode: A user device u_i that stores a file f_i in its cache operates in transmit mode if at least one of the other devices in the cluster requests f_i.

- HD-only mode: A user device u_i operates in HD-only mode if it either receives a requested file but does not transmit or it transmits its cached file but does not receive within a transmission time interval (TTI).

- FD-only mode: A user device u_i operates in FD-only mode if it simultaneously transmits its cached file and receives its requested file within a TTI.

- Mixed FD/HD mode: A user device that is capable of operating in FD or HD mode communicates using the mixed FD/HD mode if it operates in FD mode with a probability p or HD mode with the complementary probability $(1-p)$. Thus, p is the probability that the device operates in FD mode given that the device can operate in FD or HD modes.

3.3 Analysis of Device Communication Probabilities

3.3.1 Receive mode Probability

The probability that a user device is a D2D receiver is given as:

$$\Psi_{rx,d2d} = \frac{1}{N_c^2} \sum_{\forall i \in \mathcal{N}_c} \sum_{\forall f_j \in \mathcal{F}_c} \big(\sum_{k=1}^{N_c} \Psi_{f_k} - \Psi_{f_j} \big), \quad 1 \leq i \leq |\mathcal{N}_c|, \;\; 1 \leq j \leq \mathcal{F}_c, \tag{3.3}$$

where $\mathcal{N}_c$ represents the set of devices in the cluster with cardinality $|\mathcal{N}_c| = N_c$ and $\mathcal{F}_c$ is the set of all files that are cached in the cluster, also with cardinality $|\mathcal{F}_c| = N_c$.

Proof of (3.3). See Appendix A.1. □

Remark. *Note that Ψ_{f_j} is the probability that a user requests file f_j as given in* (3.2). *The term $\sum_{k=1}^{N_c} \Psi_{f_k}$ represents the probability that the requested file is cached in the cluster and Ψ_{f_j} is subtracted from $\sum_{k=1}^{N_c} \Psi_{f_k}$*

to exclude self-requests. The factor $\frac{1}{N_c^2}$ *results from averaging over the* N_c *user requests for the* N_c *cached files in the cluster.*

The probability that a user device is a cellular receiver is the complement of the probability that the user device is a D2D receiver, i.e., $\Psi_{rx,cell} = 1 - \Psi_{rx,d2d}$. Consequently, for a constant cluster size, a greater fraction of D2D receivers results in a lesser fraction of cellular receivers, and vice-versa.

3.3.2 Transmit mode Probability

The probability that a user device operates as a D2D transmitter is given as:

$$\Psi_{tx} = \frac{1}{N_c^2} \sum_{\forall k \in N_c} \sum_{\forall j \in \mathcal{F}_c} \Big(1 - (1 - \Psi_{f_j})^{N_c - 1}\Big), \tag{3.4}$$

Remark. $(1 - \Psi_{f_j})^{N_c-1}$ *represents the probability that the cached file* f_j *at the user device is not requested by any of the other* $(N_c - 1)$ *devices in a cluster and* $1 - (1 - \Psi_{f_j})^{N_c-1}$ *is the probability that at least one of the other* $(N_c - 1)$ *devices in the cluster requests* f_j*, thus making the device transmit file* f_j*.*

3.3.3 HD-only mode Probability

Following the definition of HD-only mode of communication in Section 3.2.4, the HD-only mode probability is given by:

$$\Psi_{HD} = \begin{cases} \Psi_{rx,d2d}(1 - \Psi_{tx}), & \text{user device operates as a D2D receiver in HD only mode} \\ \Psi_{tx}(1 - \Psi_{rx,d2d}), & \text{user device operates as a D2D transmitter in HD-only mode.} \end{cases} \tag{3.5}$$

3.3.4 FD-only mode Probability

The probability that a user device operates in FD-only mode of communication is given as:

$$\Psi_{FD} = \Psi_{rx,d2d}\Psi_{tx}, \tag{3.6}$$

which follows from the independence of the two events, i.e., the event that the device operates as a D2D receiver and the event that it operates as a D2D transmitter.

3.3.5 Mixed FD/HD mode Probability

The probability that a user device operates in either HD or FD modes of communication, i.e., the mixed FD/HD mode probability, given that the device is capable of operating in FD or HD modes is given as:

$$\Psi_{FD/HD} = \begin{cases} p, & \text{user device operates in FD mode} \\ 1-p, & \text{user device operates in HD mode,} \end{cases} \tag{3.7}$$

where

$$p = \frac{\Psi_{FD}}{\Psi_{FD} + \Psi_{HD}}. \tag{3.8}$$

Now, considering the case when the user device operates as a D2D receiver in HD-only mode, by substituting the corresponding expressions for Ψ_{HD} in (3.5) and Ψ_{FD} in (3.6) into (3.8), p simplifies to Ψ_{tx}, the probability that the device operates as a transmitter.

3.4 Analysis of Coverage Probability

Coverage probability is defined as the probability that the received signal-to-interference-plus-noise ratio (SINR) at a target receiver exceeds γ_T, a specified threshold for decoding received signals. First, the analysis of the coverage probability for the case when a target D2D receiver operates in mixed FD/HD mode is presented as a general case for D2D communication modes. Given that the target D2D receiver located at a distance r from the desired D2D transmitter is operating in mixed FD/HD mode, the received SINR is given by:

$$\Gamma_d(r) = \frac{P_d h_d r^{-\alpha}}{\epsilon_o + I_{intra} + I_{FD/HD}}, \tag{3.9}$$

where h_d is the channel fading power gain of the link between the desired D2D transmitter and the target D2D receiver, ϵ_o is the additive white Gaussian noise power, I_{intra} is the interference from other active D2D transmissions within the cluster, and $I_{FD/HD}$ is the self-interference (SI) at the target D2D receiver. Since the D2D receiver is capable of operating in FD or HD modes, the expression for $I_{FD/HD}$ is given by

$$I_{FD/HD} = \begin{cases} \beta P_d, & \text{D2D receiver is in FD mode w.p. } p \\ 0, & \text{D2D receiver is in HD mode w.p. } (1-p), \end{cases} \tag{3.10}$$

where βP_d is the SI of the target D2D receiver when it operates in FD mode and β is the portion of the transmit power that leaks to the D2D receiver. I_{intra} is calculated by

$$I_{intra} = \sum_{j=1}^{N_I} P_d h_j r_j^{-\alpha}, \tag{3.11}$$

where N_I is the number of D2D transmitters in the cluster that interfere with the desired D2D transmission, r_j and h_j are the distance and channel fading power gain between the j-th interfering D2D transmitter and the target D2D receiver, respectively.

The expression for the coverage probability when the target D2D receiver operates in mixed FD/HD mode, denoted by $\Upsilon_{cov,FD/HD}$ is given by:

$$\Upsilon_{cov,FD/HD} = \mathbb{E}\Big[Pr\Big(h_d > \frac{\gamma_T r^\alpha (\epsilon_o + I_{intra} + I_{FD/HD})}{P_d}\Big)\Big], \tag{3.12}$$

where the expectation is taken over the random variables r, I_{intra}, and $I_{FD/HD}$. Given that $h_d \sim \exp(1)$, (3.12) simplifies to:

$$\Upsilon_{cov,FD/HD} = \mathbb{E}_r\Big[\exp\Big(\frac{-\gamma_T r^\alpha \epsilon_o}{P_d}\Big)\mathcal{L}_{intra}\Big(\frac{\gamma_T r^\alpha}{P_d}\Big)\mathcal{L}_{FD/HD}\Big(\frac{\gamma_T r^\alpha}{P_d}\Big)\Big], \tag{3.13}$$

where $\mathcal{L}_X(s) \triangleq \mathbb{E}(\exp(-sX))$ denotes the Laplace transform of the random variable X. Taking the expectation with respect to r and considering (3.10), (3.13) expands to:

$$\Upsilon_{cov,FD/HD} = \int_{x=0}^{\infty} \exp\Big(\frac{-\gamma_T x^\alpha \epsilon_o}{P_d}\Big)\mathcal{L}_{intra}\Big(\frac{\gamma_T x^\alpha}{P_d}\Big)\big(p\exp(-\gamma_T x^\alpha \beta) + (1-p)\big) g_X(x)\, dx, \tag{3.14}$$

where $g_X(x)$ is the pdf of the distance between the desired D2D transmitter and the target D2D receiver which follows a Rayleigh distribution [19] given by:

$$g_X(x) = \frac{x}{2\sigma_c^2}\exp\Big(-\frac{x^2}{4\sigma_c^2}\Big). \tag{3.15}$$

Further, $\mathcal{L}_{intra}(s)$ is approximated by

$$\mathcal{L}_{intra}(s) \approx \exp\Bigg(-(N_a - 1)\Psi_{tx}\int_{y=0}^{\infty}\frac{sP_d}{y^\alpha + sP_d} g_Y(y)\, dy\Bigg), \tag{3.16}$$

where the parameter $s = \frac{\gamma_T x^\alpha}{P_d}$ and N_a is the maximum number of active D2D transmitters in the cluster, which depends on the mode of communication as follows:

$$N_a = \begin{cases} \frac{N_c}{2}, & \text{HD-only mode} \\ N_c, & \text{FD-only mode} \\ N_c, & \text{mixed FD/HD mode only,} \end{cases} \tag{3.17}$$

and $g_Y(y)$ is the pdf of the random variable Y, representing the distance between an interfering D2D transmitter and the target D2D receiver, which is also Rayleigh distributed [19].

Proof of (3.16) . See Appendix A.2. □

Remark. *Eqn.* (3.14) *gives the general expression of the coverage probability for all D2D communication modes in the cluster. The coverage probability expressions for HD-only mode and FD-only mode can be obtained by setting* $p = 0$ *and* $p = 1$*, respectively, in* (3.14)*.*

The analysis of the SINR and coverage probability for the case when the target receiver operates in cellular receive mode is presented next. The expression for the SINR under cellular receive mode is given as:

$$\Gamma_c(r) = \frac{P_t h_t r^{-\alpha}}{\epsilon_o + I_{inter}}, \tag{3.18}$$

where h_t is the channel fading power gain of the link between a CH and the target cellular receiver and I_{inter} is the interference from cellular transmissions outside C_o. I_{inter} is calculated by:

$$I_{inter} = \sum_{k \in \Phi_c \setminus b} P_t h_k r_k^{-\alpha}, \tag{3.19}$$

where $\Phi_c \setminus b$ represents the set of interfering cluster heads whose transmissions interfere with the desired CH labeled b. r_k and h_k are the distance and channel fading power gain between the k-th interfering CH and the target cellular receiver, respectively.

The expression of the coverage probability under the cellular communication mode is derived similar to the derivation under the D2D communication mode. Thus,

$$\Upsilon_{cov,cell} = \int_{x=0}^{\infty} \exp\Big(- \frac{\gamma_T x^{\alpha} \epsilon_0}{P_t} \Big) \mathcal{L}_{inter}(\frac{\gamma_T x^{\alpha}}{P_t}) f_X(x)\, dx \tag{3.20}$$

where $f_x(x)$ is the pdf of the location of the target receiver relative to its CH, which is given in (3.1). Further,

$\mathcal{L}_{inter}(s^*)$ is derived based on similar analysis in [126]:

$$\mathcal{L}_{inter}(s^*) = \exp\left(-2\pi\lambda_c \Psi_{rx,cell} \int_{y=0}^{\infty} \frac{s^* P_t}{y^\alpha + s^* P_t}\, dy \right), \tag{3.21}$$

where $s^* = \frac{\gamma_T x^\alpha}{P_t}$ and $\lambda_c \Psi_{rx,cell}$ represents the density of the interfering clusters heads in the cellular communication mode.

3.5 Analysis of Cluster Average Spectral Efficiency

The cluster average spectral efficiency is determined as a product of the average number of D2D/cellular transmitters and the target receiver in a cluster given by:

$$SE_{avg} = \begin{cases} N_a \Psi_{tx} \Upsilon_{cov,\delta} \log_2(1+\gamma_T), & \delta \in \{FD, HD, FD/HD\} = \text{D2D} \\ \lambda_c \Psi_{rx,cell} \Upsilon_{cov,\delta} \log_2(1+\gamma_T), & \delta = \text{cellular}, \end{cases} \tag{3.22}$$

where δ is the communication mode of the target receiver.

3.6 Analysis of Content Average Download Latency

The content average download latency (in seconds) for files that are downloaded inside a cluster is expressed as:

$$DL_{avg,\delta} = \frac{\eta W}{B_\delta \Upsilon_{cov,\delta} \log_2\left(1+\gamma_T\right)}, \tag{3.23}$$

where W is the size of the downloaded file in bits, assumed to be constant for all files, $\delta \in \{FD, HD, FD/HD, cellular\}$ is the mode of downloading a file, B_δ is the bandwidth allocation in Hz for δ-communication mode, and η is the probability that a downloaded file is not in the cache of the target receiver given that the file is in the cluster, which is calculated as:

$$\eta = \begin{cases} \frac{\Psi_{rx,d2d}}{\sum_{k=1}^{N_c} \Psi_{f_k}}, & \delta = \text{D2D} \\ \frac{\Psi_{rx,cell}}{\sum_{k=N_c+1}^{M} \Psi_{f_k}}, & \delta = \text{cellular}. \end{cases} . \tag{3.24}$$

3.7 Evaluation Methodology and Discussion of Numerical Results

The values of the performance metrics of the HetNet are computed in MATLAB by following the steps:

- Declare the values of the system parameters, i.e., $\{N_c, M, \nu_r, P_t, P_d, \dots\}$.
- Compute the value of the performance metric per user in the representative cluster C_o, e.g., cellular/D2D coverage probability based on the propagation model of Section 3.2.2, the content placement and delivery protocol of section 3.2.3, and the corresponding expressions for the performance metric.
- Compute the value of the performance metric for the HetNet by averaging over the N_c users in the representative cluster C_o.

The assumed values for the system parameters of the HetNet are chosen according to the related works on microwave-based networks [37, 38, 123, 127]. The chosen values are listed in Table 3.1 and otherwise, are stated under the discussion of the graphical results.

Table 3.1: Values of System Parameters

Notations	Definition	Assumed Values
P_t, P_d	CH transmit power, D2D transmit power	33 dBm, 23 dBm [123, 37]
α, B_δ, ϵ_o	Path loss exponent, bandwidth allocation in Hz for δ-communication mode, additive white Gaussian noise power	4, 1.4×10^6 Hz, $-174 + 10\log_{10} B_\delta + \text{NF}$ dB, NF = 3 dB [127, 38]
M, W	Number of files in file library, size of downloaded file	1000, 100 MB [123, 127, 37]

Fig. 3.2 illustrates the plot of the device communication probability vs. the Zipf exponent ν_r, where ν_r has an inverse relationship with the number of popular file requests. It can be observed that $\Psi_{rx,d2d}$ increases monotonically with ν_r because user requests become more concentrated on a few popular files resulting in an increase in the probability that the requested files are cached in the cluster. Conversely, $\Psi_{rx,cell}$ decreases monotonically with ν_r because the increase in the number of D2D receivers in the cluster decreases the number of cellular receivers. Unlike $\Psi_{rx,d2d}$ and $\Psi_{rx,cell}$, which exhibit strictly monotonic behaviors with ν_r, Ψ_{tx} exhibits a concave behavior with ν_r. In the low ν_r range ($0 < \nu_r < 1$), the requests are spread out over the user devices in the cluster and Ψ_{tx} increases with ν_r, but up to a maximum point. Beyond the maximum point, a further increase in ν_r concentrates the requests to a few distinct files, making Ψ_{tx} to decrease with ν_r.

Ψ_{FD} exhibits a similar behavior to Ψ_{tx} because it is equal to the product of Ψ_{tx} (concave with ν_r) and $\Psi_{rx,d2d}$ (strictly monotonic with ν_r). Similar reasoning applies to the behaviors of Ψ_{HD} in D2D receiver mode and Ψ_{HD} in D2D transmitter mode, which are equal to $\Psi_{rx,d2d}(1-\Psi_{tx})$ and $\Psi_{tx}(\Psi_{rx,d2d})$, respectively.

As expected, the curve for $\Psi_{FD/HD}$ is identical to the curve for Ψ_{tx} when the target D2D receiver operates in FD mode given, that it can operate in either FD mode or HD mode.

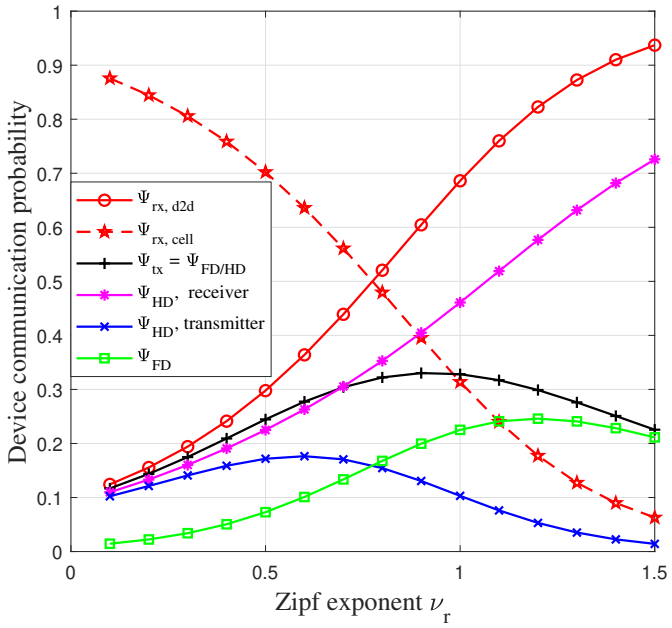

Figure 3.2: Device communication probability vs. Zipf exponent ($M = 1000$, $N_c = 100$).

The sensitivity of the device communication probability to the number of user devices in a cluster N_c is presented in Fig. 3.3. The selected value of ν_r is chosen to ensure that the user requests are concentrated on a few popular files. As explained in Fig. 3.2, there is a high probability of finding the requested file in the cluster which serves as a reason for the increase of $\Psi_{rx,d2d}$ with ν_r and conversely, the decrease of $\Psi_{rx,cell}$ with ν_r. However, as the value of N_c tends towards the constant value of the number of available files $M = 1000$, $\Psi_{rx,d2d}$ eventually converges to $\frac{M-1}{M}$ (≈ 1) and $\Psi_{rx,cell}$ converges to $1 - \frac{M-1}{M}$ (≈ 0). The explanation for the concave behavior of Ψ_{tx} with N_c is similar to the provided explanation in Fig. 3.2. In addition, the explanation for the behaviors of Ψ_{FD}, Ψ_{HD} (transmit and receive modes), and $\Psi_{FD/HD}$ follow those provided for the corresponding probabilities in Fig. 3.2.

The impact of N_c on the D2D coverage probability is illustrated in Fig. 3.4, where a typical receiver in HD-only mode exhibits the highest coverage probability while a typical receiver in FD-only mode exhibits the smallest. Accounting for the non-ideal SI cancellation circuitry further degrades the coverage probability in FD-only mode. The coverage probability obtained under the mixed FD/HD mode lies between that of the FD-only mode and the HD-only mode because of the following reason: The coverage probability expression for the mixed FD/HD mode is a weighted sum of the FD-only mode and HD-only mode coverage probabilities with respective weighting factors Ψ_{tx} and $(1 - \Psi_{tx})$ as presented in (3.14). From Fig. 3.3, the weighting

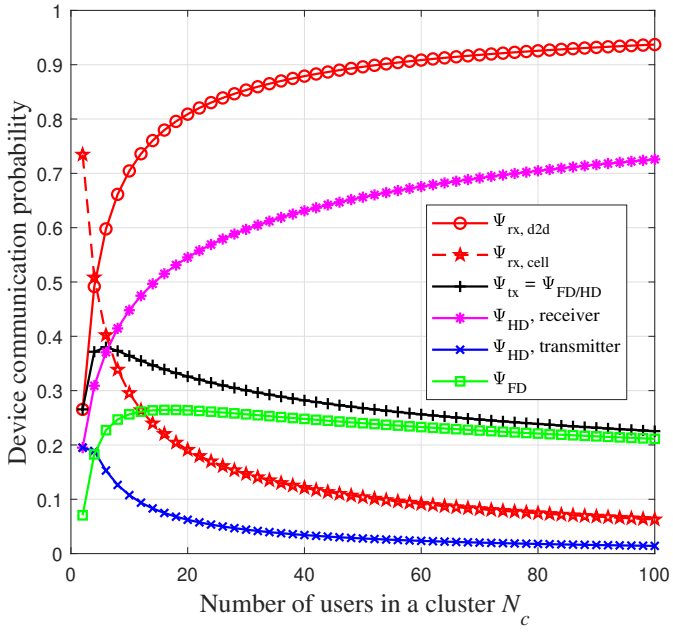

Figure 3.3: Device communication probability vs. Number of users in a cluster ($M = 1000$, $\nu_r = 1.5$).

factor for Ψ_{HD}, receive mode ($= 1 - \Psi_{tx}$) is always higher than that for $\Psi_{FD} (= \Psi_{tx})$ because over the range of N_c considered, P_{tx} is strictly less than 0.5. Hence, it follows that the performance of the mixed FD/HD coverage probability is closer to that of the HD-only mode than that of the FD-only mode. The impact of the scattering/clustering of the devices on the performance of the cellular coverage probability is illustrated in Fig. 3.5 where an increase in the cluster standard deviation σ_c decreases the cellular coverage probability due to longer link lengths within a cluster. Moreover, the cellular coverage probability decreases with an increase in the SINR threshold γ_T as seen in Fig. 3.5 because of the higher received SINR which is required to decode received file signals.

Fig. 3.6 presents the cluster average SE plotted versus N_c for the D2D communication modes. The SE of the FD-only mode with perfect SI cancellation is higher than that of the HD-only mode because of the higher number of active D2D transmitters, but only up to $N_c = 30$ users, beyond which HD-only mode exhibits slightly better performance. However, the SE performance of the FD-only mode with imperfect SI cancellation is always worse than that of the HD-only mode, which implies that SI limits the performance of the FD-only mode. The mixed FD/HD mode provides the best SE performance among the D2D communication modes because of the following reasons: First, the coverage probability of the mixed FD/HD mode is always higher than that for the FD-only mode and closer to the HD-only mode as observed in Fig. 3.4. Second, the average number of active transmitters of the mixed FD/HD mode is greater than that of the HD-only mode. In Fig. 3.7, the cluster average SE for cellular receive mode is plotted versus the density of

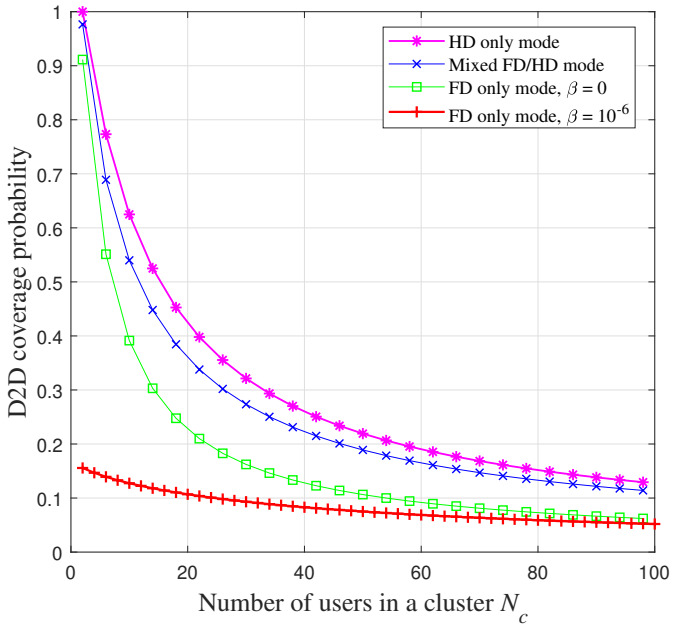

Figure 3.4: D2D coverage probability vs. Number of users in a cluster ($M = 1000,\ \gamma_T = -6\text{dB},\ \ \nu_r = 1.5$).

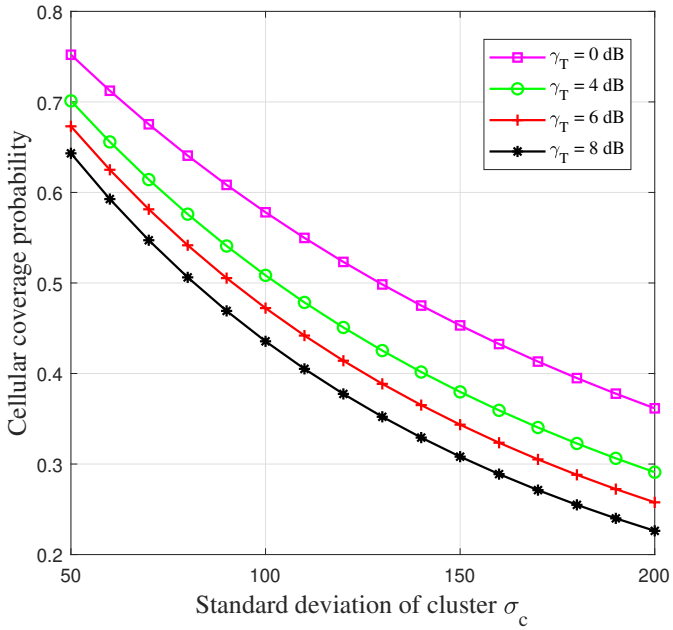

Figure 3.5: Cellular coverage probability vs. Standard deviation of cluster at different SINR thresholds ($M = 1000,\ \ \nu_r = 0.8,\ \ N_c = 100,\ \ \lambda_c = 10^{-4}\text{m}^{-2}$).

cluster heads λ_c where the average SE is observed to increase with λ_c which follows from (3.22). Moreover, a larger value of N_c diminishes the SE performance because of the corresponding decrease in the average number of transmitting cluster heads as shown in Fig. 3.3.

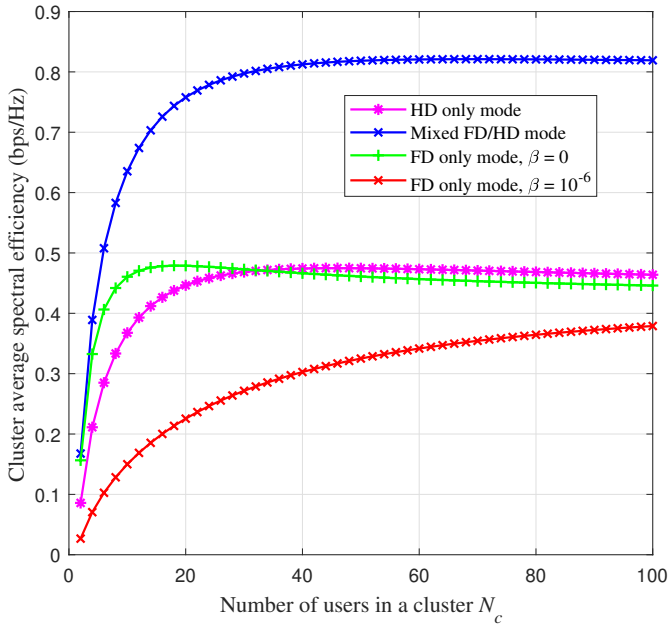

Figure 3.6: Cluster average spectral efficiency vs. Number of users in a cluster ($M = 1000$, $\lambda_c = 10^{-3}\text{m}^{-2}$, $\nu_r = 1.5$).

Lastly, Fig. 3.8 depicts the content average download latency for both cellular and D2D communication modes. Note that (3.23) illustrates the inverse relationship between content average download latency and the coverage probability. Thus, FD-only mode achieves the longest latency among the D2D communication modes while HD-only mode provides the shortest. The latency of the mixed FD/HD mode is between that of the HD-only mode and FD-only mode because of the explanation provided for its coverage probability performance in Fig. 3.5.

3.8 Summary

In this chapter, the performance of a HetNet, which comprises cluster heads and user devices capable of operating in multiple communication modes, was investigated. The analytical expressions for the key performance metrics of communication probability, coverage probability, cluster average SE, and content average download latency were derived in terms of the system parameters. In addition, graphical results were presented to compare the performance of user devices that operate in different communication modes.

The findings in this chapter show that the cellular communication mode is desirable when requests are

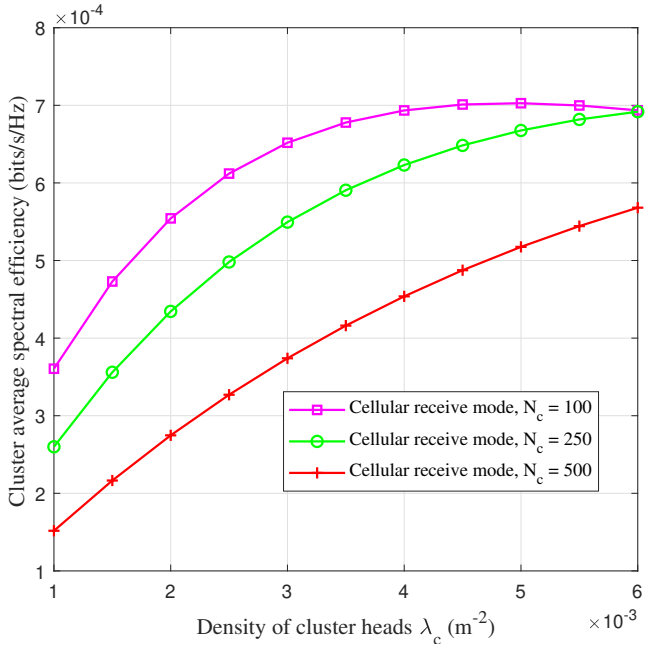

Figure 3.7: Cluster average spectral efficiency vs. Density of cluster heads for different cluster sizes ($M = 1000$, $\nu_r = 1.5$).

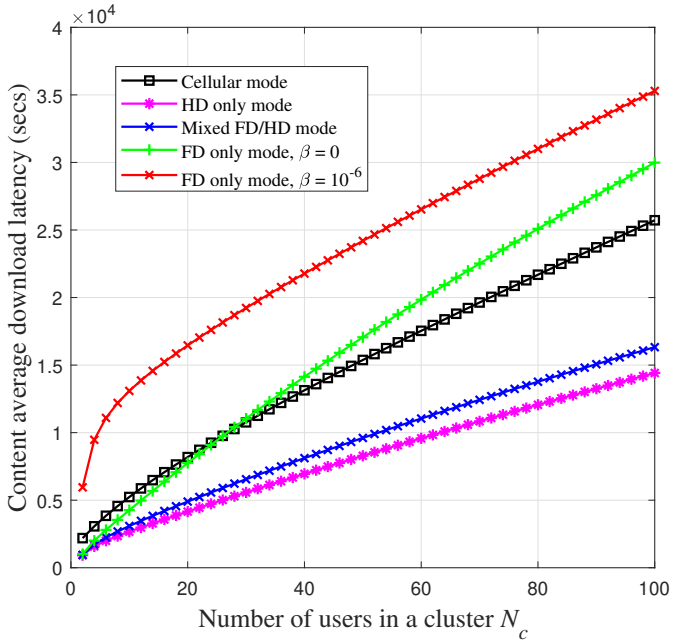

Figure 3.8: Content average download latency vs. Number of users in a cluster ($M = 1000$, $\gamma_T = -6$dB, $\nu_r = 1.5$).

spread out over less popular files, while the D2D communication mode is desirable when the requests are concentrated on a few popular files. In addition, none of the D2D communication modes can simultaneously satisfy the design objectives of high cluster average SE and low content average download latency. The FD-only mode was shown to achieve high cluster average SE at the cost of high content average download latency while the HD-only mode was shown to achieve lower content average download latency compared to the FD-only mode, but at the cost of lower cluster average SE. Finally, the mixed FD/HD mode was seen to provide the best balance in the tradeoff between high cluster average SE and low content average download latency in D2D-enabled HetNets.

Chapter 4

Spectral Efficiency and Energy Efficiency Analyses of Device-to-Device-Enabled Millimeter Wave Networks [1]

4.1 Introduction

This chapter discusses the performance analysis of a mmWave network comprising users that can associate with a BS for cellular communication or neighboring users for D2D communication. The main contributions of this chapter are outlined in the following: First, an association scheme that is characterized by a distance threshold is proposed for activating cellular and D2D links. The proposed association scheme accounts for the underlying system conditions, including out-of-cell interference, antenna radiation, and blockage effects. Second, the analytical expressions for the D2D and cellular association probabilities, coverage probability assuming noise and interference-limited scenarios, SE, and EE are derived. Finally, a goal attainment algorithm is proposed to maximize the network area SE and EE. The goal attainment algorithm incorporates system design parameters as optimization variables, including transmit power and bandwidth allocations to the cellular and D2D tiers. The performance of the proposed algorithm is studied and compared with the

[1] The content of this chapter has generated a journal paper publication [51], O. E. Ochia and A. O. Fapojuwo, "Energy and Spectral Efficiency Analysis for a Device-to-Device-Enabled Millimeter-Wave OFDMA Cellular Network," in IEEE Transactions on Communications, vol. 67, no. 11, pp. 8097-8111, Nov. 2019, doi: 10.1109/TCOMM.2019.2935728.

performance that is achieved under a baseline scheme that is characterized by constant transmit power and bandwidth allocations to the cellular and D2D tiers.

The demand for enhanced mobile broadband services and ultra-low latency applications in the fifth generation and future networks has prompted studies on higher frequency bands beyond the microwave frequency band. The mmWave frequency band, which extends from 30-300 GHz [128], is of current research interest and existing studies on the 28GHz, 38 GHz, and 73GHz bands have revealed much promise in terms of providing significant enhancements in the capacity of cellular networks [9, 129, 12]. D2D communication, which has been introduced in Chapter 3, can leverage the highly directional characteristics of mmWave links to supplement the capacity of cellular systems that operate in mmWave bands. D2D communication schemes have also been studied, including power control, device clustering, and spectrum partitioning schemes [15, 41, 130]. Similar studies have focused on the joint optimization of the SE and the EE performance of D2D-enabled mmWave systems [14, 131]. In this regard, the design problem of achieving coverage probability, SE, and EE performance objectives in a D2D-enabled mmWave cellular network, while ensuring efficient load balancing between cellular and D2D tiers, is investigated in this chapter. Also, the system-level performance of the proposed association scheme and the goal attainment algorithm form the other topics in this chapter.

4.2 System Model

4.2.1 Network Topology

The mmWave cellular network consists of BSs and users that are deployed in an outdoor urban environment. The BSs are assumed to be distributed according to a homogeneous PPP Φ_1 with density λ_1 and the users are assumed to be distributed according to a second independent homogeneous PPP Φ_3 with density λ_3 within the network area of radius r_{net}. The user devices in a particular cell are located within the coverage area of a BS, which is defined by an average cell radius r_c. The BS PPP Φ_1 is divided into a line-of-sight (LOS) PPP denoted by $\Phi_{1\mathrm{L}}$ and a non-line-of-sight (NLOS) PPP denoted by $\Phi_{1\mathrm{N}}$ with respect to a typical receiver and based on blockage models that will be described in Section 4.2.3. Similarly, the user PPP Φ_3 is divided into a LOS PPP denoted by $\Phi_{3\mathrm{L}}$ and a NLOS PPP denoted by $\Phi_{3\mathrm{N}}$ with respect to a typical receiver. Fig. 4.1 illustrates the described network topology.

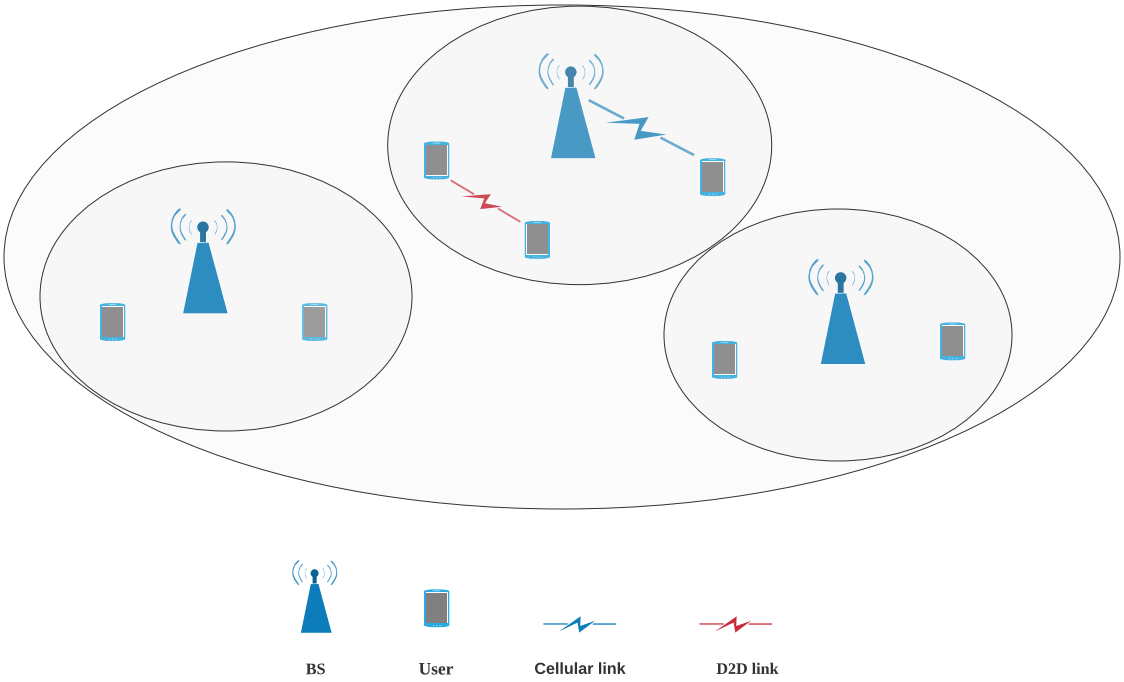

Figure 4.1: Topology of a mmWave cellular network with 3 cells comprising base stations, users, a typical cellular link, and a typical D2D link.

4.2.2 Path Loss and Channel Fading Models

The urban macrocell model [132] is adopted to describe the large-scale path loss experienced by both LOS and NLOS links and is expressed as:

$$PL(x) = \begin{cases} \epsilon_L \cdot \max\{d_0, x\}^{-\alpha_L}, & \text{LOS link}, \\ \epsilon_N \cdot \max\{d_0, x\}^{-\alpha_N}, & \text{NLOS link}, \end{cases} \tag{4.1}$$

where $PL(x)$ represents the path loss experienced by a link of length x, ϵ_L and ϵ_N denote the path loss intercept for a LOS link and NLOS link, respectively, α_L and α_N represent the LOS path loss exponent and NLOS path loss exponent, respectively, and d_0 denotes the close-in reference distance.

An independent Nakagami-m_ν distributed channel fading envelope is assumed to model the small-scale channel fading effect on a desired mmWave link [12, 44] where m_ν is the fading depth parameter and the subscript $\nu \in \{\text{LOS}, \text{NLOS}\}$. Similarly, independent Nakagami-M_ν distribution is assumed for each interfering link where M_ν has the same definition as m_ν. Thus, the channel fading power gain is Gamma distributed with parameter set $\rho_\nu = m_\nu$ as the shape parameter and $\varsigma_\nu = \frac{1}{m_\nu}$ as the scale parameter. The pdf of the Gamma distributed channel fading power gain H_ν is given by [133]:

$$f_{H_\nu}(h_\nu;\rho_\nu,\varsigma_\nu)=\frac{\varsigma_\nu^{-\rho_\nu}h_\nu^{\rho_\nu-1}e^{-\frac{h_\nu}{\varsigma_\nu}}}{\Gamma(\rho_\nu)},\quad h_\nu>0,\ \ \varsigma_\nu>0,\ \ \varsigma_\nu>0. \tag{4.2}$$

Similar pdf of the channel fading power gain for each interfering link can be written.

4.2.3 Blockage Models and Antenna Array Pattern

The rectangular Boolean model [11, 43, 134, 135, 136], defined as *blockage model-A*, and the generalized LOS ball model [12, 44, 137], defined as *blockage model-B*, are adopted to model the probability that a link of length x is either LOS or NLOS with respect to a target receiver. The expression for the LOS probability under blockage model-A is:

$$P_L(x)=e^{-\frac{x}{C}}, \tag{4.3}$$

where $P_L(x)$ is the probability that a link of length x is LOS and C is a constant parameter defined as the average LOS range of the network which depends on the deployment environment [11, 43]. The expression for the LOS probability under blockage model-B is:

$$P_L(x)=p_L\mathbf{1}(x<R_L), \tag{4.4}$$

where $P_L(x)$ is the probability that a link of length x is LOS, R_L is LOS range, $p_L\in[0,1]$ is the LOS probability given that $x<R_L$ [137], and $\mathbf{1}(.)$ is the indicator function. The NLOS probability of a link of length x is given by $P_N(x)=1-P_L(x)$ under the blockage models.

The radiation pattern of an antenna array is characterized by using the uniform linear array model and is approximated by a sectored antenna model for analytical tractability [138, 139]. Under the sectored antenna model, the array gain of a node type $k\in\{\text{BS},\text{user}\}$ is described as follows: The angles in the main lobe beam are assumed to have a constant array gain Z_k and the angles in the side lobe beams are assumed to have a different constant array gain ζ_k where $\zeta_k<Z_k$. Moreover, a typical transmitter-receiver link is assumed to perform perfect beam alignment to achieve a maximum array gain G_o. In contrast, an interfering link has a random array gain G_i, which is modeled as a discrete random variable [12]. The expressions for G_o and G_i are given in (4.5) and (4.6), respectively as:

$$G_o=Z_1Z_3, \tag{4.5}$$

$$G_i = \begin{cases} \phi_{i,1} = Z_1 Z_3 \quad \text{w.p.} \quad \xi_1 = \left(\frac{\theta_1}{2\pi}\right)\left(\frac{\theta_3}{2\pi}\right), \\ \phi_{i,2} = \zeta_1 Z_3 \quad \text{w.p.} \quad \xi_2 = \left(\frac{2\pi-\theta_1}{2\pi}\right)\left(\frac{\theta_3}{2\pi}\right), \\ \phi_{1,3} = Z_1 \zeta_2 \quad \text{w.p.} \quad \xi_3 = \left(\frac{\theta_1}{2\pi}\right), \left(\frac{2\pi-\theta_3}{2\pi}\right), \\ \phi_{1,4} = \zeta_1 \zeta_2 \quad \text{w.p.} \quad \xi_4 = \left(\frac{2\pi-\theta_1}{2\pi}\right)\left(\frac{2\pi-\theta_3}{2\pi}\right), \end{cases} \tag{4.6}$$

where θ_k is the main lobe signal beamwidth of node type k, and $\phi_{i,u}$ is the sample value of G_i at combination u occurring with probability ξ_u, where $u \in [1, 4]$.

4.3 Association Schemes and Resource Allocation

4.3.1 Distance Threshold-Based and Interference-Aware Association

A typical user can associate with a BS for cellular communication or a neighboring user for D2D communication according to the following protocol: A D2D link can be established between a transmitter-receiver pair of users if there exists at least one user located inside a ball of radius r_d that is centered at a receiving user's location and LOS with respect to the receiving user. Further, a user is randomly selected out of the LOS users inside the ball as the D2D transmitter for establishing a D2D link. On the other hand, if no LOS user exists inside the ball of radius r_d, a LOS BS that is located inside the annular region bounded by r_d and the average cell radius r_c is randomly selected as the transmitting BS. Based on the described association protocol, the pdfs of the lengths of a cellular link and a D2D link are:

$$f_X(x) = \begin{cases} \frac{2x}{\pi r_d^2}\left[2\arccos\left(\frac{x}{2r_d}\right) - \frac{x\sqrt{(4r_d^2-x^2)}}{2r_d^2}\right], & 0 \le x \le 2r_d \\ 0, & \text{otherwise}, \end{cases} \tag{4.7}$$

$$g_X(x) = \begin{cases} \frac{2x}{\pi r_c^2}\left[2\arccos\left(\frac{x}{2r_c}\right) - \frac{x\sqrt{(4r_c^2-x^2)}}{2r_c^2}\right], & r_d \le x \le 2r_c \\ 0, & \text{otherwise}, \end{cases} \tag{4.8}$$

where $f_X(x)$ represents the pdf of a D2D link of random length X and sample value x, The expression on the right hand side of (4.7) arises from considering the pdf of the distance between two random points that are uniformly distributed inside a circle according to the results in Section 2.3.5 and 2.3.6 of [140]. On the other hand, $g_X(x)$ represents the pdf of a cellular link of random length X and sample value x, while the expression on the right hand side of (4.8) is obtained similar to (4.7), except that the annular region bounded

by $[r_d, r_c]$ is considered.

The probability that the typical user associates to a BS or D2D transmitter is given respectively as:

$$\Psi_c = e^{-2\pi\lambda_3 \int_0^{r_d} xP_L(x)\,dx} \times \left(1 - e^{-2\pi\lambda_1 \int_{r_d}^{r_c} xP_L(x)\,dx}\right), \tag{4.9}$$

$$\Psi_d = 1 - e^{-2\pi\lambda_3 \int_0^{r_d} xP_L(x)\,dx}, \tag{4.10}$$

where Ψ_c is the cellular association probability and the expression on the right hand side of (4.9) is obtained by considering the independent events that there is no LOS user inside the ball of radius r_d that is centered at the receiving user, and there is at least one LOS BS inside the annular region bounded by $[r_d, r_c]$. Additionally, Ψ_d follows from considering the event that there is at least one LOS user inside the ball of radius r_d centered at the receiving user.

A D2D overlay spectrum sharing strategy is adopted to mitigate inter-tier interference. The system bandwidth W is divided into the cellular bandwidth W_c and the D2D bandwidth W_d, and orthogonal frequency division multiple access (OFDMA) is used to allocate resource blocks (RBs) to active cellular/D2D links in a cell. A frequency reuse factor of unity is assumed across all cells such that cellular and D2D transmissions in a target cell experience interference from corresponding transmissions in other cells outside the target cell, i.e., out-of-cell interference.

The selection of r_d is based on a link-level quality of service objective where r_d is calculated by fixing the minimum SINR threshold γ for successful reception of transmitted signals. Additionally, considering that interference is the main constraint that impacts mmWave networks [43], the mean interference from D2D transmissions in neighboring cells is taken into account and r_d is derived such that the received SINR at a D2D receiver due to transmissions from a D2D transmitter is equal to γ. Small-scale fading effects are ignored by means of temporal averaging and the expression for the D2D average received SINR is given by:

$$\overline{\Gamma}_d = \frac{P_3 r_d^{-\alpha_L} Z_3^2}{N_0 + \bar{I}_{dd}}, \tag{4.11}$$

where P_3 is the user transmit power, $\bar{I}_{dd}$ is the mean interference from D2D transmissions outside the target cell, and N_0 is the thermal noise power. Setting $\overline{\Gamma}_d$ to γ and solving for r_d gives:

$$r_d = \left[\frac{\gamma}{P_3 Z_3^2}\left(\bar{I}_{dd} + N_0\right)\right]^{-\frac{1}{\alpha_L}}. \tag{4.12}$$

The expression for $\bar{I}_{dd}$ under the blockage model-A and the ULA pattern is given in (4.13), where $\Gamma(a, z) \triangleq$

$\int_z^\infty x^{a-1}e^{-x}\,dx$ is the upper incomplete Gamma function. Similarly, $\bar{I}_{dd}$ under the blockage model-B is given in (4.14).

$$\bar{I}_{dd} = 2\pi\lambda_3 P_3 \sum_{u=1}^{4} \xi_u \phi_{i,u}\Big(\mathcal{F}_1(r_{net}, d_o, C, \alpha_L) + \mathcal{F}_2(r_{net}, d_o, C, \alpha_N)\Big), \tag{4.13a}$$

$$\begin{aligned}\mathcal{F}_1(r_{net}, d_0, C, \alpha_L) =& C\epsilon_L {d_o}^{-\alpha_L} e^{-\frac{d_o}{C}}\Bigg[C\big(e^{\frac{d_o}{C}} - 1\big) - d_o + \Big(\frac{1}{C}\Big)^{\alpha_L - 1} d_o^{\alpha_L} e^{\frac{d_o}{C}} \\ &\times \Gamma\Big(2-\alpha_L, \frac{d_o}{C}\Big) - \Big(\frac{1}{C}\Big)^{\alpha_L-1} {d_o}^{\alpha_L} e^{\frac{d_o}{C}} \times \Gamma\Big(2-\alpha_L, \frac{r_{net}}{C}\Big)\Bigg],\end{aligned} \tag{4.13b}$$

$$\begin{aligned}\mathcal{F}_2(r_{net}, d_0, C, \alpha_N) =& (-1)^{1-\alpha_N}\epsilon_N(-r_{net})^{-\alpha_N}\Bigg(r_{net}^2 - 2\Big(-\frac{1}{C}\Big)^{\alpha_N} C^2(-r_{net})^{\alpha_N}\Gamma\big(2-\alpha_N\big) \\ &+ \Big(-\frac{1}{C}\Big)^{\alpha_N} C^2\big(-r_{net}\big)^{\alpha_N}\alpha_N\Gamma\big(2-\alpha_N\big) + 2\Big(-\frac{1}{C}\Big)^{\alpha_N} C^2(-r_{net})^{\alpha_N} \\ &\times \alpha_N\Gamma\big(2-\alpha_N\big) + 2\Big(-\frac{1}{C}\Big)^{\alpha_N} C^2(-r_{net})^{\alpha_N}\Gamma\Big(2-\alpha_N, \frac{r_{net}}{C}\Big) \\ &- \Big(-\frac{1}{C}\Big)^{\alpha_N}\alpha_N\Gamma\Big(2-\alpha_N, \frac{r_{net}}{C}\Big)\Bigg) - r_{net}^{\alpha_N}\Bigg(r_{net}^2 - 2\Big(\frac{1}{C}\Big)^{-2+\alpha_N} r_{net}^{\alpha_N}\Gamma(2-\alpha_N) \\ &+ \Big(\frac{1}{C}\Big)^{-2+\alpha_N} r_{net}^{\alpha_N}\alpha_N\Gamma(2-\alpha_N) + 2\Big(\frac{1}{C}\Big)^{\alpha_N-2} r_{net}^{\alpha_N}\Gamma\Big(2-\alpha_N, \frac{r_{net}}{C}\Big) \\ &- \Big(\frac{1}{C}\Big)^{-2+\alpha_N} r_{net}^{\alpha_N}\alpha_N\Gamma\Big(2-\alpha_N, \frac{r_{net}}{C}\Big)\Bigg),\end{aligned} \tag{4.13c}$$

$$\bar{I}_{dd} = \pi\lambda_3 P_3 \sum_{u=1}^{4} \xi_u \phi_{i,u}\Big(\mathcal{F}_3(d_o, \alpha_L, R_L) + \mathcal{F}_4(d_o, \alpha_N, r_{net})\Big), \tag{4.14a}$$

$$\mathcal{F}_3(d_o, \alpha_L, R_L) = \frac{\epsilon_L d_o^{-\alpha_L} R_L^{-\alpha_L} p_L\Big(d_o^2 R_L^{\alpha_L}\alpha_L - 2d_o^{\alpha_L}R_L^2\Big)}{(\alpha_L - 2)}, \tag{4.14b}$$

$$\mathcal{F}_4(d_o, \alpha_N, r_{net}) = \frac{\epsilon_N d_o^{-\alpha_N}\big(r_{net}d_o\big)^{\alpha_N}(1-p_L)\Big(d_o^2(d_o r_{net})^{\alpha_N}\alpha_N + 2{d_o}^{2+\alpha_N} r_{net}^{\alpha_N} - 2d_o^{2\alpha_N} r_{net}^2\Big)}{(\alpha_N - 2)}. \tag{4.14c}$$

Proofs of (4.13) *and* (4.14). See Appendix B.1 □

The justification for adopting the proposed distance threshold-based and interference-aware association scheme is three-fold: First, the LOS association protocol ensures that a user receives stronger LOS signals compared to the weaker NLOS signals. Second, the random transmitter selection relaxes the requirement for associating to the transmitter that gives the minimum path loss and/or the maximum average received power, allowing for the establishment of links that can support low and medium-rate applications. Third, the calculation of the distance threshold r_d accounts for path loss, blockage effects, antenna radiation pattern, and

interference which are constraints that can impact link quality. The proposed association scheme promises a reduction in the likelihood of occurrence of outage events because the determination of r_d is not arbitrary, rather its determination is based on the system parameters. However, the proposed association scheme introduces signaling overhead, including the knowledge of the transmitter density which must be retrieved via a centralized or distributed network control mechanism. In a quasi-static network, r_d only needs to be determined during a session establishment. In contrast, a dynamic network with user mobility will require more signaling resources because of the time and location-dependent fluctuation of the received signal quality at a mobile user.

4.3.2 Orthogonal Resource Allocation and Performance Tradeoffs

A transmitter can access the system bandwidth W, which is divided between the cellular and D2D tiers as noted in Section 4.3.1. Under the OFDMA scheme, orthogonal RBs are reserved for scheduled users within a cell and the RBs are reused across the cells. A typical user associates with a unique transmitter under the minimum path loss (Min PL)-based and maximum biased received power (Max BRP)-based association schemes (the state of the art) because at most one transmitter in a cell will meet the requirements for association. The probability of resource collision under the state-of-the-art schemes is low because each scheduled user will be served by a single transmitter. On the other hand, the proposed association scheme discussed in Section 4.3.1 will experience a higher number of resource collisions because a typical user can associate with more than one LOS transmitter, which is unknown a priori. Hence, a high number of potentially active transmitters would give rise to a high probability of resource collision.

The resource collision problem could be resolved by an orthogonal allocation of RBs to users in a cell. The overhead cost of resolving the collisions in a tier of node type k (BS or D2D) depends on L_k, the load per cell in a tier of node type k. Following the definitions in [66, 141], $L_k = 1 + \frac{1.28\lambda_j \Psi_l}{\lambda_k}$, where $j = 2, k = 1, l = c$ for the cellular tier and $j = 2, k = 3, l = d$ for the D2D tier. Now, to guarantee collision-free transmissions under the proposed association scheme, at least $\lceil L_k \rceil$ orthogonal RBs should be reserved for the users in a cell [2]. The loss in performance of the proposed association scheme compared to the state-of-the-art schemes is $O(\frac{1}{\lceil L_k \rceil})$ and would impact the achievable average rate.

[2] $\lceil x \rceil$ is the ceiling function of a real number x, defined as the smallest integer that is greater than or equal to x.

4.4 Coverage Probability Analysis

4.4.1 Coverage Probability under a General Network Model

Assuming that the typical user is located at the origin o, the expressions for the SINR coverage probability in the cellular and D2D tiers are given by:

$$\Gamma_c(r) = \frac{P_1 G_o h_{l,o} PL(r)}{I_{cc} + N_o}, \tag{4.15a}$$

$$\Gamma_d(r) = \frac{P_3 G_o h_{l,o} PL(r)}{I_{dd} + N_o}, \tag{4.15b}$$

where

$$I_{cc} = \sum_{u \in \Phi_{1\mathrm{L}} \setminus \{bs(o)\}} P_1 G_{i,u} h_{l,u} PL(y) + \sum_{m \in \Phi_{1\mathrm{N}}} P_1 G_{i,u} h_{l,u} PL(y) \tag{4.16a}$$

and

$$I_{dd} = \sum_{p \in \Phi_{2\mathrm{L}} \setminus \{user(o)\}} P_3 G_{i,p} h_{l,p} PL(y') + \sum_{q \in \Phi_{2\mathrm{N}}} P_3 G_{i,q} h_{n,q} PL(z'). \tag{4.16b}$$

P_1 and P_3 denote the BS transmit power and user transmit power, respectively, I_{cc} and I_{dd} denote the intra-cellular tier interference (i.e., when the typical user associates to a LOS BS) and the intra-D2D tier interference (i.e., when the typical user associates to a D2D transmitter), respectively, and the interference powers are divided into LOS and NLOS components. Further, the notations y and z represent the link lengths for LOS and NLOS interferers, respectively. The corresponding link lengths in the D2D association mode are denoted by y' and z', respectively. The terms G_o and $G_{i,\cdot}$ denote the array gains for a target and interfering link, respectively, while h_l and h_n are the channel fading power gains for a LOS and NLOS link, respectively.

The SINR coverage probability under δ- association mode ($\delta \in \{\mathrm{c} = \text{cellular}, \mathrm{d} = \text{D2D}\}$) is the probability that the received SINR at a typical user exceeds the threshold γ for successful reception, and is expressed as:

$$\Upsilon_{cov,\delta}(\gamma) = Pr\Big(\Gamma_\delta(o) > \gamma\Big). \tag{4.17}$$

The SINR coverage probability is derived by conditioning on the length of a target link and taking the mean over its pdf. Starting with cellular association mode,

$$\Upsilon_{cov,c}(\gamma) = \int_{r_d}^{\infty} Pr\Big(\Gamma_c(o) > \gamma \;\Big|\; x\Big) g_X(x)\, dx$$
$$= \int_{r_d}^{\infty} \sum_{j=0}^{m_L-1} \frac{1}{j!}\Big(\frac{\gamma x^{\alpha_L}}{P_1 G_{o,c}}\Big)^j \sum_{q=0}^{j} \binom{j}{q} \mathbb{E}_{I_{cc}}\Big[I_{cc}^q\Big] N_o^{j-q} \mathcal{L}_{I_{cc}}(s)\Big|_{s=\frac{\gamma x^{\alpha_L}}{P_1 G_{o,c}}} e^{-\frac{\gamma x^{\alpha_L} N_o}{P_1 G_{o,c}}} g_X(x)\, dx, \tag{4.18}$$

where $G_{o,c}$ is the array gain for the target link in cellular association mode and $\mathcal{L}_{I_{cc}}(s)$, the Laplace transform of I_{cc} in cellular association mode, is derived using the tools of stochastic geometry as:

$$\mathcal{L}_{I_{cc}}(s) = \mathcal{L}_{I_{cc,L}}(s) \times \mathcal{L}_{I_{cc,N}}(s)$$
$$= \big(2\pi\lambda_1\big)^2 \prod_{u=1}^{4} \xi_u \exp\left(-\int_{r_d}^{\infty} \sum_{j=1}^{M_L} \binom{M_L}{j} \frac{\big(sP_1\phi_{i,u}\epsilon_L\sigma_L x^{-\alpha_L}\big)^j}{\big(sP_1\phi_{i,u}\epsilon_L\sigma_L x^{-\alpha_L}+1\big)^{M_L}} \right) x P_L(x)\, dx$$
$$\times \prod_{u=1}^{4} \xi_u \exp\left(-\int_{r_d}^{\infty} \sum_{j=1}^{M_N} \binom{M_N}{j} \frac{\big(sP_1\phi_{i,u}\epsilon_N\sigma_N x^{-\alpha_N}\big)^j}{\big(sP_1\phi_{i,u}\epsilon_N\sigma_N x^{-\alpha_N}+1\big)^{M_N}} \right) x P_N(x)\, dx, \tag{4.19}$$

where $\sigma_L = \frac{1}{M_L}$, $\sigma_N = \frac{1}{M_N}$, and $\mathbb{E}_{I_{cc}}\Big[I_{cc}\Big]^q$ in (4.18) is the q^{th} moment of I_{cc}, which is calculated by: $\mathbb{E}_{I_{cc}}\Big[I_{cc}\Big]^q = (-1)^q \left.\frac{d^q \mathcal{L}_{I_{cc}}(s)}{ds^q}\right|_{s=0}$.

Proof of (4.18) *and* (4.19) . See Appendix B.2 and Appendix B.3, respectively.

□

Eqns. (4.18) and (4.19) represent the derivation of the coverage probability expression under a general network setting with arbitrary fading and path loss. The coverage probability analysis under Nakagami-m fading considering special path loss laws, a noise-limited network, and an interference limited network is presented next.

4.4.2 Special Case I: Noise-Limited Network with Nakagami-m Fading

Assume Nakagami-m fading with LOS shape parameter $M_L = 3$ and NLOS shape parameter $M_N = 2$. In addition, consider a typical path loss law with a LOS exponent $\alpha_L = 2.5$ and a NLOS exponent $\alpha_N = 4$. The expression for the coverage probability for a noise-limited network is obtained by setting $\mathcal{L}_{I_{cc}}(s)$ in (4.18) to unity. Further, setting $M_L = 3, \alpha_L = 2.5$, $\alpha_N = 4$, and expanding the resulting expression gives:

$$\Upsilon_{cov,c}(\gamma) = \int_{r_d}^{r_{net}} \exp\Big(- K\big(\gamma, x, SNR\big)\Big)\Big(1 + K\big(\gamma, x, SNR\big) + \frac{1}{2}K^2\big(\gamma, x, SNR\big)\Big) g_X(x)\, dx$$
$$\approx 1 - \frac{1}{2}\int_{r_d}^{r_{net}} K^2(\gamma, x, SNR) g_X(x)\, dx, \tag{4.20}$$

where $K\big(\gamma, x, SNR\big) = 3\frac{\gamma x^{2.5}}{G_{o,c}SNR}$ and SNR denotes the signal-to-noise-ratio.

Remark. *The value of the integrand in* (4.20) *depends on* $K(\gamma, x, SNR)$ *which is a non-decreasing function of SNR. Thus, a high received SNR guarantees a high coverage probability for a noise-limited network.*

4.4.3 Special Case II: Interference-Limited Network with Nakagami-m Fading

Consider an interference-limited network with Nakagami-m fading shape parameters $M_L = 3, M_N = 2$, and path loss exponents $\alpha_L = 2, a_N = 4$. To obtain the expression under an interference-limited scenario, set N_o in (4.18) to zero. The resulting expression is an integral of a second order differential equation that is parameterized by the Laplace transform of the LOS and NLOS terms. Hence,

$$\Upsilon_{cov,c}(\gamma) = \int_{r_d}^{r_{net}} \sum_{j=0}^{2} \frac{1}{j!}\mathbb{E}_{I_{cc}}\left[\Big(\frac{\gamma x^2 I_{cc}}{P_1 G_{o,c}\epsilon_L}\Big)^j \exp\Big(- \frac{\gamma x^2 I_{cc}}{P_1 G_{o,c}\epsilon_L}\Big)\right] g_X(x)\, dx$$
$$\overset{(a)}{=} \int_{r_d}^{r_{net}} \sum_{j=0}^{2} \frac{1}{j!}(-1)^j \frac{d^j \mathcal{L}_{I_{cc}}(s)}{ds^j} g_X(x)\, dx$$
$$\overset{(b)}{=} \int_{r_d}^{r_{net}} \left(\frac{1}{2}\mathcal{L}^{''}_{I_{cc}}(s) - \mathcal{L}^{'}_{I_{cc}}(s) + \mathcal{L}_{I_{cc}}(s)\right) g_X(x)\, dx, \tag{4.21}$$

where the result in (a) follows from applying the relation in [142]: $\mathbb{E}\big[x^j \exp(-x)\big] \triangleq (-1)^j \left.\frac{d^j \mathcal{L}_X(x)}{ds^j}\right|_{s=1}$ and (b) follows from expanding the result in (a). $\mathcal{L}^{'}_{I_{cc}}(s)$ and $\mathcal{L}^{''}_{I_{cc}}(s)$ denote the first and second order derivatives of the Laplace transform of the interference, respectively. Lastly, the derived coverage probability expression in (4.21) can be computed by using numerical integration techniques.

4.5 Joint Optimization of Spectral Efficiency and Energy Efficiency

4.5.1 Analysis of Average Rate, Spectral Efficiency, and Energy Efficiency

The per-user rate for cellular association mode, per-user rate for D2D association mode, and the per-user average rate, denoted by $\mathcal{R}_c, \mathcal{R}_d$, and $\bar{\mathcal{R}}$, respectively, are given as:

$$\mathcal{R}_c = \frac{W_c}{\mathcal{N}_c}\Big(\Upsilon_{cov,c}(\gamma) \times log_2(1+\gamma)\Big), \tag{4.22a}$$

$$\mathcal{R}_d = \frac{W_d}{\mathcal{N}_d}\Big(\Upsilon_{cov,d}(\gamma) \times log_2(1+\gamma)\Big), \tag{4.22b}$$

$$\bar{\mathcal{R}} = \Psi_c \mathcal{R}_c + \Psi_d \mathcal{R}_d, \tag{4.22c}$$

where $\mathcal{N}_c$ and $\mathcal{N}_d$ symbolize the number of active users in cellular and D2D association modes, respectively.

The area SE is defined as the rate per unit bandwidth per unit area in bits/s/Hz/km^2. The expressions for the cellular SE, D2D SE, and area SE are:

$$\mathcal{S}_c = \lambda_1 \Upsilon_{cov,c}(\gamma) \log_2(1+\gamma), \tag{4.23a}$$

$$\mathcal{S}_d = \lambda_3 \Upsilon_{cov,d}(\gamma) \log_2(1+\gamma), \tag{4.23b}$$

$$\bar{\mathcal{S}} = \Psi_c \mathcal{S}_c + \Psi_d \mathcal{S}_d, \tag{4.23c}$$

where $\mathcal{S}_c$ is the area SE for a user that is in cellular association mode, $\mathcal{S}_d$ is the area SE for a user that is in D2D association mode, and $\bar{\mathcal{S}}$ is the network area SE.

Similarly, the EE is the amount of data bits transmitted per unit energy consumption in bits/J. The corresponding expressions for the EE are given as:

$$\mathcal{E}_c = \frac{\mathcal{S}_c}{\lambda_1(\Omega + P_1)}, \tag{4.24a}$$

$$\mathcal{E}_d = \frac{\mathcal{S}_d}{\lambda_3(\Omega + P_3)},$$

$$\bar{\mathcal{E}} = \frac{\bar{\mathcal{S}}}{\lambda_1(\Omega + P_1) + \lambda_3(\Omega + P_3)}, \tag{4.24b}$$

where $\mathcal{E}_c$ is the EE for users in cellular association mode, $\mathcal{E}_d$ is the EE for users in D2D association mode, $\bar{\mathcal{E}}$ is the network EE, and Ω is the power consumption in the baseband and radio frequency circuitry, excluding the power amplifier. In the following section, the network area SE and network EE are coupled into a joint

optimization problem. For the problem formulation, the BS and user transmit powers are assumed to be variables and $P_1, P_3 >> \Omega$.

4.5.2 Problem Formulation for Spectral Efficiency and Energy Efficiency Optimization

This section considers several design issues in the problem formulation for the SE and EE, including: (i) the determination of the optimum transmit power for a BS and a D2D transmitter under the assumption of full network load, and (ii) the determination of the optimum bandwidth fraction to allocate to scheduled cellular and D2D links. The rate coverage probability metric is adopted as the SE-EE coupling constraint and is defined by $Pr(\bar{\mathcal{R}} > \tau) \geq \eta_{obj}$, where η_{obj} is a specified rate coverage probability objective. Let $\mathbf{P^c} = \{P_{1,i}\}_{i=1}^{\mathcal{N}_c}$ denote the set of transmit powers of the LOS BSs that are designated to transmit to scheduled users in cellular association mode. Similarly, let $\mathbf{P^d} = \{P_{2,j}\}_{j=1}^{\mathcal{N}_d}$ denote the set of transmit powers of the LOS D2D transmitters that are designated to transmit to the scheduled users in D2D association mode. The maximum array gain G_o is assumed on all desired links and an OFDMA scheme is assumed where each active link is allocated with a single RB. In addition, the system bandwidth W is divided between the cellular and D2D tiers such that a fraction κ is reserved for the cellular tier and $(1-\kappa)$ is reserved for the D2D tier. Thus, the network area SE can be expressed as:

$$\bar{\mathcal{S}}(\kappa, \mathbf{P^c}, \mathbf{P^d}) = \kappa \Psi_c \mathcal{S}_c + (1-\kappa)\Psi_d \mathcal{S}_d. \tag{4.25}$$

Combining (4.22a)-(4.25) with the rate coverage constraint, a multi-objective optimization problem (MOOP) is formulated as:

$$\max_{\kappa, \mathbf{P^c}, \mathbf{P^d}} \{\bar{\mathcal{S}}(\kappa, \mathbf{P^c}, \mathbf{P^d}), \bar{\mathcal{E}}(\kappa, \mathbf{P^c}, \mathbf{P^d})\}, \tag{4.26a}$$

$$s.t.\ \ Pr(\bar{\mathcal{R}} > \tau) \geq \eta_{obj},\ \ 0 < \kappa < 1,\ \ P_{1,min} \leq P_{1,i} \leq P_{1,max},$$

$$\forall P_{1,i} \in \mathbf{P^c},\ \ P_{2,min} \leq P_{2,j} \leq P_{2,max},\ \ \forall P_{2,j} \in \mathbf{P^d}, \tag{4.26b}$$

where $P_{1,min}$ and $P_{1,max}$ are the minimum and maximum BS transmit powers, respectively, $P_{2,min}$ and $P_{2,max}$ are the minimum and maximum user transmit powers, respectively, $\bar{\mathcal{R}}$ is parameterized by the minimum SINR coverage threshold γ expressed in (4.22a). The MOOP in (4.26a) is reformulated as a single objective optimization problem (SOOP) using the weighted-Tchebycheff method [143] as follows:

$$\max_{\kappa,\mathbf{P^c},\mathbf{P^d}} \{\omega\bar{\mathcal{S}}(\kappa,\mathbf{P^c},\mathbf{P^d}) - \beta(1-\omega)\bar{\mathcal{E}}(\kappa,\mathbf{P^c},\mathbf{P^d})\}, \tag{4.27a}$$

$$s.t.\ \ Pr(\bar{\mathcal{R}} > \tau) \geq \eta_{obj},\ \ 0 < \kappa < 1,\ \ P_{1,min} \leq P_{1,i} \leq P_{1,max},$$

$$\forall P_{1,i} \in \mathbf{P^c},\ \ P_{2,min} \leq P_{2,j} \leq P_{2,max},\ \ \forall P_{2,j} \in \mathbf{P^d}, \tag{4.27b}$$

where ω is a specified weight objective and β is a conversion factor that is applied in (4.26a) to ensure consistency in the units of SE and EE. Next, (4.24a) is substituted into the coupled objective function in (4.27a) to obtain a transformed objective function $\bar{\mathcal{S}}_T$:

$$\bar{\mathcal{S}}_T = \mathcal{A}_c\Psi_c\mathcal{S}_c + \mathcal{A}_d\Psi_d\mathcal{S}_d, \tag{4.28a}$$

$$\mathcal{A}_c = \kappa\Big(\omega - \frac{\beta(\omega-\beta)}{P_N}\Big), \tag{4.28b}$$

$$\mathcal{A}_d = (1-\kappa)\Big(\omega - \frac{\beta(\omega-1)}{P_N}\Big), \tag{4.28c}$$

where $P_N = \sum_{i=1}^{\mathcal{N}_c} P_{1,i} + \sum_{j=1}^{\mathcal{N}_d} P_{2,j}$ is the total power consumption in the network. In addition, $\mathcal{A}_c$ and $\mathcal{A}_d$ can be interpreted as the transformed bandwidth fraction allocations to the cellular tier and D2D tier, respectively, constrained by the decision variables, i.e., $\kappa, \mathbf{P^c}, \mathbf{P^d}$. Moreover, the transformed bandwidth constraint can be written as $0 < \mathcal{A}_c, \mathcal{A}_d < 1$ and the power constraints can be written as $\mathcal{N}_c P_{1,min} + \mathcal{N}_d P_{3,min} < P_N < \mathcal{N}_c P_{1,max} + \mathcal{N}_d P_{3,max}$. The transformed problem of (4.28) is shown to be non-convex by applying Jensen's inequality [144] and the proof of its non-convexity is provided in Appendix B.4. A goal attainment algorithm for solving (4.28) and the selection of ω is discussed next.

4.5.3 A Goal Attainment Algorithm for Spectral Efficiency and Energy Efficiency Optimization

In design problems for systems that comprise many design variables, a targeted performance goal is set and several possible solutions that meet the performance goal are tested within tolerance ranges. This approach is necessary because it is impossible to satisfy multiple competing objectives simultaneously due to the finite system resources. Hence, the goal attainment method described in [143] is adopted to solve the SE-EE SOOP. The goal attainment method provides a linear formulation for MOOPs and aims to find the vector of decision variables that minimizes the maximum of the scaled deviation of a set of objectives from a set of desired goals [143].

Starting from (4.25), (4.27), and (4.28) and applying the goal attainment method, the SOOP becomes

$$\min_{\kappa,\mathbf{P^c},\mathbf{P^d}} \Big(\frac{\bar{\mathcal{S}}^* - \bar{\mathcal{S}}_T(\kappa,\mathbf{P^c},\mathbf{P^d})}{\omega} \Big), \tag{4.29a}$$

$$s.t.\ \ Pr(\bar{\mathcal{R}} > \tau) \geq \eta_{obj},\ \ 0 < \mathcal{A}_c, \mathcal{A}_d < 1,$$

$$\mathcal{N}_c P_{1,min} + \mathcal{N}_d P_{3,min} < P_N < \mathcal{N}_c P_{1,max} + \mathcal{N}_d P_{3,max}, \tag{4.29b}$$

where $\bar{\mathcal{S}}^*$ is a specified network SE goal. The selection of ω measures the relative tradeoff between the objective performance in the cellular tier and the D2D tier [145]. For example, if ω is set to 1, (4.29b) becomes an unscaled goal attainment problem i.e., $\min_{\kappa,\mathbf{P^c},\mathbf{P^d}} \Big(\bar{\mathcal{S}}^* - \bar{\mathcal{S}}_{\mathcal{T}}\big(\kappa,\mathbf{P^c},\mathbf{P^d}\big) \Big)$, where $\mathcal{A}_c = \kappa\big(1 - \frac{\beta(1-\beta)}{P_N}\big)$ and $\mathcal{A}_d = (1-\kappa)$. In this case, $\mathcal{A}_d$ is independent of ω and the goal attainment is skewed towards optimizing the performance objective in the cellular tier. An iterative algorithm for implementing (4.29) is proposed in Algorithm 4.1.

The decision and non-decision variables of the SOOP are initialized in Lines 1 and 2 of Algorithm 4.1, respectively. Lines 3-6 allocate the transmit powers to the active BS and D2D transmitters with ϱ_1 and ϱ_2 denoting small values for updating the BS transmit power and D2D transmit power, respectively at each iteration index of the outer **while** loop. The BS and D2D transmit power allocations are stored in Line 7 and the allocated bandwidth fraction to the cellular tier is incremented, while the value of the objective function is computed in Lines 8 and 9. Lines 10-12 determine whether or not the rate coverage and bandwidth constraints of the SOOP are satisfied and the computed value of the objective function is saved in Line 13. Lines 14-20 examine the behavior of the discretized Jacobian matrix and, depending on which condition is met, the values of the objective function, the decision, and the non-decision variables are saved in Line 23. The algorithm terminates at Line 25.

The proposed Algorithm 4.1 has polynomial asymptotic complexity because its search space comprises the power allocation vectors for the BS and D2D transmitters over the maximum number of iterations in order to determine the values of a decision variable and the objective function based on the rate coverage constraint. Thus, the complexity is $O(\chi \times max(\mathcal{N}_c, \mathcal{N}_d) \times maxITER)$ where χ is the number of decision variables.

4.6 Evaluation Methodology and Discussion of Numerical Results

The performance of the main system metrics, including coverage probability, SE, and EE is discussed and compared under the proposed association scheme and the state of the art, considering the assumed system

Algorithm 4.1: Proposed SE-EE Goal Attainment Algorithm

Input: $P_{1,min}$, $P_{1,max}$, $P_{3,min}$, $P_{3,max}$, $\mathcal{N}_c$, $\mathcal{N}_d$, $\bar{\mathcal{S}}^*$, β, γ, τ, ω, η_{obj}, $maxITER$.
Output: $\bar{\mathcal{S}}_T^{opt}$, $\mathbf{P}^{c,opt}$, $\mathbf{P}^{d,opt}$, κ^{opt}.

1: Initialize: $\mathbf{P}^c = ones(1, \mathcal{N}_c) \times P_{1,min}$, $\mathbf{P}^d = ones(1, \mathcal{N}_d) \times P_{3,min}$.
2: Initialize: $\mathbf{O} = zeros(1, maxITER)$, $\varrho_1 = 0.1$, $\varrho_2 = 0.1$, n= 1, $\kappa = 0.1$.
3: **while** $n < maxITER$ **do**
4: **for** $j = 1$ to $max(\mathcal{N}_c, \mathcal{N}_d)$ **do**
5: Increment the BS and D2D transmit powers: $P_{1j,n} = P_{1j,n-1} + \varrho_1$, $P_{2j,n} = P_{2j,n-1} + \varrho_2$.
6: **end for**
7: Update the BS and D2D transmit power allocations at index n in the transmit power vectors $\mathbf{P}^c$ and $\mathbf{P}^d$, respectively and increment the BS bandwidth i.e., $\kappa_n = \kappa_{n-1} + \varrho_1$.
8: Compute $P_{cov,c}(\gamma)$ and $P_{cov,d}(\gamma)$.
9: Compute $Pr(\bar{\mathcal{R}} > \tau)$, $\mathcal{A}_c$, $\mathcal{A}_d$, and $\bar{\mathcal{S}}_{\mathcal{T}}(\kappa_n, \mathbf{P}^c, \mathbf{P}^d)$ using (4.28). Compute the objective function value $\mathcal{O}_n$ using (4.29).
10: **if** $Pr(\bar{\mathcal{R}} > \tau) < \eta_{obj} \parallel \mathcal{A}_c, \mathcal{A}_d \notin (0, 1)$ **then**
11: Discard $\mathcal{O}_n$.
12: **end if**
13: Save $\mathcal{O}_n$ in $\mathbf{O}$.
14: Compute the discretized Jacobian matrix $\mathbf{J} = [\frac{\Delta \mathbf{O}}{\Delta k}, \frac{\Delta \mathbf{O}}{\mathbf{P}_n^c}, \frac{\Delta \mathbf{O}}{\mathbf{P}_n^d}]$.
15: **if** $det(\mathbf{J}) < 0$ **then**
16: Go to Line 21.
17: **end if**
18: **if** $det(\mathbf{J}) \geq 0$ **then**
19: Go to Line 22.
20: **end if**
21: Increment n by 1. Repeat Lines 1 to 15.
22: **if** $n == maxITER$ **then**
23: $O^{opt} = \min(\mathbf{O})$, $\bar{\mathcal{S}}_T^{opt} = \bar{\mathcal{S}}_T(\kappa, \mathbf{P^c}, \mathbf{P^d})$, $\mathbf{P}^{c,opt} = \mathbf{P^c}$, $\mathbf{P}^{d,opt} = \mathbf{P^d}$, $\kappa^{opt} = \kappa$ at the index of O^{opt}. Go to Line 25.
24: **end if**
25: **end while**

parameters. Additionally, the joint SE-EE performance under the proposed goal attainment scheme is compared with a baseline scheme where BSs are assumed to transmit with equal transmit power and D2D transmitters transmit with equal transmit power different than the BS transmit power.

The values of the system performance metrics are computed based on their corresponding expressions and using numerical algorithms in Mathematica. Besides, Algorithm 4.1 is executed by calling user-defined functions within a MATLAB script. The assumed values of the system parameters are listed in Table 4.1.

Table 4.1: Values of System Parameters

Notations	Definition	Assumed Values
$P_{1,max}, P_{1,min}$, $P_{3,max}, P_{3,min}$, f, W	Maximum BS transmit power, minimum BS transmit power, maximum user transmit power, minimum user transmit power, carrier frequency, system bandwidth	46 dBm, 43 dBm, 20 dBm, 17 dBm, 28 GHz, 1 GHz [15, 66]
κ, α_L, α_N, ϵ_L, ϵ_N, C, R_L, p_L	Cellular bandwidth fraction, LOS path loss exponent, NLOS path loss exponent, LOS path loss intercept, NLOS path loss intercept, LOS range under blockage model-A, LOS range under blockage model-B, LOS probability under blockage model-B	$0.5, 2.0, 4$, $\frac{1}{10^{2.8}f^2}$, $\frac{1}{10^{3.24}f^2}$, 141.4 m, 200 m, 1 [132, 43, 12, 137, 41]
$G_{o,c}$, $G_{o,d}, N_0$	Array gain for a target link in cellular association mode, array gain for a target link in D2D association mode, thermal noise power	20 dB, 0 dB, -174dBm/Hz $+ 10\log_{10} W$ [43, 15]

Figs. 4.2a and 4.2b show the plots of the cellular association probability vs. the average cell radius and the D2D association probability vs. the average cell radius, respectively, assuming blockage model-A. The average cell radius $r_{cell} \triangleq \frac{1}{\sqrt{\pi\lambda_1}}$ [12, 43] is such that a sparse network results in a large inter-site distance, and vice-versa. In addition, the proposed association scheme is compared with the state-of-the-art Min PL-based and Max BRP-based association schemes [15, 39, 43]. The Max BRP-based association scheme includes a biasing factor $T \in [0, \infty)$ with $T = 0$ indicating no D2D association and $T \to \infty$ indicating no cellular association [15, 66]. When $T = 1$, the Max BRP-based scheme reduces to the Max RP-based scheme under which a user can connect to a BS or a neighboring user that offers the strongest average received power [42]. The cellular association probability is monotonically decreasing with r_c under the proposed and state-of-the-art association schemes because a sparse network reduces the probability that a BS is LOS with respect to a user. Moreover, the cellular association probability under the proposed scheme matches the Min PL-based scheme and the Max BRP-based scheme at low T (for example, $T = 0.01$ implies that users are biased to associate to BSs). The close match among the schemes is because a random LOS BS will likely incur a small path loss or provide a high received power at a receiver. In contrast, when T is set to a high value (for example, $T = 100$), the D2D association probability under the Max BRP-based scheme is the highest among the association schemes because of its strong bias towards D2D association. The D2D

association probability is monotonically increasing with r_c because of the increased likelihood of users to associate with neighboring users in close range compared to BSs that are more distant.

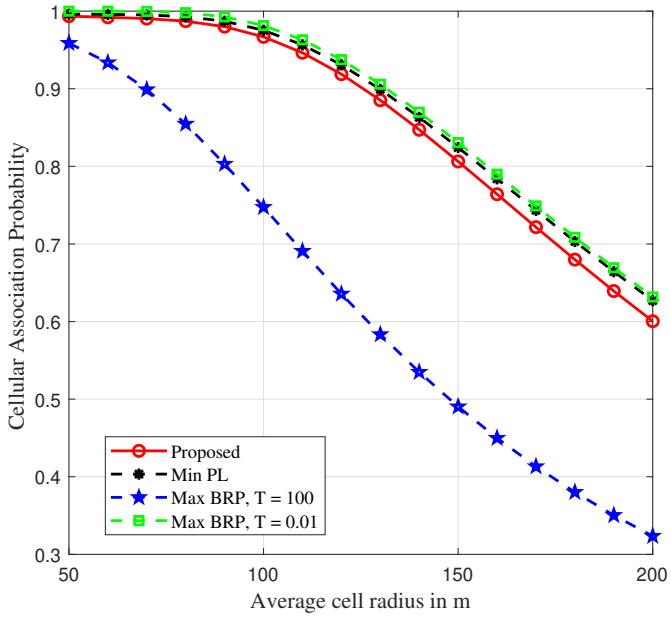

(a) Cellular association probability vs. average cell radius.

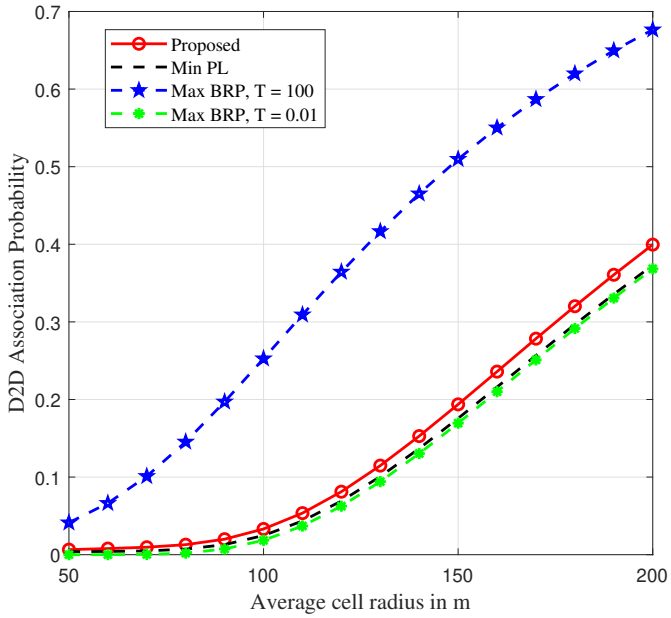

(b) D2D association probability vs. average cell radius.

Figure 4.2: Cellular and D2D association probabilities vs. average cell radius under blockage model-A where $r_{net} = 1$km and $\lambda_3 = 100$ users/km^2 (BS = base station, D2D = device-to-device, Min PL = minimum path loss, Max BRP = maximum biased received power).

Figs. 5.9 and 4.4 illustrate the comparison between blockage model-A and blockage model-B where it is observed that blockage model-A achieves a higher D2D association probability because it achieves a higher value of the D2D distance threshold r_d at each value of r_c, hence, permits a wider D2D coverage area. The converse is true for cellular association probability, which is higher under blockage model-B. The aforementioned observations confirm the intuition that the cellular deployment environment impacts the association mode. An urban environment with a large number of potential blockers (modeled by blockage model-B) reduces the likelihood of D2D association, whereas a rural and suburban environment with a small number of potential blockers (modeled by blockage model-A) favors D2D association.

The variation of the SNR coverage probability with the SNR coverage threshold is presented in Figs. 4.5a and 4.5b. There are two notable points regarding the behavior of the proposed association scheme in a noise-limited network. First, the parameter r_d is defined by the out-of-cell interference and, hence, has no impact in a noise-limited network. Second, the lower limit of the integral term in (4.20) is zero because a link length in cellular association mode can assume any real positive value. Fig. 4.5a shows that the SNR coverage probability of the proposed scheme under blockage model-A (the overlapping blue and red curves) is higher than the Min PL-based scheme and the Max BRP-based scheme at $T = 0.01$ when the typical user is associated to a BS and when the SNR threshold is high (SNR $>$ 15 dB) because of the non-existence of a constraint on the link length. Moreover, at $T = 100$, the Max BRP-based scheme achieves the highest SNR coverage probability because the number of users in cellular association mode is the least among all the schemes. However, the proposed scheme gives the worst D2D coverage probability under the severe blocking conditions of blockage model-B because it achieves the least received power and, consequently, the least SNR.

In Figs. 4.6a and 4.6b, the performance of the SIR coverage probability in an interference-limited network is illustrated for cellular and D2D association modes, respectively. The proposed association scheme under the cellular association mode is upper bounded by the Max BRP-based scheme at $T = 0.01$ and lower bounded by the Max BRP-based scheme at $T = 100$ because user association to BSs is favored at a low value of T, whereas D2D association is favored at a high value of T. Moreover, the proposed scheme is sub-optimal at a low SIR threshold (SIR $<$ 20 dB) and the state-of-the-art schemes achieve up to 60% higher SIR coverage probability. Fig. 4.6b shows that the proposed scheme achieves the best performance under blockage model-A in D2D association mode, while it achieves the least performance under blockage model-B.

The performance of the coverage probability, area SE, and EE at 25 dB SINR threshold is studied under varying BS densities and presented in Figs. 4.7 and 4.8. The proposed scheme achieves the highest coverage probability in both cellular and D2D association modes because it exploits the high availability

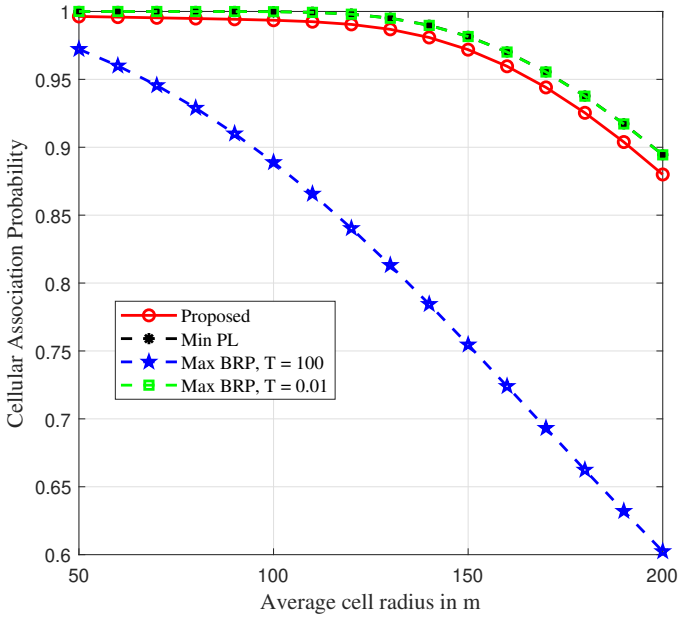

(a) Cellular association probability vs. average cell radius.

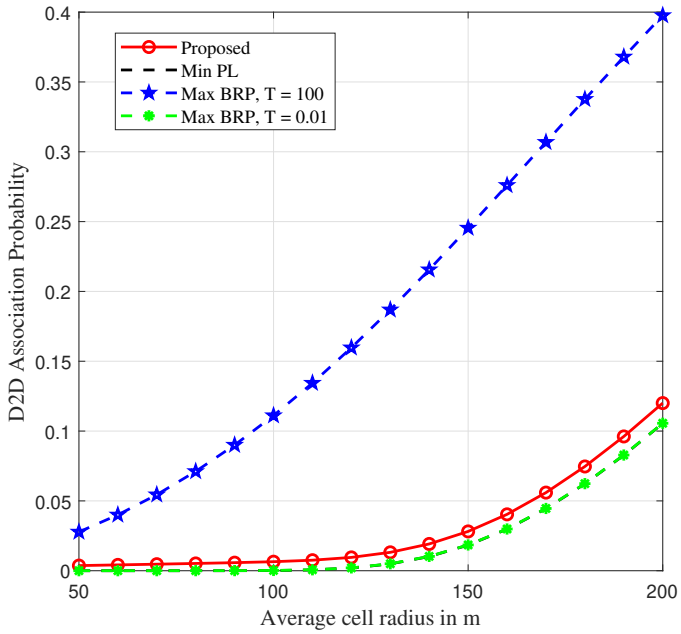

(b) D2D association probability vs. average cell radius.

Figure 4.3: Cellular and D2D association probabilities vs. average cell radius under blockage model-B.

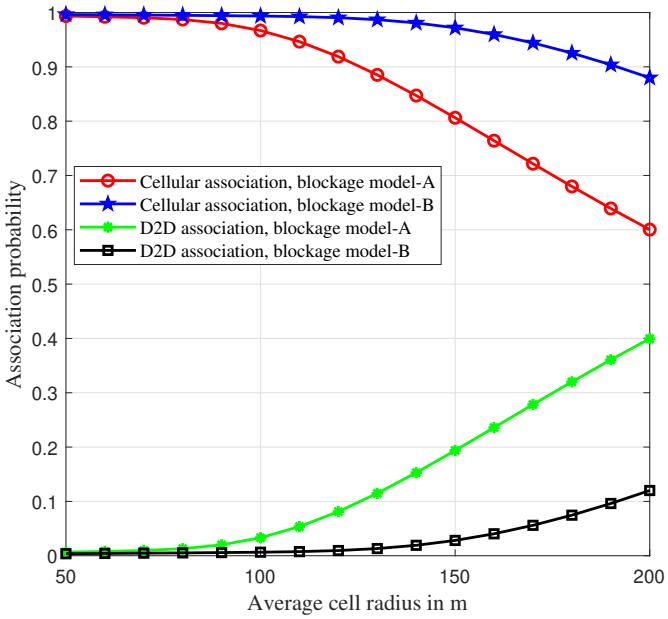

(a) Association probability vs. average cell radius.

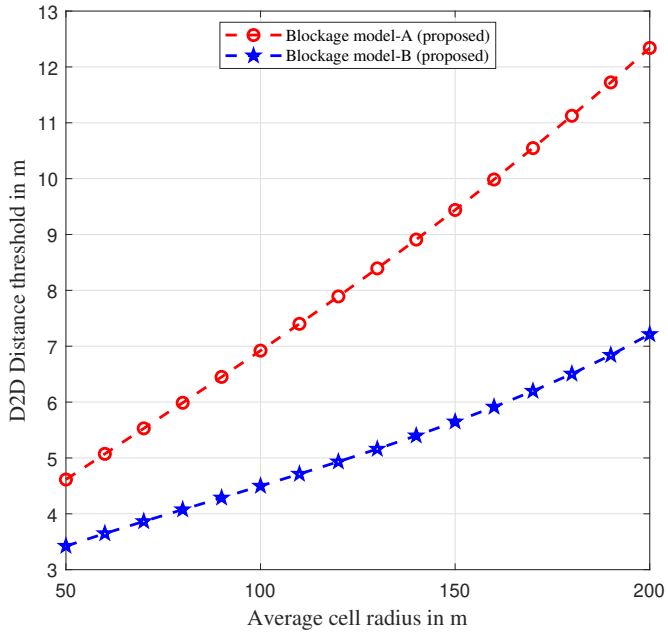

(b) D2D distance threshold vs. average cell radius.

Figure 4.4: Association probability and D2D distance threshold vs. average cell radius for the proposed association scheme and under the blockage models.

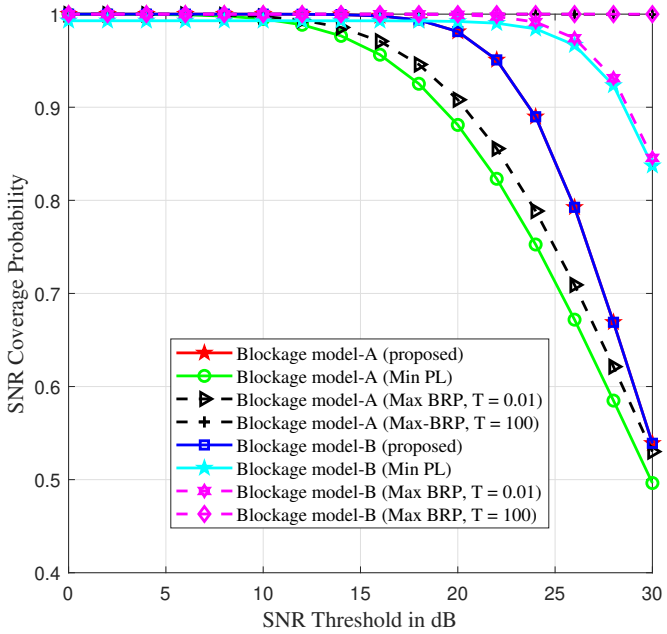

(a) Cellular association mode.

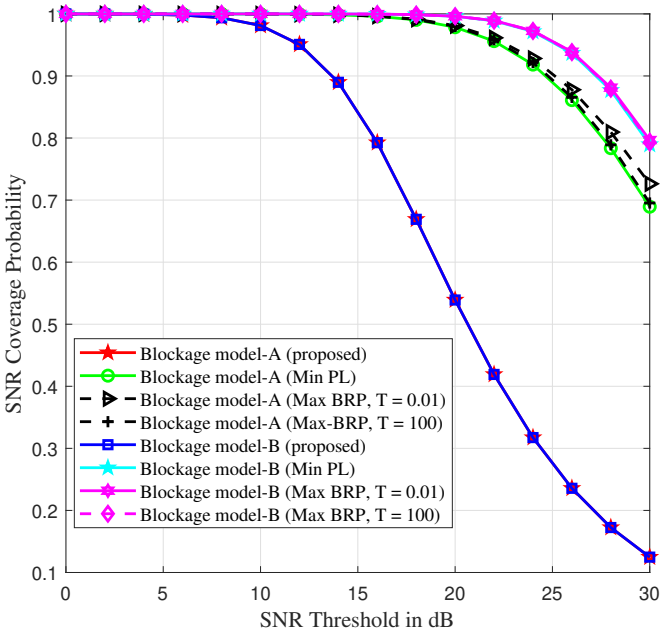

(b) D2D association mode.

Figure 4.5: SNR coverage probability vs. SNR threshold for BS and D2D association modes where $\lambda_3 = 100$ users/km^2 and $r_{cell} = 200$m.

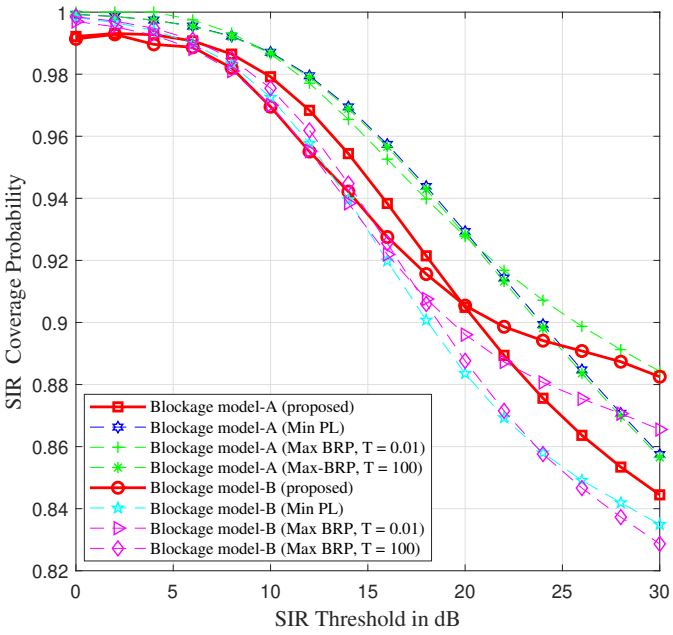

(a) Cellular association mode.

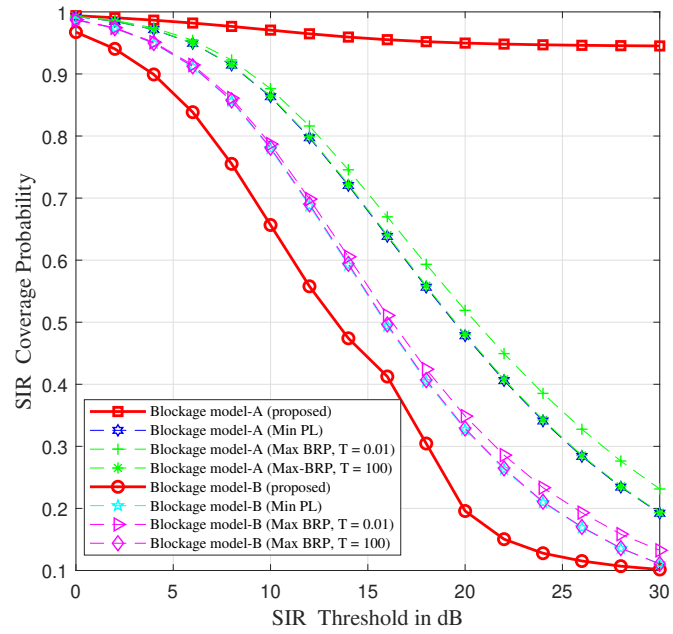

(b) D2D association mode.

Figure 4.6: SIR coverage probability vs. SIR threshold for Cellular and D2D association modes where $\lambda_3 = 100$ users/km^2 and $r_{cell} = 200$m.

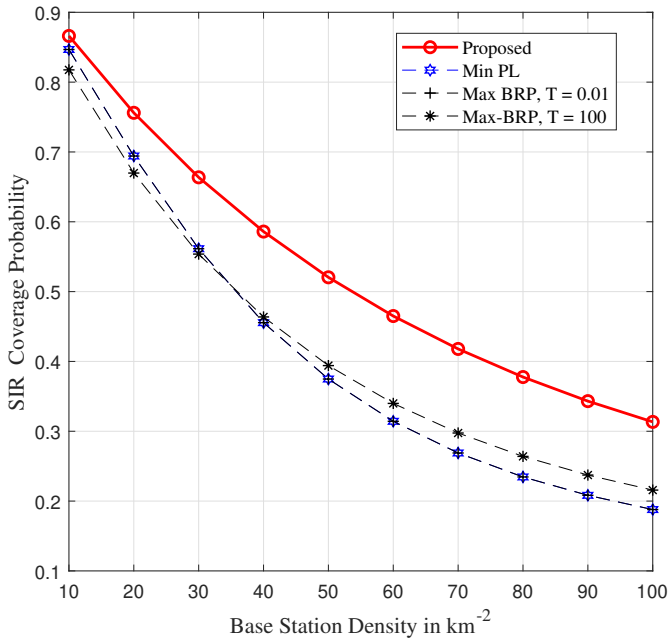

(a) Cellular association mode.

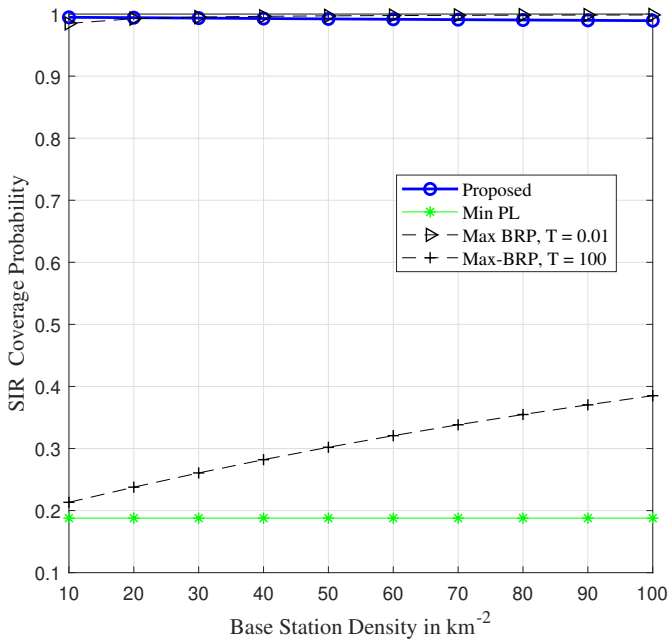

(b) D2D association mode.

Figure 4.7: SINR Coverage Probability vs. BS density λ_1 with $\lambda_3 = 100$ users/km^2 and $\gamma = 25$ dB.

of transmitters to maximize the fraction of serviced users. The load balancing between the cellular and D2D tiers results in a higher network area SE and EE performance under the proposed scheme as seen in Figs. 4.8a and 4.8b, respectively. The load balancing mechanism of the proposed scheme contrasts with the Min PL-based scheme that prioritizes BS transmissions over D2D transmissions because of the higher BS transmit power. In addition, the Max BRP-based scheme requires a high value of T (for example, $T = 100$) to match the performance of the proposed and Min PL-based schemes.

Lastly, Fig. 4.9 shows a comparison of the performance of the proposed goal attainment algorithm with the performance under a baseline constant transmit power and bandwidth allocation scheme. The network objective function is investigated in Fig. 4.9a and the network power consumption is investigated in Fig. 4.9b. The network objective function under the proposed goal attainment algorithm, defined as the scaled deviation from the SE goal of 20 b/s/Hz is lower than the corresponding value obtained under the baseline scheme. Further, the goal attainment algorithm achieves the highest EE, achieving up to 50% decrease in the network power consumption (at $\lambda_1 = 50$ BSs/km^2), compared to the baseline scheme. The higher EE that is achieved by the goal attainment algorithm results from the power control mechanism that contrasts with the baseline scheme where all the BSs and users transmit with no power control. Moreover, the jagged nature of Fig. 4.9b arises from the random power allocation mechanism of Algorithm 4.1. Hence, there is a non-zero probability that the mean value of the transmit power allocation vector at a higher BS density is less than the mean value at a lower BS density, which can result in a lower network power consumption at a higher BS density.

4.7 Summary

This chapter analyzed the performance of the EE and SE of a mmWave cellular network comprising users that are capable of associating with BSs for cellular communication or neighboring users for D2D communication. A D2D distance threshold-based and interference-aware association scheme was proposed as a means of activating cellular and D2D communication modes in a cell. In addition, the analytical expressions for cellular and D2D association probabilities, coverage probability, SE, and EE were derived considering typical system parameters and deployment settings. Lastly, the competing SE and EE metrics were coupled into a joint SE-EE optimization problem and a goal attainment algorithm was proposed to solve the joint SE-EE optimization problem. Lastly, graphical results were presented to compare the performance of the proposed distance threshold-based and interference-aware association scheme with the state-of-the-art Min PL-based and Max BRP-based association schemes.

The findings in this chapter indicate that the proposed association scheme is desirable for adoption in a

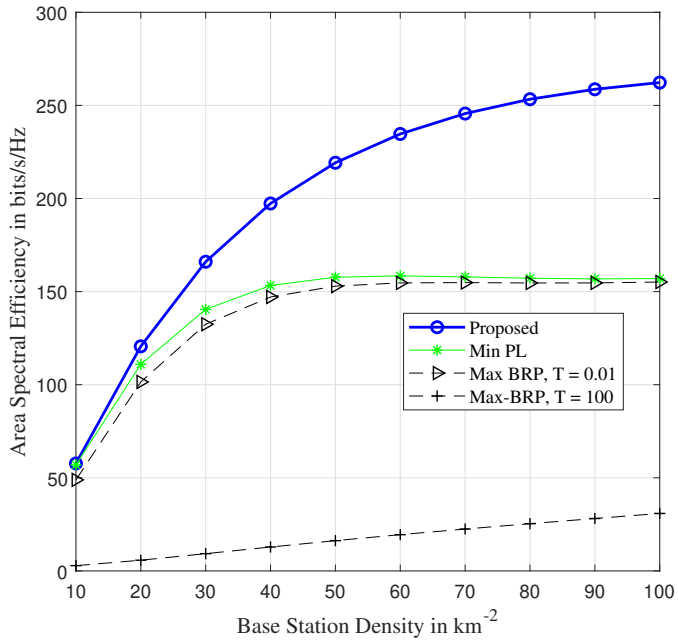

(a) Area SE vs. BS density.

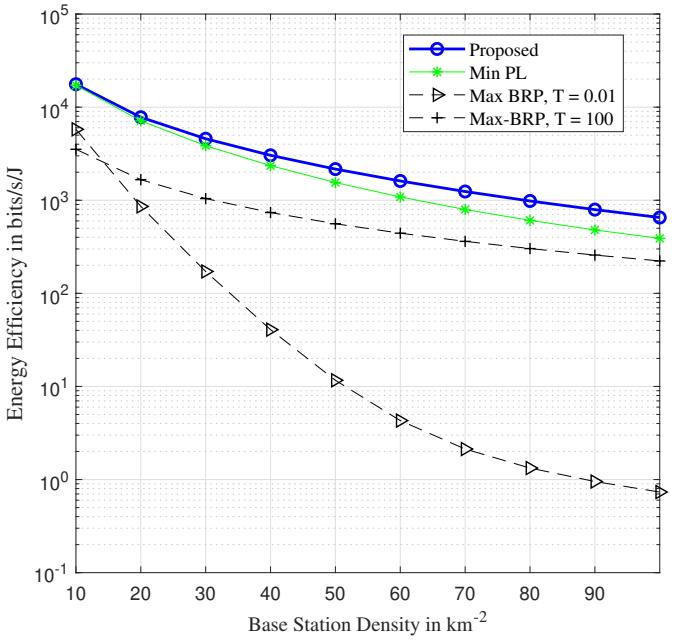

(b) EE vs. BS density.

Figure 4.8: Area SE and EE vs. BS density λ_1 with $\lambda_3 = 100$ users/km^2 and $\gamma = 25$ dB.

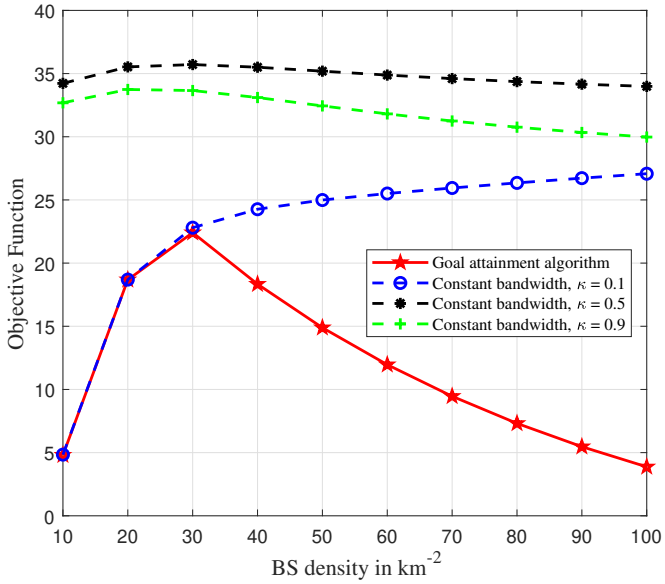

(a) Network Objective Function vs. BS density.

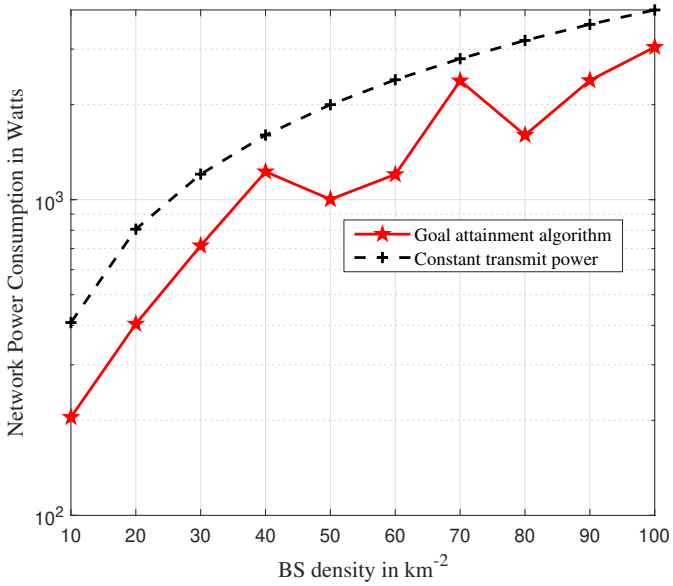

(b) Network Power Consumption vs. BS density.

Figure 4.9: Network Objective Function and Power Consumption vs. BS density λ_1 with $\lambda_3 = 100$ users/km^2, $\{P_{1,min}, P_{1,max}\} = \{43, 46\}$dBm, $\{P_{3,min}, P_{3,max}\} = \{17, 20\}$dBm, $\omega = \beta = \tau = 0.5$, $\eta_{obj} = 5$ b/s/Hz, and $\bar{\mathcal{S}}^* = 20$ b/s/Hz.

D2D-enabled mmWave cellular network to meet high coverage and load balancing requirements. Moreover, the efficacy of the goal attainment algorithm in optimizing the bandwidth allocation and transmit power control of the D2D-enabled mmWave cellular system was validated by the graphical comparison with a baseline system with no integration of the goal attainment algorithm.

Chapter 5

Popularity and Size-Aware Caching with Cooperative Transmission in Hybrid Microwave/Millimeter wave Heterogeneous Networks [1]

5.1 Introduction

This chapter proposes and analyzes the performance of a file popularity and size-aware (PSA) caching scheme in a hybrid HetNet that comprises a file server, a macro BS tier operating in the microwave frequency bands, a pico BS tier operating in the mmWave frequency bands, and a user tier. The main contributions of this chapter are outlined in the following: First, the macro BSs and the pico BSs of the hybrid HetNet are assumed to be equipped with caches that can store files whose sizes are drawn from independent Pareto and lognormal distributions. The choice of the file size models is justified by existing studies on the file size statistics in content servers, however, the PSA caching scheme works for any file size distribution. Second, the problem of maximizing the average cache hit probability of the hybrid HetNet under the PSA caching scheme is formulated as a zero-one knapsack problem (0-1 KP). Moreover, two algorithms that leverage dynamic programming and branch and bound techniques are proposed to solve the 0-1 KP. In addition, the problem of maximizing the network average success probability of the hybrid HetNet subject to the available cache

[1] The content of this chapter has generated a journal paper, currently undergoing peer review in IEEE Transactions on Communications.

capacity is shown to be non-convex and the assumption of prior knowledge of the file caching strategy in the pico BS tier is employed to resolve its non-convexity. Based on the assumption of prior knowledge of the file caching strategy in the pico BS tier, the expressions for the optimal file caching probabilities are derived under noise-limited and interference-limited HetNets with typical path loss exponents. Finally, the results of the analysis under the PSA caching scheme are compared with the state-of-the-art size-weighted popularity (SWP)-based and popularity-based caching schemes. Besides, the performance of cooperative transmission with coded caching is studied in the pico BS tier to reveal the achievable gains over a non-cooperative transmission scheme without coded caching.

The design of efficient caching schemes is critical because of the problem of maximizing competing performance metrics that are subject to constrained system resources such as the cache capacity of a cache-enabled network. Caching schemes that prioritize the caching of popular files, i.e., popularity-based caching do so at the expense of the diversity of the cached files [146, 147]. Other caching schemes including random caching, probabilistic caching, and coded caching have been proposed to optimize the content delivery in multi-cellular and hybrid networks [88]. On the other hand, the inhomogeneous nature of files has prompted studies on content-aware caching. In this regard, the performance of the PSA caching scheme that considers the file size and file popularity distributions in enhancing the performance of a hybrid HetNet is studied in this chapter. The design of a cooperative transmission and coded caching scheme to leverage the file storage redundancy in the pico BS tier of the hybrid HetNet is also presented in this chapter.

5.2 System Model

5.2.1 Network Topology

A hybrid HetNet of radius R that consists of a centralized file server, a macro BS tier, a pico BS tier, and a user tier is considered. The locations of the macro BSs, pico BSs, and users are assumed to be distributed as points of independent homogeneous Poisson point processes (PPPs) Φ_1, Φ_2, and Φ_3 with densities λ_1, λ_2, and λ_3, respectively. The hybrid nature of the HetNet is such that the pico BS tier operates in the mmWave frequency bands to provide high data rate coverage using directional beamforming, while the macro BSs operate in the microwave (sub 6 GHz) frequency bands to provide wide area coverage. Additionally, the available files of the HetNet are stored in the file server, which is connected to the BSs through backhaul links. The macro and pico BSs are equipped with caches that store files according to the file PSA caching scheme that is discussed in Section 5.4. The topology of the hybrid HetNet is illustrated in Fig. 5.1.

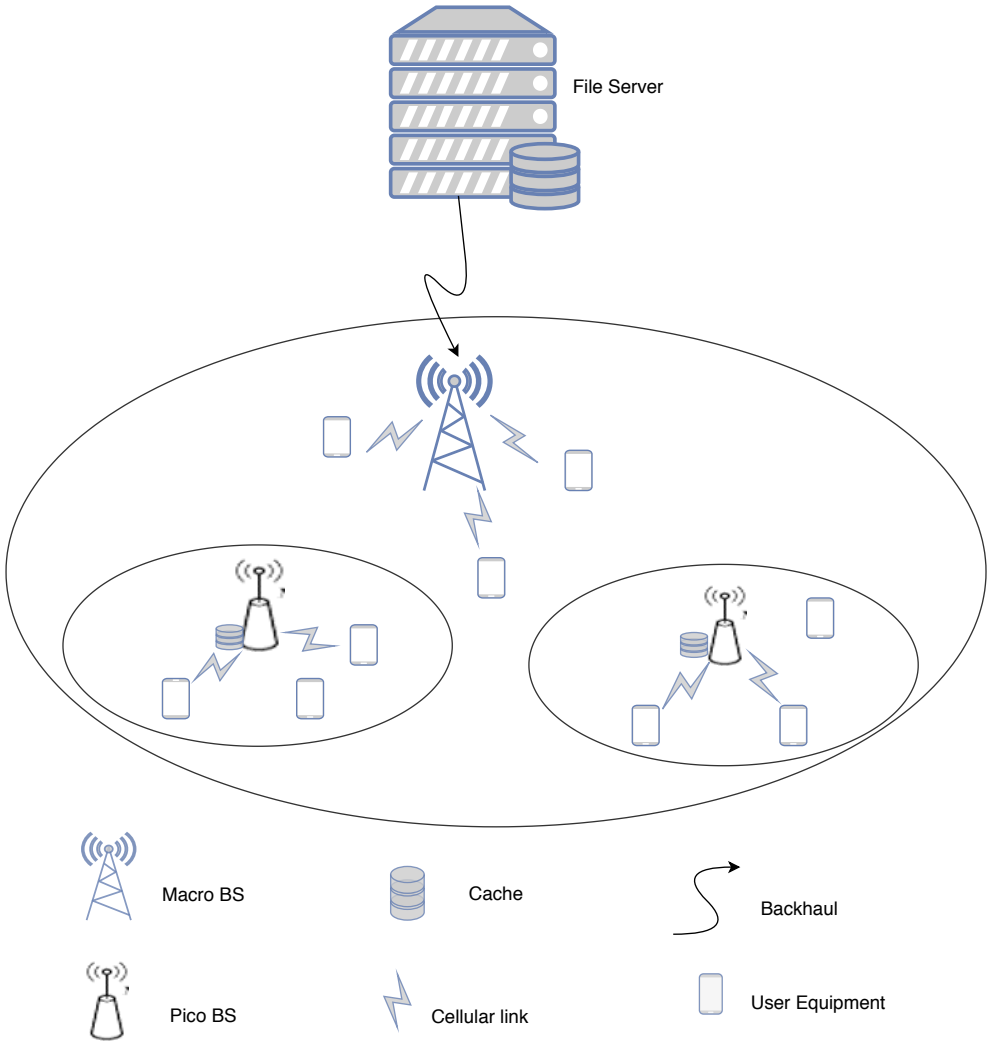

Figure 5.1: Hybrid HetNet architecture with macro BSs (operating in the microwave frequency bands) and pico BSs (operating in the mmWave frequency bands).

5.2.2 Radiation Pattern and Directional Beamforming

The antennas of the pico BSs are assumed to have a radiation pattern that is modeled according to a uniform linear array because of the extremely small wavelength of mmWave signals [45]. Under the linear array model, a pico BS is capable of steering the orientation of its antennas in a direction that aligns with the orientation of the desired receiver to achieve the maximum beamforming gain G_2 where the subscript "2" denotes a pico BS. Further, the uniform linear array pattern of the pico BSs is approximated by a sectored antenna model for tractability of the analysis. Under the sectored antenna model, the array gain function is a discrete random variable that is characterized by the main lobe gain Ψ_k and the side lobe gain ψ_k with $k \in \{2, u\}$ [33, 45]. The subscript k denotes a node type with a value "2" representing a pico BS and a value "u" representing a user. The array gain equations for both a desired link and an interfering link are given by [33, 45]:

$$G_2 = \Psi_2 \Psi_u, \tag{5.1}$$

$$G_{2,i} = \begin{cases} \phi_{i,1} = \Psi_2 \Psi_u, \;\; w.p \;\; \zeta_1 = (\frac{\theta_2}{2\pi})(\frac{\theta_u}{2\pi}), & \text{(5.2a)} \\ \phi_{i,2} = \Psi_2 \psi_u, \;\; w.p \;\; \zeta_2 = (\frac{\theta_2}{2\pi})(\frac{2\pi - \theta_u}{2\pi}), & \text{(5.2b)} \\ \phi_{i,3} = \psi_2 \Psi_u, \;\; w.p \;\; \zeta_3 = (\frac{2\pi - \theta_2}{2\pi})(\frac{\theta_u}{2\pi}), & \text{(5.2c)} \\ \phi_{i,4} = \psi_2 \psi_u, \;\; w.p \;\; \zeta_4 = (\frac{2\pi - \theta_2}{2\pi})(\frac{2\pi - \theta_u}{2\pi}). & \text{(5.2d)} \end{cases}$$

$G_{2,i}$ denotes the random array gain due to the i-th interfering pico BS. Φ_k denotes the main lobe signal beamwidth of node type k, $\phi_{i,w}$ denotes the sample value of $G_{2,i}$ at gain combination w occurring with probability ζ_w and $w \in \{1, 2, 3, 4\}$. On the other hand, the antenna gain of a macro BS is assumed to have an omnidirectional pattern with an array gain $G_1 = 0$ dB [49].

From a practical perspective, the sample values of $G_{2,i}$, i.e., $\{\phi_{i,w}\}$ and the sample space probabilities, i.e., $\{\zeta_w\}$ account for the possible orientations of the antenna of a random interfering pico BS with respect to the orientation of the typical receiver's antenna including i)- $\phi_{i,1}$ with probability ζ_1, corresponds to the alignment between the main lobe of an interferer's antenna and the main lobe of the typical receiver's antenna, ii)- $\phi_{i,2}$ with probability ζ_2, corresponds to the alignment between the main lobe of an interferer's antenna and the side lobe of the typical receiver's antenna, iii)- $\phi_{i,3}$ with probability ζ_3, corresponds to the alignment between the side lobe of an interferer's antenna and the main lobe of the typical receiver's antenna, and (iv)- $\phi_{i,4}$ with probability ζ_4, corresponds to the alignment between the side lobe of an interferer's antenna and the side lobe of the typical receiver's antenna. Additionally, the impact of the main lobe beamwidth θ_k on

$G_{2,i}$ is captured in the equations for $\{\zeta_w\}$.

5.2.3 Path Loss, Fading, and Blockage Modeling

The path loss of the hybrid HetNet follows the slope-intercept model [148], where the expression for the path loss experienced by a link of length y in the macro BS tier is given by:

$$L_1(y) = C_1 y^{-\alpha_1}, \tag{5.3}$$

where C_1 and α_1 denote the frequency-dependent intercept and path loss exponent in the macro BS tier, respectively.

The exponential blockage model is adopted to capture the random blockage pattern experienced by mmWave links in the pico BS tier. Under the exponential blockage model, a mmWave link may experience one out of three states, namely LOS, NLOS, or outage [149]. Thus, the state probability equations for a mmWave link of length y are [150]:

$$\ell_{outage}(y) = \max(0, 1 - e^{-Ay+B}), \tag{5.4a}$$

$$\ell_{LOS}(y) = \big(1 - \ell_{outage}(y)\big)e^{-Dy}, \tag{5.4b}$$

$$\ell_{NLOS}(y) = 1 - \ell_{out}(y) - \ell_{LOS}(y), \tag{5.4c}$$

where $\ell_{\digamma}$ is the probability that a link is in state $\digamma \in \{\text{LOS, NLOS, outage}\}$, and A, B, and D are parameters that depend on the propagation environment [149]. The path loss equation in the pico BS tier depends on the link state and is given by:

$$L_2(y) = C_{2,\varsigma} y^{-\alpha_\varsigma}, \tag{5.5}$$

where $C_{2,\varsigma}$ and α_ς denote the frequency-dependent intercept and path loss exponent, respectively for a link in state $\varsigma \in \{\text{LOS, NLOS}\}$.

Small-scale fading in the macro BS tier is assumed to be Rayleigh distributed where the channel fading power gains of the microwave links follow independent and identically distributed (i.i.d) exponential distributions with unit mean. On the other hand, Nakagami-m distribution with shape parameter m is assumed to model the small-scale fading in the pico BS tier. Under a Nakagami-m fading model, the channel fading power gains of the LOS mmWave links follow i.i.d Gamma distributions with parameter set $\{\eta_L, \frac{1}{\eta_L}\}$, where

$\eta_L = m$ denotes the shape parameter [33].

5.2.4 File Request and File Size Distributions

The file request and file size distributions are described in this section and are assumed to be uncorrelated. The probability that a typical user requests a file f out of N files that are stored in the file server is assumed to follow the Mandelbrot-Zipf (MZipf) distribution and is given by [151]:

$$p_f = \frac{(f+\tau)^{-\delta}}{\sum_{a=1}^{N}(a+\tau)^{-\delta}}, \quad 1 \leq f \leq N, \;\; f \in \{1, 2, \ldots, N\}, \tag{5.6}$$

where δ denotes the Zipf factor of the file popularity distribution and τ denotes the Mandelbrot plateau factor. When δ is high, i.e., $1 < \delta < 2$, the number of requests for unique files is small, whereas when δ is low, i.e., $0 < \delta < 1$, a high fraction of the requests are for unique files. In addition, the popularity distribution becomes flattened as $\tau \to \infty$ [151] and the file requests become uniform.

The Pareto and lognormal probability distributions are adopted to model the file size s_f based on studies of file size distributions in content servers [89, 90, 152]. The pdf for s_f that follows a Pareto distribution is given by [89, 152]:

$$\epsilon_{s_f} = \frac{\beta}{\xi}\left(\frac{\xi}{s_f+\xi}\right)^{\beta+1}, \quad \{\xi, s_f\} > 0, \;\; 0 < \beta \leq 2, \tag{5.7}$$

where ξ denotes the Pareto scale parameter, which represents the smallest file size based on the file encoding format, and β denotes the Pareto shape parameter, which represents the tail index of the file size. A low value of β indicates a high variance in the file size, for example, $\beta = 0.5$ results in a range of $s_f \sim O(10^1) - O(10^5)$ gigabytes (GB). On the other hand, a high value of β results in a low variance in the file size, for example, $\beta = 1.9$ generates a range of $s_f \sim O(10^1) - O(10^3)$ GB.

The pdf of s_f that follows a lognormal distribution is given by [89, 152]:

$$\nu_{s_f} = \frac{1}{s_f\left(2\pi\sigma^2\right)^{1/2}} \exp\left[\frac{-(\log s_f - \mu)^2}{2\sigma^2}\right], \quad \mu, \sigma > 0, \tag{5.8}$$

where μ denotes the lognormal location parameter, which represents the logarithmic mean of the file size distribution, while σ denotes the lognormal scale parameter, which represents the logarithmic standard deviation of the file size distribution.

5.2.5 User Association Scheme and Cooperative Transmission Design

The typical user is assumed to request the file f and can associate with either a macro BS or a LOS pico BS that stores the file f and gives the maximum average received power [42]. The justification for adopting the LOS criterion in the pico BS tier is to ensure that a user receives stronger LOS signals compared to the weaker NLOS signals. Denote the probability that the typical user associates to a macro BS by $\varrho_{1,f}$. Similarly, denote the probability that the typical user associates with an LOS pico BS by $\varrho_{2,f}$. On the other hand, denote the probability of storing the file f in a macro BS by $q_{1,f}$ and denote the probability of storing the file f in a pico BS by $q_{2,f}$. According to the thinning theorem for homogeneous PPPs [27], the density of macro BSs that store the file f is $\Lambda_{1f} = q_{1,f}\lambda_1$ and the density of pico BSs that store the file f is $\Lambda_{2f} = q_{2,f}\lambda_2$. The expressions for $\varrho_{1,f}$ and $\varrho_{2,f}$ are given based on similar derivations in [49] as:

$$\varrho_{1,f} = \frac{\Lambda_{1f} P_1^{\frac{2}{\alpha_1}}}{\Lambda_{1f} P_1^{\frac{2}{\alpha_1}} + \Lambda_{2f} P_2^{\frac{2}{\alpha_{2,LOS}}}}, \quad \varrho_{2,f} = \frac{\Lambda_{2f} P_2^{\frac{2}{\alpha_{2,LOS}}}}{\Lambda_{1f} P_1^{\frac{2}{\alpha_1}} + \Lambda_{2f} P_2^{\frac{2}{\alpha_{2,LOS}}}}. \tag{5.9}$$

Remark. *Observation of* (5.9) *confirms that users tend to associate to a tier with a higher density of BSs and higher transmit power. Moreover, the higher density and the lower transmit power of the pico BS tier compared to the macro BS tier ensures load balancing between the macro BS tier and the pico BS tier.*

Based on the maximum average received power-based association scheme, the pdf for the link length y when the typical requesting user associates to a macro BS or an LOS pico BS is given based on similar derivation in [42], i.e.,

$$g_{1,f}(y) = \frac{2\pi\Lambda_{1f} y \exp\Big(-\pi\Big(\Lambda_{1f} + \Lambda_{2f}\big(\frac{P_2 G_2 C_{2,LOS}}{P_1 G_1 C_1}\big)^{\frac{2}{\alpha_{2,LOS}}}\Big) y^{\frac{2\alpha_1}{\alpha_{2,LOS}}}\Big)}{\varrho_{1,f}}, \tag{5.10a}$$

$$g_{2,f}(y) = \frac{2\pi\Lambda_{2f} y \exp\Big(-\pi\Big(\Lambda_{2f} + \Lambda_{1f}\big(\frac{P_1 G_1 C_1}{P_2 G_2 C_{2,LOS}}\big)^{\frac{2}{\alpha_1}}\Big) y^{\frac{2\alpha_{2,LOS}}{\alpha_1}}\Big)}{\varrho_{2,f}}. \tag{5.10b}$$

Cooperative transmission is employed in the pico BS tier to exploit its high density and the high file storage redundancy in the caches of the pico BSs. The pico BSs that comprise the cooperative transmission set $\mathcal{C}$ are selected according to the maximum average received power based-scheme which is equivalent to the path loss-based scheme because the pico BSs transmit with equal power [39, 49]. Hence, the joint pdf $g_{2,f}(\mathbf{y})$ of the link distance vector $\mathbf{y} = [y_1, \ldots, y_K]$ between the K pico BSs in $\mathcal{C}$ and the typical user is derived based on similar derivation for the joint distribution of the nearest points in a homogeneous PPP

[153], i.e.,

$$g_{2,f}(\mathbf{y}) = \left(2\pi\Lambda_{2f}\right)^{K} e^{-\pi\Lambda_{2f} y_K^2} \prod_{j=1}^{K} y_j. \tag{5.11}$$

In order to further enhance the probability of successful transmission of files, cooperative transmission is combined with coded caching [154] in the pico BS tier where each file is subdivided into fragments, stored in the pico BSs belonging to the set $\mathcal{C}$, and multicasted to the requesting users with the cooperative transmission scheme. As an illustration, consider a file library comprising 3 files whose indices are $i = 1, 2, 3$, with sizes 5 GB, 6 GB, and 8 GB, respectively, and with popularity values 1, 3, and 2, respectively. Also, consider $K = 3$ cooperating pico BSs where each pico BS is designed with a cache capacity of $M_2 = 20$ GB and files 1 and 3 are selected as the optimal set of files based on their aggregate popularity values and the cache capacity of a pico BS. Under the coded caching scheme, the file server divides the files 1 and 3 into $K = 3$ equal fragments and each separate fragment is stored in one of the $K = 3$ cooperating pico BSs. In the delivery phase, each pico BS transmits the stored file fragment in its cache to a requesting user and the user combines the 3 separate fragments to form the entire file. The macro BSs can also employ coded caching with non-cooperative transmission, however, the analysis assumes a non-cooperative transmission scheme without coded caching in the macro BS tier, i.e., files 1 and 3 are stored without fragmentation in the macro BS tier, and the files are delivered to a requesting user from a single macro BS.

5.3 Performance Analysis

5.3.1 Analysis of Cache Hit Probability

Let c_{kf} denote the cache hit probability of a file f conditioned on a user associating to the k-th tier, which is the probability that at least one BS in the k-th tier stores the file f. The expression for c_{kf} is given by: $c_{kf} = 1 - e^{-\pi\Lambda_{kf}R^2}, k \in \{1, 2\}$. Moreover, c_{kf} is a monotonically increasing and a concave function of Λ_{kf} because $\frac{\partial c_{kf}}{\partial \Lambda_{kf}} > 0$ and $\frac{\partial^2 c_{kf}}{\partial \Lambda_{kf}^2} < 0$. The network average cache hit probability for any file f is obtained by averaging over requests for the N files and the two tiers, given by:

$$\bar{c} = \sum_{k\in\{1,2\}} \sum_{f=1}^{N} p_f \varrho_{k,f} c_{kf}. \tag{5.12}$$

5.3.2 Analysis of Coverage Probability

The file f is assumed to be requested by the typical user from either the macro BS tier or the pico BS tier. Recall from Section 5.2.5 that the K cooperating pico BSs that store the file f are selected according to the

maximum average received power-based scheme. Assuming the K pico BSs cooperatively transmit the same file symbol ϑ over a symbol duration, the received signal at the user is

$$z_{2,f} = \sum_{j=1}^{K} \sqrt{P_2 G_2 L_2(y_j)} \varphi_{j,o} \vartheta + \sum_{i \in \Phi_{2,f} \setminus \mathcal{C}} \sqrt{P_2 G_2 L_2(y_i)} \varphi_{2,i} \vartheta_i + \sum_{i \in \Phi_{2,f'}} \sqrt{P_2 G_2 L_2(y_i)} \varphi_{2,i} \vartheta'_i + n_o, \quad (5.13)$$

where $\varphi_{j,o}$ denotes the channel fading coefficient between the k-th pico BS that stores the file f and the typical user, $\varphi_{2,i}$ denotes the channel fading coefficient between the i-th interfering pico BS and the typical user, $\Phi_{2,f} \setminus \mathcal{C}$ denotes the set of interfering pico BSs that store the file f and transmit a file symbol ϑ_i, $\Phi_{2,f'}$ denotes the set of interfering pico BSs that do not store the file f and transmit a different file symbol ϑ'_i, and n_o denotes the thermal noise voltage.

Based on (5.13), the SINR expression in the pico BS tier is given by [6]:

$$\Gamma_{2,f}(o) = \frac{\left| \sum_{j=1}^{K} \sqrt{P_2 G_2 L_2(y_j)} \varphi_{j,o} \right|^2}{N_o + I_{2,f} + I_{2,f'}}, \quad (5.14)$$

where N_o is the thermal noise power at the receiver circuit of the typical user,
$I_{2,f} = \sum_{i \in \Phi_{2,f} \setminus \mathcal{C}} P_2 G_{2,i} L_2(y_i) |\varphi_{2,i}|^2$ denotes the interference power from the pico BSs that store the file f, $I_{2,f'} = \sum_{i \in \Phi_{2,f'}} P_2 G_{2,i} L_2(y_i) |\varphi_{2,i}|^2$ is the interference power from the pico BSs that do not store the file f, and $\Phi_{2,f} \cup \Phi_{2,f'} = \Phi_2$.

Similarly, when the typical user requests for the file f that is stored in the macro BS tier, the macro BS that stores the file and gives the maximum average received power is selected by the file server to service the user. Assuming the macro BS transmits the file symbol ϑ over a given symbol duration, the received signal at the user is

$$z_{1,f} = \sqrt{P_1 G_1 L_1(y)} \varphi_{1,o} \vartheta + \sum_{i \in \Phi_{1,f} \setminus b(o)} \sqrt{P_1 G_1 L_1(y_i)} \varphi_{1,i} s_i + \sum_{i \in \Phi_{1,f'}} \sqrt{P_1 G_1 L_1(y_i)} \varphi_{1,i} \vartheta'_i + n_o, \quad (5.15)$$

where the terms in (5.15) have the same definitions as the corresponding terms in the pico BS tier which are defined under (5.13).

Based on (5.13), the SINR expression in the macro BS tier is given by:

$$\Gamma_{1,f}(o) = \frac{P_1 G_1 {\varphi_{1,o}}^2 L_1(y)}{N_o + I_{1,f} + I_{1,f'}}, \quad (5.16)$$

where the terms in (5.16) have similar definitions to the corresponding terms in the pico BS tier which are defined under (5.14).

Let $\Upsilon_{cov,k}(\gamma, f)$ denote the SINR coverage probability which is defined as the probability that the received SINR at the typical user that requests for a file f from the k-th tier is larger than a threshold γ for successfully decoding the received file. Mathematically,

$$\Upsilon_{cov,k}(\gamma, f) = \mathbb{P}(\Gamma_{k,f}(o) > \gamma), \quad k \in \{1, 2\}, \tag{5.17}$$

where $\Gamma_{k,f}(o)$ is the received SINR at the typical user that requests for the file f from the k-th tier.

Theorem 5.1. *The expression for the SINR coverage probability in the pico BS tier $\Upsilon_{cov,2}(\gamma, f)$ when K pico BSs cooperatively transmit a file f is derived as*

$$\begin{aligned}\Upsilon_{cov,2}(\gamma, f) \approx \int\limits_{0<y_1<\cdots<y_K<R} & \sum_{n=1}^{\rho}(-1)^{n+1}\binom{\rho}{n}\exp\Big(-\frac{\bar{\rho}\gamma N_o \kappa(\mathbf{y})}{C_2 G_2}\Big) \\ & \times \mathcal{L}_{2,I}\Big(\kappa(\mathbf{y}), \gamma, n\Big) \cdot \mathcal{L}_{2,I'}\Big(\kappa(\mathbf{y}), \gamma, n\Big) \cdot g_{2,f}(\mathbf{y})\, \mathrm{d}y_1 \cdots \mathrm{d}y_K, \end{aligned} \tag{5.18}$$

where $\rho = K\eta_L$, $\bar{\rho} = \eta(\rho!)^{-\frac{1}{\rho}}$, $\kappa(\mathbf{y}) = \frac{1}{\sum_{j=1}^{K} y_j^{-\alpha_2}}$, $\mathcal{L}_{2,I}\Big(\kappa(\mathbf{y}), \gamma, n\Big)$ and $\mathcal{L}_{2,I'}\Big(\kappa(\mathbf{y}), \gamma, n\Big)$ are the n-th partial Laplace transform terms resulting from the interfering pico BSs in $\Phi_{2,f} \setminus \mathcal{C}$ and $\Phi_{2,f'}$, respectively, which are given by:

$$\mathcal{L}_{2,I}\Big(\kappa(\mathbf{y}), \gamma, n\Big) = \exp\Big(-2\pi\Lambda_{2,f}\sum_{a=1}^{4}\zeta_a \int_{y_k}^{\infty}\Big[1 - \frac{1}{\big(1 + \frac{n\overline{\phi}_{i,a}\bar{\rho}\gamma\kappa(\mathbf{y})}{\rho w^{\alpha_2}}\big)^{\rho}}\Big] \cdot w \cdot \mathbf{U}(R_L - w)\, \mathrm{d}w\Big), \tag{5.19a}$$

$$\begin{aligned}\mathcal{L}_{2,I'}\Big(\kappa(\mathbf{y}), \gamma, n\Big) = \exp\Big(-2\pi\big(\lambda_2 - \Lambda_{2,f}\big)\sum_{a=1}^{4}\zeta_a \int_{0}^{\infty}\Big[1 - \frac{1}{\big(1 + \frac{n\overline{\phi}_{i,a}\bar{\rho}\gamma\kappa(\mathbf{y})}{\rho w'^{\alpha_2}}\big)^{\rho}}\Big] \\ \times w' \cdot \mathbf{U}(R_L - w')\, \mathrm{d}w'\Big), \end{aligned} \tag{5.19b}$$

where $\overline{\phi}_{i,a} = \frac{\phi_{i,a}}{G_2}$.

Proof. See Appendix C.1.

Theorem 5.1 shows a positive relationship between $\Upsilon_{cov,2}(\gamma, f)$ and the cardinality K of $\mathcal{C}$ which is evident from observing ρ, $\kappa(\mathbf{y})$, and the summand of (5.18). However, the additional gain in $\Upsilon_{cov,2}(\gamma, f)$ decreases as K increases because of the higher path loss experienced by the longer link lengths. □

The expression for the SINR coverage probability in the macro BS tier $\Upsilon_{cov,1}(\gamma, f)$ when the typical user is served by a macro BS that stores a file f is derived based on existing analysis of microwave cellular

networks and the result in [122], i.e.,

$$\Upsilon_{cov,1}(\gamma, f) = \int_{y}^{\infty} \exp\Big(- \frac{\gamma N_o y^{-\alpha_1}}{C_1 G_1}\Big) \cdot \mathcal{L}_{1,I}(y,\gamma) \cdot \mathcal{L}_{1,I'}(y,\gamma) \cdot g_{1,f}(y)\, \mathrm{d}y, \tag{5.20}$$

where $\mathcal{L}_{1,I}(y,\gamma)$ and $\mathcal{L}_{1,I'}(y,\gamma)$ denote the Laplace transform terms resulting from the interfering macro BSs in $\Phi_{1,f} \setminus \{b_o\}$ and $\Phi_{1,f'}$, respectively, and b_o denotes the transmitting macro BS. The expressions for $\mathcal{L}_{1,I}(y,\gamma)$ and $\mathcal{L}_{1,I'}(y,\gamma)$ are given by:

$$\mathcal{L}_{1,I}(\gamma, y) = \exp\Big(- 2\pi\Lambda_{1,f} \int_{y}^{\infty} \frac{w}{1 + \frac{1}{y}(\frac{w}{y})^{\alpha_1}} \mathrm{d}w\Big), \tag{5.21a}$$

$$\mathcal{L}_{1,I'}(\gamma, y) = \exp\Big(- 2\pi\big(\lambda_1 - \Lambda_{1,f}\big) \int_{0}^{\infty} \frac{w}{1 + \frac{1}{y}(\frac{w'}{y})^{\alpha_1}} \mathrm{d}w'\Big). \tag{5.21b}$$

Corollary 1. *Consider a HetNet where the interference resulting from the macro BSs in $\Phi_{1,f} \setminus \{b_o\}$ and $\Phi_{1,f'}$ is negligible, i.e., a noise-limited macro BS tier. The expression for $\Upsilon_{cov,1}(\gamma, f)$ under the noise-limited scenario is given by:*

$$\Upsilon_{cov,1}(\gamma, f) = \int_{0}^{\infty} \exp\Big(- \frac{\gamma N_o y^{\alpha_1}}{C_1 G_1}\Big) \cdot g_{1,f}(y)\, \mathrm{d}y. \tag{5.22}$$

Additionally, consider the typical path loss exponent of $\alpha_1 = 4$ in the macro BS tier and $\alpha_{2,LOS} = 2$ in the pico BS tier. Thus, (5.22) *can be integrated to give:*

$$\Upsilon_{cov,1}(\gamma, f) = \frac{\exp\Big[\frac{(\pi q_{1,f}\lambda_1 + \pi q_{2,f}\lambda_2 \frac{P_2 G_2 C_{2,LOS}}{P_1 G_1 C_1})^2}{4\varrho_{1,f}}\Big] \pi^{\frac{3}{2}} q_{1,f}\lambda_1 \operatorname{erfc} \frac{\pi\Big(q_{1,f}\lambda_1 + q_{2,f}\lambda_2 \frac{P_2 G_2 C_{2,LOS}}{P_1 G_1 C_1}\Big)}{2\sqrt{\frac{\gamma N_o}{C_1 G_1}}}}{2\varrho_{1,f}\sqrt{\frac{\gamma N_o}{C_1 G_1}}}. \tag{5.23}$$

The coverage probability of file f in the noise-limited macro BS tier is enhanced by having a high density of BSs that store the files, i.e., $q_{1,f}\lambda_1$ as seen in (5.23). On the other hand, a high probability of user association mitigates the coverage probability.

Corollary 2. *Consider a HetNet where the thermal noise power is negligible compared to the interference in the macro BS tier, i.e., an interference-limited macro BS tier. The expression for $\Upsilon_{cov,1}(\gamma, f)$ under the interference-limited scenario is given by:*

$$\Upsilon_{cov,1}(\gamma, f) = \int_0^\infty \exp\Big(- 2\pi q_{1,f}\lambda_1 \int_y^\infty \frac{w}{1+\frac{1}{\gamma}(\frac{w}{y})^{\alpha_1}} \mathrm{d}w\Big) \\ \times \exp\Big(- 2\pi\big(\lambda_1(1-q_{1,f})\big) \int_0^\infty \frac{w}{1+\frac{1}{\gamma}(\frac{w'}{y})^{\alpha_1}} \mathrm{d}w'\Big) g_{1,f}\, \mathrm{d}y. \tag{5.24}$$

For a typical path loss exponent of $\alpha_1 = 4$ in the macro BS tier and $\alpha_{2,LOS} = 2$ in the pico BS tier, the integrals of (5.24) *can be computed in closed form and simplified as:*

$$\Upsilon_{cov,1}(\gamma, f) = \frac{4\pi q_{1,f}\lambda_1 \exp\Big[\frac{-\pi\left((1-q_{1,f})\lambda_1 R\right)^2}{2}\Big]}{\varrho_{1,f}\Big[4\pi\big(q_{1,f}\lambda_1 + q_{2,f}\lambda_2\big(\frac{P_2 G_2 C_{2,LOS}}{P_1 G_1 C_1}\big)\big) + 2\pi^2 q_{1,f}\lambda_1\sqrt{\gamma} - 4\pi\lambda_1 \operatorname{arccot}(\sqrt{\gamma})\Big]}. \tag{5.25}$$

In (5.25), the coverage probability of the file f in an interference-limited macro BS tier is observed to increase when the density of the macro BSs that do not store the file f, i.e., $(1-q_{1,f})\lambda_1$ decreases.

5.3.3 Analysis of File Transmission Success Probability

The probability of successfully transmitting a file f in the k-th tier is computed by multiplying the cache hit probability in the k-th tier and the SINR coverage probability in the k-th tier, i.e.,

$$S_{k,f}(\gamma, f) = c_{kf}\Upsilon_{cov,k}(\gamma, f), \quad k = 1, 2. \tag{5.26}$$

$S_{k,f}(\gamma, f)$ depends on the parameters of the file size distribution through c_{kf} and on the SINR threshold through $\Upsilon_{cov,k}(\gamma, f)$. The network average success probability is obtained by averaging over the requests for the N files in the macro BS tier and pico BS tier, given by:

$$\bar{S} = \sum_{k\in\{1,2\}} \sum_{f=1}^{N} p_f \varrho_{k,f} S_{k,f}(\gamma, f). \tag{5.27}$$

The proposed file PSA caching scheme is discussed in Section 5.4. Based on the file PSA caching scheme, the optimizations of the network average cache hit probability and the network average success probability are discussed in Section 5.5.

5.4 File Popularity and Size-Aware Caching Scheme

Consider a centralized file server as shown in Fig. 5.1 that contains a file library $\mathcal{N}$ comprising $|\mathcal{N}| = N$ files. The N files in the file server have non-uniform file sizes, which is typical of file servers that store multiple file formats including small text files and large multimedia files. Additionally, some of the files are requested more frequently and are more popular than the other files, which is typical of content distributed networks where some files can experience high user demand during a particular period of the day, month, or year. In general, the file server can estimate the file sizes and the file popularity values via learning, using either online learning algorithms such as those proposed in [82] or via a Bayes-based learning algorithm [83]. The present study assumes that the file sizes are modeled according to independent Pareto and lognormal distributions as described in Section 5.2.4 and the file popularity values are modeled according to an MZipf distribution also described in Section 5.2.4

The file PSA caching scheme uses the knowledge of the file popularity and file size distributions at the file server to optimize the storage of the files in the HetNet. The need to exploit the non-uniform file sizes and popularity values to optimize the storage of files in caches is because of the potential for the number of files to grow exponentially large in content-centric wireless networks that serve multiple requests. The adoption of the non-uniform file sizes under the file PSA caching scheme is different than the state-of-the-art SWP-based and popularity-based caching schemes which assume equal file size and hence, cannot exploit the actual non-uniformity in the file sizes to optimize the file storage. On the other hand, the file PSA caching scheme exhibits limitations in terms of signaling overhead and additional latency compared to the state-of-the-art caching schemes. Notably, the feasibility of applying the proposed file PSA caching scheme to the hybrid HetNet relies on learning the file sizes which is not required under the SWP-based and popularity-based caching schemes. The application of the file PSA caching scheme in a hybrid HetNet is demonstrated in Section 5.5 which discusses the optimizations of the network average cache hit probability and the network average success probability under the models and assumptions of the proposed file PSA caching scheme.

5.5 Optimization Under The File PSA Caching Scheme

5.5.1 Optimization of the Network Average Cache Hit Probability

The proposed file PSA caching scheme described in Section 5.4 maximizes the network average cache hit probability $\bar{c}$ subject to the aggregate cache capacity as follows:

$$\text{Problem P1}: \quad \max_{\mathcal{F}\subseteq\mathcal{N}} \bar{c} = \sum_{j,\ k\ \in\{1,2\}\atop j\neq k} \sum_{f=1}^{N} \frac{p_f q_{k,f} \lambda_k P_k^{\frac{2}{\alpha_k}} \left(1 - e^{-\pi q_{k,f}\lambda_k R^2}\right)}{q_{k,f}\lambda_k P_k^{\frac{2}{\alpha_k}} + q_{j,f}\lambda_j P_j^{\frac{2}{\alpha_j}}}, \tag{5.28a}$$

$$\text{subject to} \quad \sum_{f\in\mathcal{N}} s_f \leq \sum_{k\in\{1,2\}} M_k, \tag{5.28b}$$

$$0 < q_{k,f}, q_{j,f} < 1, \tag{5.28c}$$

where $\bar{c}$ is given by (5.12) and the decision variables are the file caching probabilities $\{q_{k,f}, q_{j,f}\}$ that maximize $\bar{c}$. Problem P1 is non-convex because deriving the optimal file caching probabilities in the macro BS tier relies on knowledge of the file caching strategy in the pico BS tier, and vice-versa [155]. Hence, the optimal file caching probabilities $\{q^*_{k,f}\}_{f=1,\ldots,N}$ in the k-th tier are derived under the assumption of knowledge of the file caching probabilities $\{q_{j,f}\}_{j\neq k, f=1,\ldots,N}$ in the j-th tier. Further, consider the following inequality derived from the objective function in Problem P1:

$$\begin{aligned}
&\max_{\mathcal{F}\subseteq\mathcal{N}} \sum_{j,\ k\ \in\{1,2\}\atop j\neq k} \sum_{f=1}^{N} \frac{p_f q_{k,f} \lambda_k P_k^{\frac{2}{\alpha_k}} \left(1 - e^{-\pi q_{k,f}\lambda_k R^2}\right)}{q_{k,f}\lambda_k P_k^{\frac{2}{\alpha_k}} + q_{j,f}\lambda_j P_j^{\frac{2}{\alpha_j}}} \\
&\leq \max_{\mathcal{F}\subseteq\mathcal{N}} \sum_{f=1}^{N} \frac{p_f q_{k,f} \lambda_k P_k^{\frac{2}{\alpha_k}} \left(1 - e^{-\pi q_{k,f}\lambda_k R^2}\right)}{q_{k,f}\lambda_k P_k^{\frac{2}{\alpha_k}} + q_{j,f}\lambda_j P_j^{\frac{2}{\alpha_j}}} \\
&+ \max_{\mathcal{F}\subseteq\mathcal{N}} \sum_{f=1}^{N} \frac{p_f q_{j,f} \lambda_j P_j^{\frac{2}{\alpha_j}} \left(1 - e^{-\pi q_{j,f}\lambda_j R^2}\right)}{q_{k,f}\lambda_k P_k^{\frac{2}{\alpha_k}} + q_{j,f}\lambda_j P_j^{\frac{2}{\alpha_j}}}, \quad j = \text{pico BS tier},\ k = \text{macro BS tier},
\end{aligned} \tag{5.29}$$

where (5.29) follows from $\max(f+g) \leq \max(f) + \max(g)$. Thus, given the existence of the optimal file caching probabilities that independently maximize the cache hit probabilities in the macro BS tier, i.e., the k-th tier and the pico BS tier, i.e., the j-th tier, the maximum network average cache hit probability is upper bounded by the sum of the maximum average cache hit probabilities in the macro BS tier and the pico BS tier. Therefore, assuming existence of $\{q^*_{j,f}\}_{f=\{1,\ldots N}\}$, Problem P1 can be resolved by maximizing

the average cache hit probability in the macro BS tier, i.e,

$$\text{Problem P2}: \quad \max_{\mathcal{F}\subseteq\mathcal{N}} \sum_{f=1}^{N} \frac{p_f q_{k,f} \lambda_k P_k^{\frac{2}{\alpha_k}} \left(1 - e^{-\pi q_{k,f} \lambda_k R^2}\right)}{q_{k,f} \lambda_k P_k^{\frac{2}{\alpha_k}} + q_{j,f} \lambda_j P_j^{\frac{2}{\alpha_j}}}, \tag{5.30a}$$

$$\text{subject to} \quad \sum_{f\in\mathcal{N}} s_f \leq M_k, \tag{5.30b}$$

$$0 < q_{k,f} < 1, \ \ \forall\, k = 1. \tag{5.30c}$$

The optimal file caching probabilities under Problem P2 correspond to solutions of a 0-1 KP which is described in Lemma 1.

Lemma 1. *Problem P2 can be decomposed to a 0-1 KP as follows:*

$$\text{Problem P2}: \quad \max_{\mathcal{F}\subseteq\mathcal{N}} \sum_{f=1}^{N} q_{k,f}, \tag{5.31a}$$

$$\text{subject to} \quad \sum_{f\in\mathcal{N}} s_f \leq M_k, \tag{5.31b}$$

$$0 < q_{k,f} < 1, \ \ \forall\, k = 1. \tag{5.31c}$$

Proof. See Appendix C.2. □

The decision variables of Problem P2 are the file caching probabilities $\{q^*_{k,f}\}_{f=1,\ldots,N}$ that maximize the aggregate popularity $\sum_{f=1}^{N} q_{k,f}$. Besides, the Problem P2 is a 0-1 KP which is NP-hard [46, 156], thus, dynamic programming with backtracking [157] and a branch and bound algorithm [158] are employed to derive local optimum values of the file caching probabilities.

5.5.2 Dynamic Programming with Backtracking

The dynamic programming with backtracking technique for solving the 0-1 KP is discussed in this section. In order to decide whether or not to store the file f, the maximum aggregate popularity value for the $(f-1)$ files cached in a BS whose cache capacity is m GB, $0 \leq m \leq M_k$, is used to derive the maximum aggregate popularity value for the f files cached by solving the Bellman recurrence equations [159]:

$$Opt[f,m] = \begin{cases} \max\left(Opt[f-1,m], \ \ q_{k,f} + Opt[f-1, m-s_f]\right), & \mathrm{s}_f \leq m, \quad (5.32a) \\ Opt[f-1,m], & \text{otherwise}, \quad (5.32b) \end{cases}$$

where $Opt[f, m]$ is an array variable that stores the maximum aggregate popularity of any subset of files $\{1, 2, \ldots, f\}$ of total size at most m GB, for $1 \leq f \leq N$, $0 \leq m \leq M_k$. The recursive equation (5.32a) is valid provided $s_f \leq m$, ensuring that the file f can be stored. The maximum aggregate popularity of the already cached files $\{1, 2, ..., f-1\}$ and used cache space $(m - s_f)$ is therefore $Opt[f-1, m-s_f]$. If the file cannot be stored, (5.32b) gives the maximum aggregate popularity. Starting from the initial condition: $Opt[0, m] = 0$, $0 \leq m \leq M_k$, (5.32) is solved in a bottom-up manner to obtain $Opt[N, M_k]$ which is the maximum aggregate popularity of the files that can fit into the BS type k cache with capacity M_k. Lastly, the files that comprise $\mathcal{F}^* \subseteq \mathcal{N}$, which is the set of files that results in $Opt[N, M_k]$, are determined by backtracking. Algorithm 5.1 highlights the steps in the dynamic programming technique.

Line 1 of Algorithm 5.1 initializes the array variable $Opt[N, M_k]$ to zero and initializes the solution set $\mathcal{F}^*$ as empty. In lines 4-6, the size s_f of the file f is compared to the available cache capacity m. If the file f can be stored, i.e., $s_f \leq m$, the aggregate popularity values when the file is stored and when the file is not stored are compared and the greater of the two values is selected as the maximum aggregate popularity for the f cached files. Lines 6-8 consider the case when the file f cannot be stored because its size exceeds the available cache capacity. Line 11 returns the last element of the array $Opt[N, M_k]$ as the maximum aggregate popularity of all the files that can fit into the BS of cache capacity M_k GB, an approximate solution to Problem P2 in (5.31). However, up to this point, Algorithm 5.1 does not yet provide the set of files that gives the optimal solution. This set is determined by the backtracking process, discussed next.

Line 12 begins the backtracking process with the necessary initializations. Lines 13-15 consider the case when the maximum aggregate popularity does not change for each preceding file, meaning that such a file does not constitute a member of the set $\mathcal{F}^*$. Lines 17 and 18 consider the case when the maximum aggregate popularity changes, meaning that such a file is an element of $\mathcal{F}^*$. Lines 19, 20, and 21 update the available cache capacity after adding a file to the set $\mathcal{F}^*$, the file index in the backtracking procedure, and the maximum aggregate popularity, respectively. The backtracking procedure is continued until all the member files of the set $\mathcal{F}^*$ are determined. Line 23 returns the complete set $\mathcal{F}^*$.

5.5.3 Branch and Bound Algorithm

The branch and bound algorithm for the 0-1 KP is discussed in this section. First, the files are sorted in descending order according to $\bar{q}_{k,f} = \frac{q_{k,f}}{s_f}$ into a new set $\bar{\mathcal{Q}} \triangleq \{\bar{q}_{k,1}, \ldots, \bar{q}_{k,N}\}$. Moreover, the subscripts $1, \ldots, N$ in the sorted set $\bar{\mathcal{Q}}$ do not necessarily correspond to the subscripts $1, \ldots, N$ in the set $\mathcal{F}$. For example, file 1 in the set $\mathcal{F}$ may not be the file with the largest ratio $\frac{q_{k,f}}{s_f}$. The storage of files under the branch and bound algorithm follows the steps in Algorithm 5.2, which are described as follows: Line 1 of

Algorithm 5.1: Dynamic Programming with Backtracking

Input: $\mathcal{S}$, $\mathcal{R}^*$, M_k.
Output: $\mathcal{F}^*$.

```
1: Initialize: Opt[0, m] = 0,  ∀ m = 0 to M_k,   F* = {}.
2: for f = 0 to N do
3:    for m = 0 to M_k do
4:       if s_f ≤ m then
5:          Opt[f, m] = max(Opt[f − 1, m],  q_{k,f} + Opt[f − 1, m − s_f]).
6:       else
7:          Opt[f, m] = Opt[f − 1, m].
8:       end if
9:    end for
10: end for
11: Return Opt[N, M_k].
12: T = Opt[N, M_k],  f = N,  Y = M_k.
13: while T > 0 do
14:    while Opt[f, Y] == T do
15:       f = f − 1.
16:    end while
17:    f = f + 1.
18:    Insert file f in F*.
19:    Y = Y − s_f.
20:    f = f − 1.
21:    T = Opt[f, Y].
22: end while
23: Return F*.
```

Algorithm 5.2 initializes the elements of the branch and bound algorithm, including i) an upper bound B on the maximum aggregate popularity. B is computed by adding the popularity values of the first f files in the set $\bar{\mathcal{Q}}$ that can be stored in the BS cache to a positive variable $\varkappa$ multiplied by the popularity value of the $(f+1)$-th file which, if added as a whole, will cause BS cache overflow. The variable $\varkappa$ is computed by dividing the available BS cache capacity after storing the first f files by the size of the $(f+1)$-th file. The other elements to be initialized are: ii) the maximum aggregate popularity of the cached files, denoted by A, is initialized to zero, iii) a variable U, denoting the BS available cache capacity after each file is considered, is initialized to M_k, iv) the file index f is initialized to zero when no file has been considered, and v) the solution set $\mathcal{F}^*$, is initialized as empty. Line 3 begins with the file whose index matches the first index in $\bar{\mathcal{Q}}$. In lines 5, 6, and 7, the values of the maximum aggregate popularity, BS available cache capacity, and the upper bound on the maximum aggregate popularity are updated, respectively, when file f is considered for caching. Line 8 compares the current upper bound B to the current maximum aggregate popularity A when file f is considered, adds file f to the set $\mathcal{F}^*$ in line 9 if the upper bound is greater than or equal to A, and repeats the branching procedure. Otherwise if the current upper bound is less than the current maximum aggregate popularity A, the branch terminates at the current file index and returns the set $\mathcal{F}^*$ in line 16 which provides the maximum aggregate popularity A.

Algorithm 5.2 achieves $O(N)$ complexity by making use of a tight upper bound on the maximum aggregate

popularity. The upper bound is computed based on the assumption that the cache capacity of a BS can be filled with a combination of whole numbers or segments of files and the algorithm uses the upper bound to determine the cached files as those whose maximum aggregate popularity lies in the neighborhood of the upper bound.

Table 5.1 provides the formal problem description and complexity of the proposed file PSA caching scheme along with those of two state-of-the-art schemes used as benchmarks for comparison. Notably, the dynamic programming and the branch and bound algorithm have pseudo-polynomial time complexity and give approximate solutions to the Problem P2.

Table 5.1: Comparison of the Proposed File PSA and State-of-the-art Caching Schemes.

Caching Scheme	**Formal Problem Description**	**Complexity**
Proposed File PSA, Dynamic Programming	$\max\limits_{\mathcal{F}\subseteq\mathcal{N}} \sum_{f=1}^{N} q_{k,f}, \quad \text{s.t.} \sum\limits_{f\in\mathcal{N}} s_f \leq M_k$	$O(M_k N)$
Proposed File PSA, Branch and Bound	$\max\limits_{\mathcal{F}\subseteq\mathcal{N}} \sum_{f=1}^{N} q_{k,f}, \quad \text{s.t.} \sum\limits_{f\in\mathcal{N}} s_f \leq M_k$	$O(M_k N)$
SWP-based [46]	$\max\limits_{\mathcal{F}\subseteq\mathcal{N}} \sum\limits_{f=1}^{N} s_f^{\theta} p_f, \quad \theta = -1, \quad \text{s.t} \sum\limits_{f\in\mathcal{N}} s_f \leq M_k$	$O(N)$
Popularity-based [49]	$q_{kf} = \mathbf{U}(M_k - \sum\limits_{j=1}^{f} s_f)$	$O(N)$

Algorithm 5.2: Branch and Bound Algorithm

Input: $\mathcal{S}$, $\bar{\mathcal{R}}$, M_k.
Output: $\mathcal{F}^*$.

1: Initialize: $B = \sum\limits_{j=1}^{f} \bar{q}_{k,j} + \varkappa \bar{q}_{k,f+1}$, such that $\varkappa = \frac{M_k - \sum_{j=1}^{f} \bar{s}_j}{\bar{s}_{f+1}}$; $A = 0$; $U = M_k$; $f = 0$; $\mathcal{F}^* = \{\}$.
2: **while** $f <= N$ **do**
3: $f = f + 1$
4: **while** $U > 0$ **do**
5: $A = A + q_{k,f}$
6: $U = U - s_f$
7: $B = B - q_{k,f}$
8: **if** $B \geq A$ **then**
9: Insert file f in $\mathcal{F}^*$.
10: Go to Line 3.
11: **else**
12: Go to Line 16.
13: **end if**
14: **end while**
15: **end while**
16: Return $\mathcal{F}^*$.

5.5.4 Optimization of the Network Average Success Probability

Starting from (5.26) and the expression for the network average success probability $\bar{S}$, the optimization problem that aims to maximize $\bar{S}$ is formulated as Problem P3, i.e.,

$$\text{Problem P3}: \quad \max_{\mathcal{F}\subseteq\mathcal{N}} \bar{S} = \sum_{k\in\{1,2\}}\sum_{f=1}^{N} \frac{p_f q_{k,f}\lambda_k P_k^{\frac{2}{\alpha_k}}\left(1-e^{-\pi q_{k,f}\lambda_k R^2}\right)}{q_{k,f}\lambda_k P_k^{\frac{2}{\alpha_k}} + q_{j,f}\lambda_j P_j^{\frac{2}{\alpha_j}}} \times \Upsilon_{cov,k}(\gamma, f), \tag{5.33a}$$

$$\text{subject to} \quad \sum_{f\in\mathcal{N}} s_f \leq \sum_{k\in\{1,2\}} M_k, \tag{5.33b}$$

$$0 < q_{k,f}, q_{j,f} < 1, \tag{5.33c}$$

where $\bar{S}$ is given by (5.27). In general, Problem P3 is not a concave function of the file caching probabilities because of the integral terms in $\Upsilon_{cov,k}(\gamma, f),\ k \in \{1,2\}$. The expressions for the optimal file caching distribution under special network conditions are provided next.

Case 1: Noise-limited HetNet ($\alpha_1 = 4$, $\alpha_{2,LOS} = 2$)

Based on Corollary 1 and the expression for $\Upsilon_{cov,1}(\gamma, f)$ given in (5.23), the optimal set of file caching probabilities $\{q_{1,f}^*\}$ in the macro BS tier conditioned on knowledge of the optimal set of file caching probabilities $\{q_{2,f}^*\}$ in the pico BS tier can be obtained as a numerical solution to the equation:

$$\begin{aligned}
&\exp\left[-\frac{\pi\left(q_{1,f}\lambda_1 + q_{2,f}^*\lambda_2\left(\frac{P_2G_2C_{2,LOS}}{P_1G_1C_1}\right)\right)^2}{4\frac{\gamma N_o}{C_1G_1}}\right] \times \left[(1-e^{-\pi q_{1,f}\lambda_1 R^2})\pi^{\frac{5}{2}} q_{1,f}^2\lambda_1^2(\pi q_{1,f}\lambda_1 + \pi\varrho_{2,f}q_{2,f}^*)\lambda_2\right] \\
&\times \operatorname{erfc}\left[\frac{\pi(q_{1,f}\lambda_1 + (\frac{P_2G_2C_{2,LOS}}{P_1G_1C_1})q_{2,f}^*\lambda_2)}{2\sqrt{\frac{\gamma N_o}{C_1G_1}}}\right] \times \left(\frac{1}{4\sqrt{\frac{\gamma N_o}{C_1G_1}}}\right)^3 \\
&+ \exp\left[-\pi q_{1,f}\lambda_1 R^2 + \frac{(\pi(q_{1,f}\lambda_1 + q_{2,f}^*\lambda_2(\frac{P_2G_2C_{2,LOS}}{P_1G_1C_1})))^2}{4\frac{\gamma N_o}{C_1G_1}}\right] \\
&\times \pi^{\frac{5}{2}} q_{1,f}^2 R^2\lambda_1^2 \operatorname{erfc}\left[\frac{\pi(q_{1,f}\lambda_1 + q_{2,f}^*\lambda_2(\frac{P_2G_2C_{2,LOS}}{P_1G_1C_1}))}{2\sqrt{\frac{\gamma N_o}{C_1G_1}})}\right] \cdot \frac{1}{2\sqrt{\frac{\gamma N_o}{C_1G_1}}(\frac{P_2G_2C_{2,LOS}}{P_1G_1C_1})} = 0,
\end{aligned} \tag{5.34}$$

where erfc[.] is the complementary error function and $\{q_{2,f}^*\}$ are determined by applying Algorithm 5.1 or Algorithm 5.2 for file caching in the pico BS tier.

Proof. See Appendix C.3. □

Remark. (5.34) *reveals that* $\{q_{1,f}^*\}$ *depends on* $\{q_{2,f}^*\}$*, the thermal noise power* N_o*, and the system design parameters* $(\lambda_1, \lambda_2, P_1, P_2, G_1, G_2, \gamma, R)$*. Moreover, for a given* $\{q_{2,f}^*\}$*, a numerical algorithm that executes* (5.34) *will require an input memory of* $O(N)$ *to store* $(\{q_{2,f}^*\}, N_o, \lambda_1, \lambda_2, P_1, P_2, G_1, G_2, \gamma, R)$ *and this presents a memory overhead compared to the SWP-based and popularity-based caching schemes which do not require the system design parameters to compute the optimal file caching probabilities.*

Case 2: Interference-limited HetNet ($\alpha_1 = 4$, $\alpha_{2,LOS} = 2$)

Based on Corollary 2 and the expression for $\Upsilon_{cov,1}(\gamma, f)$ given in (5.24), the optimal set of caching probabilities $\{q_{1,f}^*\}$ in the macro BS tier conditioned on knowledge of the optimal set of caching probabilities $\{q_{2,f}^*\}$ in the pico BS tier can be obtained as a numerical solution to the equation:

$$\frac{4\exp\Big[-\pi q_{1,f}\lambda_1\big(\pi-2\arctan(\frac{1}{\sqrt{\gamma}})\big)\Big]\Big(1-\exp(-\pi q_{1,f}\lambda_1 R^2)\Big)\pi q_{1,f}\lambda_1}{\varrho_{2,f}\Big(2\pi q_{1,f}\lambda_1+2\pi q_{2,f}^*\lambda_2\Big(\frac{P_2G_2C_{2,LOS}}{P_1G_1C_1}\Big)\Big)}$$
$$+\frac{2\exp\Big[-\pi q_{1,f}\lambda_1 R^2-\pi q_{1,f}\lambda_1\big(\pi-2\arctan(\frac{1}{\sqrt{\gamma}})\big)\Big]\pi^2 q_{1,f}^2\lambda_1^2R^2}{\varrho_{2,f}\Big(2\pi q_{1,f}\lambda_1+2\pi q_{2,f}^*\lambda_2\Big(\frac{P_2G_2C_{2,LOS}}{P_1G_1C_1}\Big)\Big)}$$
$$-\frac{4\exp\Big[-\pi q_{1,f}\lambda_1\big(\pi-2\arctan(\frac{1}{\sqrt{\gamma}})\big)\Big]\Big(1-\exp(-\pi q_{1,f}\lambda_1 R^2)\Big)\big(\pi-2\arctan(\frac{1}{\sqrt{\gamma}})\big)\pi^2 q_{1,f}^2\lambda_1^2}{\varrho_{2,f}\Big(2\pi q_{1,f}\lambda_1+2\pi q_{2,f}^*\lambda_2\Big(\frac{P_2G_2C_{2,LOS}}{P_1G_1C_1}\Big)\Big)^2}$$
$$-\frac{2\exp\Big[-\pi q_{1,f}\lambda_1\big(\pi-2\arctan(\frac{1}{\sqrt{\gamma}})\big)\Big]\Big(1-\exp(-\pi q_{1,f}\lambda_1 R^2)\Big)\big(\pi-2\arctan(\frac{1}{\sqrt{\gamma}})\big)\pi^2 q_{1,f}^2\lambda_1^2}{\varrho_{2,f}\Big(2\pi q_{1,f}\lambda_1+2\pi q_{2,f}^*\lambda_2\Big(\frac{P_2G_2C_{2,LOS}}{P_1G_1C_1}\Big)\Big)}=0. \quad (5.35)$$

where erfc[.] is the complementary error function and $\{q_{2,f}^*\}$ are determined by applying Algorithm 5.1 or Algorithm 5.2 to the pico BS tier.

Proof. Similar proof for the noise-limited case in Appendix C.3 is applicable to the interference-limited case by starting from (5.24). □

Remark. *Similar to the noise-limited case,* (5.35) *reveals that* $\{q_{1,f}^*\}$ *depends on* $\{q_{2,f}^*\}$*, the thermal noise power* N_o*, and the system design parameters* $(\lambda_1, \lambda_2, P_1, P_2, G_1, G_2, R)$*. Thus, a numerical algorithm that executes* (5.35) *will also incur an* $O(N)$ *memory overhead compared to the SWP-based and popularity-based caching schemes.*

5.6 Evaluation Methodology and Discussion of Numerical Results

The impact of the parameters of the file size distribution and the SINR threshold on the performance metrics under the file PSA caching scheme and the state-of-the-art caching schemes is investigated in this section.

5.6.1 Evaluation Methodology

The values of the optimized file caching probabilities $\{q_{1,f}^*\}$ and $\{q_{2,f}^*\}$ are generated using Monte-Carlo simulations in MATLAB and numerical algorithms in Mathematica as follows:

- Declare the network parameter values, i.e., $\{\lambda_1, \lambda_2, P_1, P_2, \alpha_1, \alpha_2, N, \dots\}$.
- Specify the number of simulation runs $n_{sim} = O(10^4)$.
- Generate PPP realizations of the macro BS tier and pico BS tier of the hybrid HetNet based on the network topology in Section 5.2.1.
- Compute the file caching probabilities $\{q_{2,f}^*\}$ in the pico BS tier based on the dynamic programming with backtracking and branch and bound algorithm by following the steps for Algorithm 5.1 and Algorithm 5.2, respectively.
- Compute the file caching probabilities $\{q_{1,f}^*\}$ in the macro BS tier using numerical algorithms in Mathematica and based on the expressions for $\{q_{1,f}^*\}$ in (5.34) and (5.35) for noise-limited and interference-limited HetNets, respectively.
- Compute the value of the performance metric, e.g., the network average cache hit probability of (5.12) as a function of $\{q_{1,f}^*\}$ and $\{q_{2,f}^*\}$. Save the result for the realization.
- Compute the average of the performance metric over the n_{sim} realizations of the hybrid HetNet and return the result.

The assumed values of the network parameters are listed in Table 5.2 and are borrowed from existing literature [33, 46, 49, 156, 160, 161, 162, 163]. Notably, a macro BS antenna is assumed to have an omnidirectional radiation pattern with a gain $G_1 = 0$ dB, while a desired pico BS performs directional beamforming and can align its signal transmission in the direction of the typical receiver to achieve the maximum array gain $G_2 = \phi_{i,1} = 10$ dB.

Table 5.2: Values of System Parameters.

Notations	Parameter Definition	Assumed Values
P_1, P_2	Macro BS transmit power, pico BS transmit power	40 dBm, 30 dBm [49]
λ_1, λ_2, λ_u	Macro BS density, pico BS density, user density	$1/(250^2\pi)\text{m}^2, 20/(250^2\pi)\text{m}^2, 30/(250^2\pi)\text{m}^2$ [49]
f_1, f_2	microwave carrier frequency, mmWave carrier frequency	2 GHz, 70 GHz [162]
α_1, $\alpha_{2,LOS}$, c, C_1, $C_{2,LOS}$, η_L	Path loss exponent in macro BS tier, LOS path loss exponent in pico BS tier, speed of light, path loss intercept in macro BS tier, LOS path loss intercept in pico BS tier, LOS Nakagami shape parameter	4, 2, $3 \times 10^8 \text{m s}^{-1}$, $(\frac{c}{4\pi f_1})^{\alpha_1}$, $C_2 = (\frac{c}{4\pi f_2})^{\alpha_{2,LOS}}$, 3 [33, 49]
G_1, G_2, R	Array gain of a macro BS, maximum array gain of a pico BS, network radius	0 dB, 10 dB, 1000 m [49, 162]
M_1, M_2, N, δ, τ	Cache capacity of a macro BS, cache capacity of a pico BS, number of files in file library, Zipf factor, Mandelbrot plateau factor	$[2, 4]$ GB, $[1, 2]$ GB, 100, 0.8, 0 [46, 160, 163]
ξ, β, σ, μ	Scale parameter of Pareto file size distribution, shape parameter of Pareto file size distribution, scale parameter of lognormal file size distribution, location parameter of lognormal file size distribution	$[0.01, 0.1]$ GB, $[0.1, 2]$, $[\log 0.01, \log 0.1]$ GB, $[\log 0.01, \log 0.1]$ GB [160]

5.6.2 Impact of the File Size Distribution on the Network Average Cache Hit Probability

In Fig. 5.2a and Fig. 5.2b, the network average cache hit probabilities are plotted versus the aggregate cache capacity ($= M_1 + M_2$) under the Pareto and lognormal file size distributions, respectively. The network average cache hit probability increases with the aggregate cache capacity in all the schemes because more files can be stored when the available cache capacity is increased. The proposed file PSA caching scheme branch and bound algorithm achieves the best performance and the proposed file PSA caching scheme dynamic programming algorithm achieves the next best performance under the Pareto file size distribution. On the other hand, the proposed file PSA caching schemes branch and bound algorithm, dynamic programming

algorithm, and SWP-based scheme exhibit identical performance under the lognormal file size distribution. The explanation of the behavior of the proposed and state-of-the-art schemes depends on the choice of the heuristic and the parameters of the file size distribution. The proposed file PSA caching scheme branch and bound algorithm sorts the files in descending order according to the popularity-per-size metric and computes the upper bound on the aggregate popularity to serve as a target in determining the set of cached files. In contrast, the proposed scheme dynamic programming algorithm does not rely on an upper bound in determining the set of cached files. The SWP-based scheme sorts the files in a greedy manner according to a size-weighted popularity metric without considering whether or not the aggregate popularity of the cached files approaches a feasible upper bound. Moreover, when the variance in the file sizes is large, as captured by $\beta = 2.0$ under the Pareto file size distribution, a few files dominate the cache memory and the branch and bound algorithm exploits the large file size variance in its branching procedure to achieve up to 10% gain compared to the dynamic programming algorithm. On the other hand, the smaller variance in the lognormal file size distribution with $\sigma = \log 0.1$ GB results in a more uniform distribution of file size compared to the Pareto file size distribution. Thus, the proposed file PSA and SWP-based caching schemes achieve similar performance in the network average cache hit probability, as observed in Fig. 5.2b. The popularity-based scheme achieves the least network average cache hit probability performance because it does not consider the impact of the different file sizes, but only caches the files in descending order of popularity.

In Fig. 5.3a and Fig. 5.3b, the network average cache hit probability is plotted versus the Pareto shape parameter and Pareto scale parameter, respectively with a Mandelbrot plateau factor $\tau = 0$. The network average cache hit probability increases monotonically with the Pareto shape parameter because the variance of the Pareto file size distribution decreases with an increase in the Pareto shape parameter, as explained in Section 5.2.4. Thus, more files whose sizes fall within a small range are cached when the Pareto shape parameter is high (e.g. $\beta = 2.0$) compared to a low Pareto shape parameter (e.g. $\beta = 0.5$). In contrast, the network average cache hit probability decreases monotonically with the Pareto scale parameter because a high Pareto scale parameter results in a distribution of files that is skewed towards a few files that fill up the cache memory. Similar behavior is observed under the lognormal file size distribution in Fig. 5.4 where the network average cache hit probability decreases with the lognormal location parameter and the proposed file PSA and SWP-based caching schemes exhibit similar performance because of the low variance of the lognormal file size distribution.

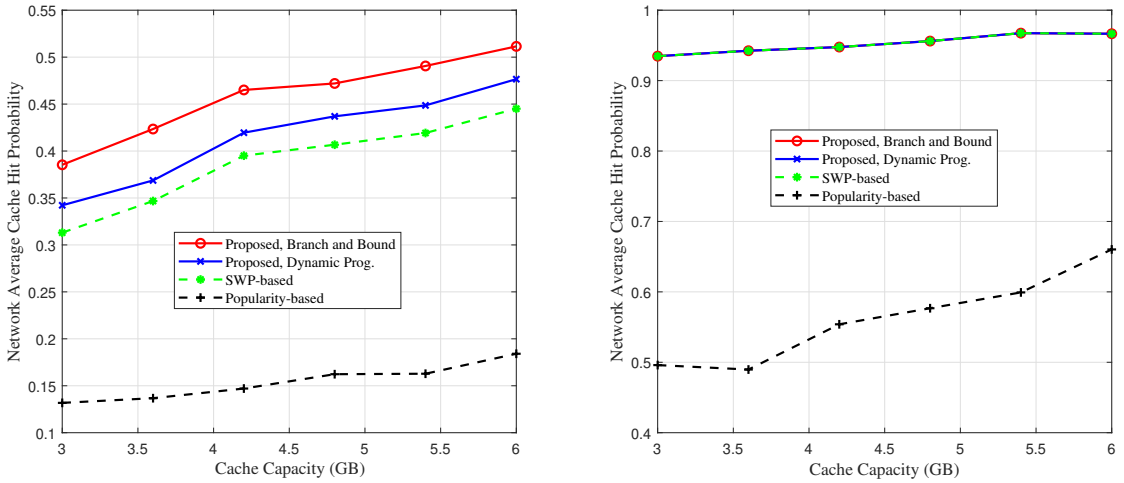

(a) Pareto file size distribution with $\beta = 0.5$, $\xi = 0.01$ GB.

(b) Lognormal file size distribution with $\mu = \log 0.01$ GB, $\sigma = \log 0.1$ GB.

Figure 5.2: Network average cache hit probability vs. aggregate cache capacity.

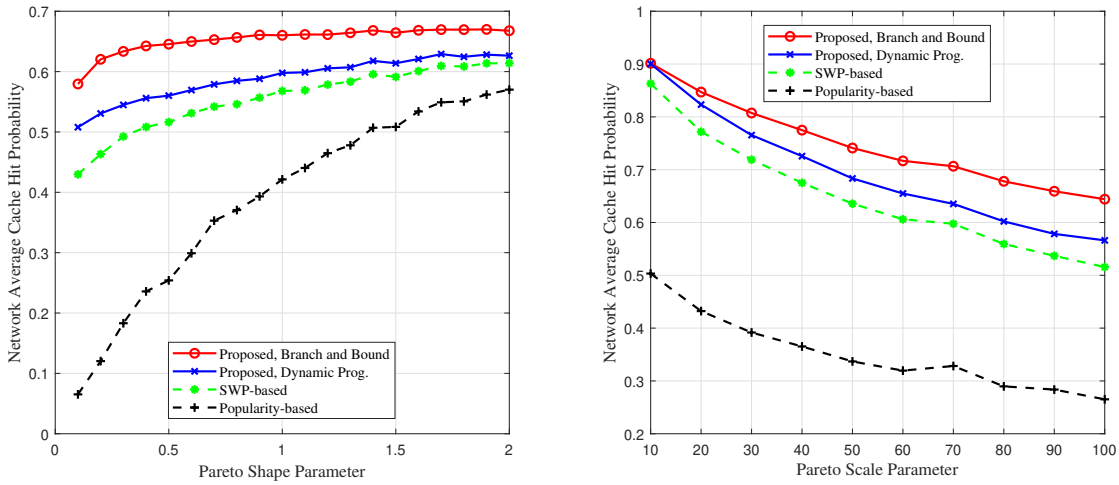

(a) Network average cache hit probability vs. Pareto shape parameter with $\xi = 0.1$ GB, $M_1 = 2$ GB, $M_2 = 1$ GB.

(b) Network average cache hit probability vs. Pareto scale parameter with $\beta = 2.0$, $M_1 = 2$ GB, $M_2 = 1$ GB.

Figure 5.3: Network average cache hit probability vs. Pareto shape parameter and Pareto scale parameter.

5.6.3 Impact of the File Size Distribution on the Network Average Success Probability

Figs. 5.5 and 5.6 depict the variation of the network average success probability with the SINR threshold under the Pareto and lognormal file size distributions, respectively. The results for the noise-limited and interference-limited HetNets are generated based on numerical evaluations of the file caching probabilities of

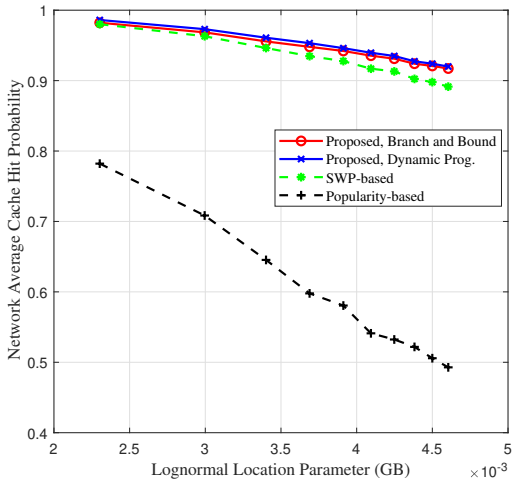

Figure 5.4: Network average cache hit probability vs. lognormal location parameter with $\sigma = \log 0.01$ GB, $M_1 = 2$ GB, and $M_2 = 1$ GB.

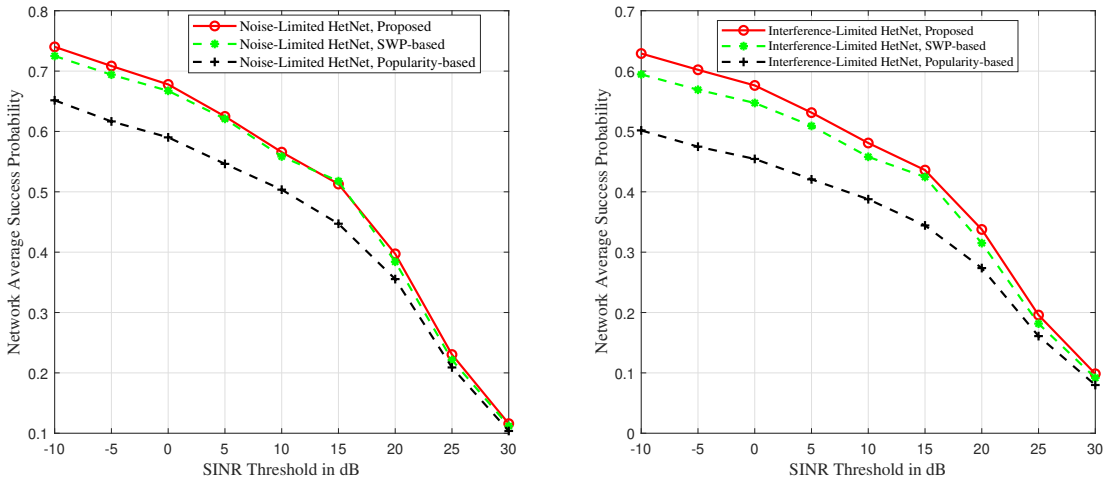

(a) Noise-limited HetNet.

(b) Interference-limited HetNet.

Figure 5.5: Network average success probability vs. SINR threshold under Pareto file size distribution with $\xi = 0.1$ GB, $\beta = 2.0$, $M_1 = 2$ GB, and $M_2 = 1$ GB.

(5.34) and (5.35) in Mathematica. The proposed file PSA and SWP-based caching schemes achieve similar performance under the noise-limited HetNet, whereas the proposed file PSA scheme achieves up to 7% gain in the network average success probability over that of the SWP-based scheme. Thus, it can be concluded that optimizing the caching of files is useful when other transmitting BSs interfere with file transmissions from a desired BS.

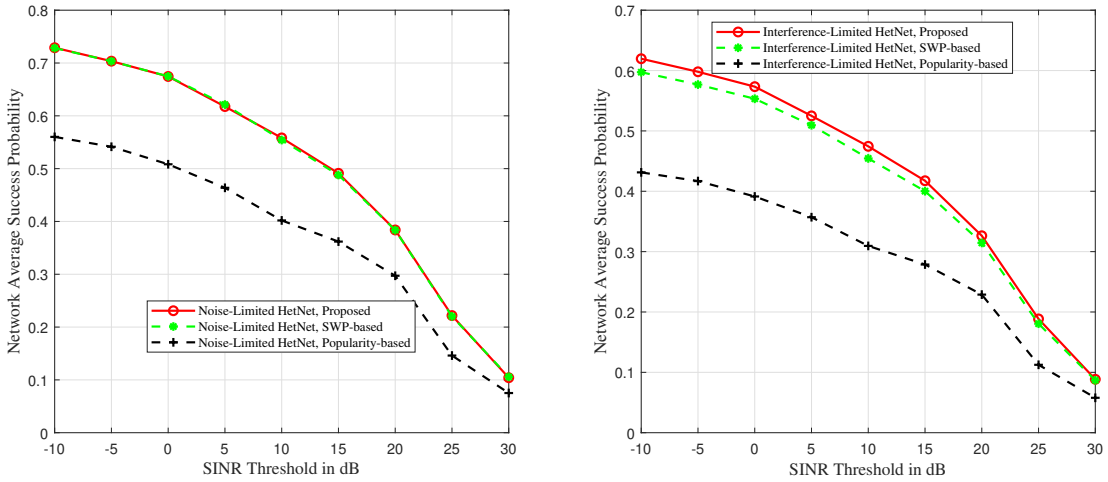

(a) Noise-limited HetNet.

(b) Interference-limited HetNet.

Figure 5.6: Network average success probability vs. SINR threshold under lognormal file size distribution with $\mu = \log 0.01$ GB, $\sigma = \log 0.1$ GB, $M_1 = 2$ GB, and $M_2 = 1$ GB.

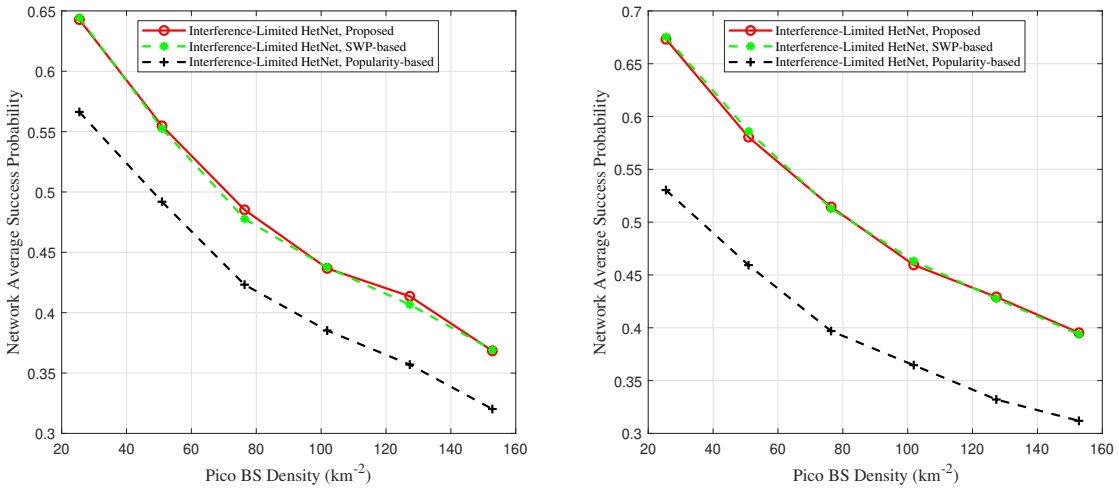

(a) Pareto file size distribution.

(b) Lognormal file size distribution.

Figure 5.7: Network average success probability vs. pico BS density with $\xi = 0.1$ GB, $\beta = 2.0$, $\mu = \log 0.01$ GB, $\sigma = \log 0.1$ GB, $M_1 = 2$ GB, and $M_2 = 1$ GB.

5.6.4 Impact of Dense Pico BS Deployment and Cooperative Transmissions With Coded Caching

The impact of a dense pico BS deployment is illustrated in Fig. 5.7 where the network average success probability decreases by approximately 20% as the pico BS density doubles. On the other hand, Fig. 5.8 shows that cooperative transmission with coded caching can be employed in the dense pico BS tier to enhance the gain in the network average success probability. Up to 40% gain is achieved with 2 cooperating pico

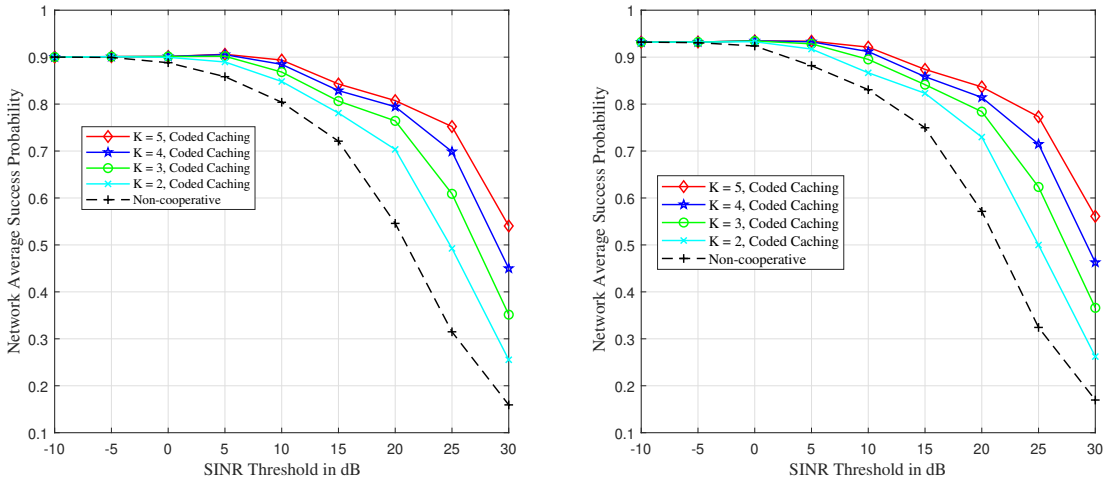

(a) Pareto file size distribution.

(b) Lognormal file size distribution.

Figure 5.8: Comparison between cooperative transmission with coded caching and non-cooperative transmission without coded caching.

BSs with coded caching compared to non-cooperative transmission without coded caching, however, the gain diminishes as the cooperative set increases with only 14% gain achieved between 4 and 5 cooperating pico BSs.

5.7 Summary

This chapter presented and analyzed the performance of a file popularity and size-aware caching scheme in a hybrid HetNet comprising a macro BS tier that operates in the microwave frequency bands and a pico BS tier that operates in the mmWave frequency bands. The set of files that are stored in a macro BS and a pico BS to maximize the HetNet average cache hit probability were obtained as a solution to a 0-1 KP. In addition, the 0-1 KP was solved using dynamic programming and branch and bound algorithms, whereas numerical evaluation techniques were used to efficiently determine the optimal set of files that maximize the HetNet average success probability. Cooperative transmission with coded caching was integrated into the pico BS tier to enhance the performance of the file popularity and size-aware caching scheme in a dense pico BS tier. Lastly, the performance gains achieved by the file popularity and size-aware caching scheme with cooperative transmission and coded caching when compared to the state-of-the-art SWP and popularity-based caching schemes were illustrated using graphical results.

The findings in this chapter show that the file popularity and size-aware caching scheme provides significant gains in a hybrid microwave/mmWave HetNet with sufficient cache capacity and a sparse deployment of BSs. Moreover, the successful transmission of files in the hybrid HetNet can be enhanced by adopting

cooperative transmission and coded caching techniques that leverage file storage redundancy.

Chapter 6

Popularity and Size-Aware Caching in Millimeter Wave Networks with Device-to-Device Communication and Large-Scale Antenna Arrays [1]

6.1 Introduction

This chapter studies the performance of the PSA caching scheme in a cache-enabled mmWave cellular network with D2D communication and large-scale antenna arrays. The mmWave network comprises a centralized file server, BSs, and users whose locations form independent and finite homogeneous Poisson point processes. The main contribution of this chapter is the downlink performance analysis of the mmWave network under the PSA caching scheme and the linear precoding technique of maximum-ratio-transmission. Mathematical expressions are derived for the cache hit probability, average achievable rate, and successful content delivery probability, and the analytical results are validated with the aid of Monte-Carlo simulations. The impact of the large-scale antenna arrays on the system performance is also investigated.

[1] The content of this chapter is being finalized for submission to the IEEE Transactions on Communications.

6.2 System Model

6.2.1 Network Architecture

Consider a mmWave network of radius R and area $\mathcal{B} \triangleq \mathbf{b}(\mathbf{o}, R)$ where $\mathbf{b}(\mathbf{o}, R)$ denotes a ball of radius R that is centered at the origin $\mathbf{o}$. The locations of the BSs and users within $\mathcal{B}$ are assumed to be distributed according to independent finite homogeneous Poisson point processes (FHPPPs) Φ_b and Φ_u, respectively. Similar to the definition of a binomial Poisson point process given in [30], the FHPPP that represents the locations of the BSs, i.e., $\Phi_b \triangleq \Upsilon_b \cap \mathcal{B}$ where Υ_b is an HPPP with density λ_b [164]. Similarly, the FHPPP that represents the locations of the users, i.e., $\Phi_u \triangleq \Upsilon_u \cap \mathcal{B}$ where Υ_u is an HPPP with density λ_u.

Fig. 6.1 illustrates the architecture of the mmWave network. A typical user that requests for a file can be serviced by a BS that stores the requested file or by another user that stores the requested file via D2D transmission. Moreover, a fraction μ of the users are assumed to participate in servicing user requests for cached files within a D2D communication range r_d and the remaining fraction $(1-\mu)$ are cellular users whose requests for cached files are serviced by the BSs. Based on the thinning theorem [122], the locations of the D2D transmitters and cellular receivers follow FHPPPs $\Phi_{d,u}$ and $\Phi_{b,u}$, respectively, with densities $\mu\lambda_u$ and $(1-\mu)\lambda_u$, respectively. The BS (cellular) and D2D transmissions are assumed to occur in mmWave bands and the allocation of frequencies to the BSs and D2D transmitters are assumed to be orthogonal to suppress inter-tier interference.

Table 6.1: Summary of Major Notations

Notation	**Description**
$\Phi_b, \Phi_u, \lambda_b, \lambda_u, \mu, N_b, N_u$	FHPPP for BSs, FHPPP for users, density of BSs, density of users, D2D partition factor, number of BS antenna elements, number of user antenna elements.
$G_b(\varsigma_x, \varsigma_y), G_u(\varsigma), L(r), \alpha, C$	Array gain of a BS, array gain of a user, path loss function for a mmWave link of length r, path loss exponent, path loss intercept.
$\beta, \xi, \varpi, \varkappa, \delta, \tau, \omega_f$	Pareto file size shape parameter, Pareto file size scale parameter, Gamma file size shape parameter, Gamma file size scale parameter, Zipf factor, Mandelbrot plateau factor, size of a file f.
R, R_L, r_d, N, M_b, M_u	Radius of the mmWave network, LOS radius, D2D communication range, number of available files in the file server, cache memory capacity of a BS in GB, cache memory capacity of a user in GB.
d_x, d_y, d	Horizontal spacing between BS antenna elements, vertical spacing between BS antenna elements, uniform spacing between user antenna elements.
$q_{b,f}, q_{u,f}, \zeta_{b,f}, \zeta_{d,f}, c_{b,f}, c_{d,f}$	Caching probability of file f in a BS, caching probability of file f in a user, BS association probability, D2D association probability, cellular cache hit probability, D2D cache hit probability.
$\psi, \bar{\mathcal{A}}_{i,f}, \bar{\mathcal{A}}, \mathcal{R}_i(\psi, f), \mathcal{H}(\psi)$	Rate threshold for successful decoding of file f, average achievable rate per unit bandwidth of file f, average achievable rate per unit bandwidth, rate coverage probability of file f, successful content delivery probability.

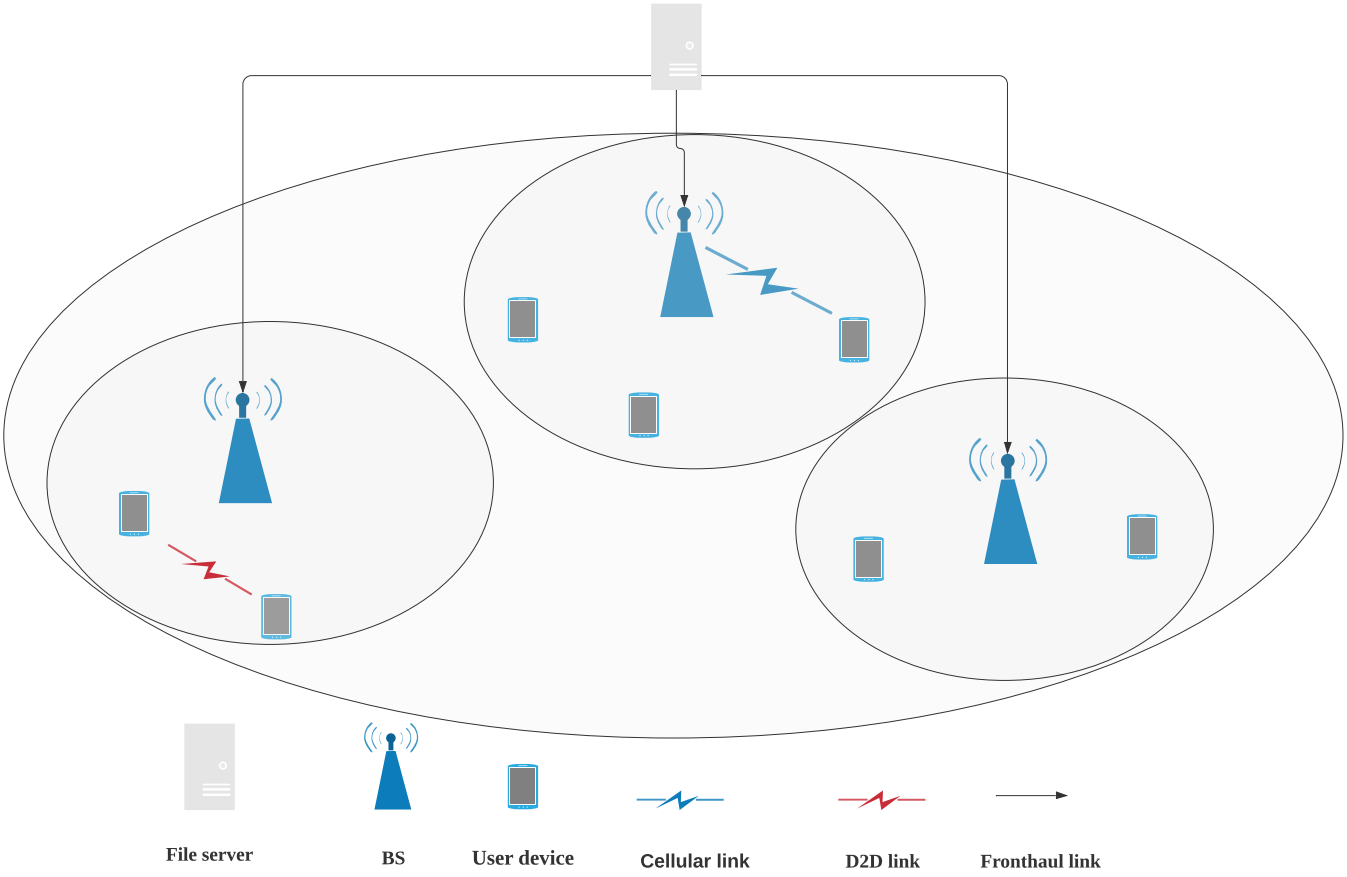

Figure 6.1: Millimeter wave network with cellular communications and device-to-device communications.

6.2.2 Antenna Design and Radiation Pattern

The transceivers of a BS and a user are assumed to be equipped with antenna arrays comprising N_b and N_u antenna elements, respectively. The N_b antenna elements of the BS are mounted in a rectangular array of dimension Q horizontal elements and M vertical elements where $N_b = Q \times M$. Additionally, d_x m is the uniform element spacing in the horizontal direction and d_y m is the uniform element spacing in the vertical direction [165, 166]. On the other hand, the N_u antenna elements of the user are mounted in a linear array pattern with a uniform element spacing of d m. [49, 167].

Based on the described antenna structure, the array gain function of a BS is given by [168]:

$$G_b(\varsigma_x, \varsigma_y) = \left[\frac{\sin^2(Q\pi\varsigma_x)}{Q^2\sin^2(\pi\varsigma_x)}\right]\left(\frac{\sin^2(M\pi\varsigma_y)}{M^2\sin^2(\pi\varsigma_y)}\right], \tag{6.1}$$

where ς_x and ς_y are uniformly distributed random variables in the range $[-\frac{d_x}{\nu}, \frac{d_x}{\nu}]$ and $[-\frac{d_y}{\nu}, \frac{d_y}{\nu}]$, respectively, and ν is the wavelength of the mmWave signals. Similarly, the array gain function of a user is given by [49, 169]:

$$G_u(\varsigma) = \frac{\sin^2(\pi N_u\varsigma)}{N_u^2\sin^2(\pi\varsigma)}, \tag{6.2}$$

where ς is a uniformly distributed random variable in the range $[-\frac{d}{\nu}, \frac{d}{\nu}]$.

6.2.3 Path Loss, Fading, and Blockage Modeling

The path loss experienced by the mmWave signals is modeled using the slope-intercept model [170]. Considering the small wavelength of mmWave and the severe blockage that is experienced by NLOS signals, a link of length r has a path loss function which is given by:

$$L(r) = Cr^{-\alpha}\mathbf{U}(R_L - r), \tag{6.3}$$

where α and C denote the path loss exponent and intercept, respectively, $\mathbf{U}(.)$ is the unit step function, and R_L is the LOS radius. The small-scale fading experienced by the mmWave signals is modeled using independent Nakagami-m distributions with shape parameter η [33]. Additionally, the channel fading power gains of the mmWave links follow independent and identically distributed (i.i.d) Gamma distributions with parameter set $\{\eta, \frac{1}{\eta}\}$.

6.2.4 File Request and File Size Distributions

A typical user can request for a random file out of the N available files in the centralized file server. The probability p_f that the typical user requests for a file $f = \{1, 2, \ldots, N\}$ is assumed to follow a Mandelbrot-Zipf (MZipf) distribution [151] given by:

$$p_f = \frac{(f+\tau)^{-\delta}}{\sum_{a=1}^{N}(a+\tau)^{-\delta}}, \quad 1 \leq f \leq N, \;\; f \in \{1, 2, \ldots, N\}, \tag{6.4}$$

where τ denotes the Mandelbrot plateau factor and δ denotes the Zipf factor of the file popularity distribution. The Mandelbrot plateau factor τ controls the tail of the distribution which becomes flattened as $\tau \to \infty$ and the Zipf factor δ controls the skewness of the distribution. When δ is high, i.e., $1 < \delta < 2$, the fraction of requests for unique files is small and when δ is low, i.e., $0 < \delta < 1$, a high fraction of the requests is for unique files.

The size of the file f ω_f is modeled according to Pareto and lognormal probability distributions based on experimental studies of file sizes in content distribution networks [89, 152, 90]. Under the Pareto distribution, the pdf of ω_f is given by [89, 152]:

$$\epsilon_{\omega_f}(u_f) = \frac{\beta}{\xi}\left(\frac{\xi}{u_f+\xi}\right)^{\beta+1}, \quad \{\xi, u_f\} > 0, \;\; 0 < \beta \leq 2, \tag{6.5}$$

where β denotes the Pareto shape parameter which represents the tail index of the file size and ξ denotes the Pareto scale parameter which represents the smallest file size that is determined by the file encoding format. A low value of β indicates a high variance in the file size, for example, $\beta = 0.5$ generates a range of $\omega_f \sim O(10^1) - O(10^5)$ GB. On the other hand, a high value of β results in a low variance in the file size, for example, $\beta = 1.9$ generates a range of $\omega_f \sim O(10^1) - O(10^3)$ GB.

Similarly, the pdf of a Gamma file size distribution is expressed as [171]:

$$\upsilon_{\omega_f}(u_f) = \frac{u_f^{\varpi-1} e^{-\frac{u_f}{\varkappa}}}{\Gamma(\varpi)\varkappa^{\varpi}}, \;\; \varpi, \varkappa > 0, \;\; u_f \geq \varkappa, \tag{6.6}$$

where $\Gamma(.)$ denotes the complete Gamma function and ϖ, $\varkappa$ are the shape parameter and the scale parameter of the Gamma file size distribution, respectively.

6.2.5 Association Scheme and Signal Transmission Model

Assume that the typical user is located at the origin and requests for a file f. Denote a node type i where $i = b$ indicates a BS that stores the file f and $i = u$ indicates a user that stores the file f. The typical user is

assumed to associate to the node type i that is in LOS and guarantees the maximum average received power to enhance the received signal strength [49]. Let the BS and D2D association probabilities conditioned on requesting for the file f be denoted as $\zeta_{b,f}$ and $\zeta_{d,f}$, respectively. Denote the probability of caching the file f in a BS as $q_{b,f}$ and the probability of caching the file f in a user as $q_{u,f}$. Following similar derivations in [49] and the thinning theorem for HPPPs [27], the expressions for $\zeta_{b,f}$ and $\zeta_{d,f}$ are given by:

$$\zeta_{b,f} \approx \frac{q_{b,f}\lambda_b P_b^{\frac{2}{\alpha}}}{q_{b,f}\lambda_b P_b^{\frac{2}{\alpha}} + \mu q_{u,f}\lambda_u P_u^{\frac{2}{\alpha}}}, \tag{6.7a}$$

$$\zeta_{d,f} \approx \frac{\mu q_{u,f}\lambda_u P_u^{2/\alpha}}{q_{b,f}\lambda_b P_b^{\frac{2}{\alpha}} + \mu q_{u,f}\lambda_u P_u^{\frac{2}{\alpha}}}. \tag{6.7b}$$

Based on the maximum received power-based association scheme [42], the pdfs of the link lengths in BS and D2D association modes are given by:

$$g_{b,f}(r) = \frac{2\pi q_{b,f}\lambda_b r \exp\Big(-\pi\Big(q_{b,f}\lambda_b + \mu q_{u,f}\lambda_u \big(\frac{P_u N_u}{P_b N_b}\big)^{\frac{2}{\alpha}}\Big) r^2\Big)}{1-\exp\big(-\pi\lambda_b q_{b,f} R_L^2\big)} \times \mathbf{U}(R_L - r), \tag{6.8a}$$

$$g_{u,f}(r) = 2\pi\mu q_{u,f}\lambda_u r \times \mathbf{U}(r_d - r) \frac{\exp\Big(-\pi\Big(\mu q_{u,f}\lambda_u + q_{b,f}\lambda_b \big(\frac{P_b N_b}{P_u N_u}\big)^{\frac{2}{\alpha}}\Big) r^2\Big)}{\big(1-\exp(-\pi\mu\lambda_u q_{u,f} r_d^2)\big)}. \tag{6.8b}$$

Remark. *Observation of* (6.7a) *and* (6.7b) *validates the intuition that the fraction of users that request for the file f and associate in BS mode decreases when the density of D2D transmitters that store the file f, i.e., $\mu q_{u,f}\lambda_u$ increases, and vice-versa. On the other hand, the fraction of users that request for the file f and associate in D2D mode increases when the density of the D2D transmitters that store the file f increases, and vice-versa.*

After the association phase for the typical user, the next phase is the file symbol transmission phase. The desired node type i is assumed to employ the linear precoding technique of maximum-ratio-transmission (MRT) to service the typical user's request. The feasibility of the MRT technique relies on the knowledge of the channel state information at the desired BS or D2D transmitter, permitting the construction of the channel precoder matrix that maximizes the transmitted symbol power. Based on the MRT technique with equal power allocation to the transmitting antenna elements [172], the received baseband symbol vector for the file f due to the node type i is given by:

$$\mathbf{y}_{i,f} = \sqrt{P_i}\mathbf{H}_0\mathbf{W}_0\rho_0\mathbf{x}_{i,f} + \sum_{j\in\Phi'_{i,f}} \sqrt{P_i}\mathbf{H}_j\mathbf{W}_j\rho_j\mathbf{x}_{j,f} + \mathbf{n_0}, \tag{6.9}$$

where $\mathbf{x}_{i,f}$ is the $N_u \times 1$ symbol vector due to the desired node type i, $\mathbf{y}_{i,f}$ is the $N_u \times 1$ symbol vector received at the typical user, $\mathbf{H}_0$ is the $N_u \times N_b$ channel matrix between the desired node type i and the typical user and comprises i.i.d Nakagami random elements $\{h_o\}$ with shape parameter m, $\mathbf{W}_o = \mathbf{H_o}^\dagger$ represents the $N_b \times N_u$ channel precoder matrix between the desired node type i and the typical user with " † " denoting the conjugate transpose operator, $\rho_0 = G_b(\varsigma_x, \varsigma_y)G_u(\varsigma)L(r_0)$, where r_0 is the link length between the desired node type i and the typical user, and P_i is the transmit power of the desired node type i. On the other hand, $\mathbf{x}_{j,f}$ is the $N_u \times 1$ symbol vector due to an interfering node $j \in \Phi'_{i,f}$, where $\Phi'_{i,f}$ is the FHPPP of nodes of type i which store the file f and interfere with the signal transmission. $\mathbf{H}_j$ is the $N_u \times N_b$ channel matrix between an interfering node type i and the typical user and comprises independent Nakagami random elements $\{h_j\}$, $\mathbf{W}_j = \mathbf{H}_j^\dagger$ represents the $N_b \times N_u$ channel precoder matrix between the interfering node j of type i and the typical user, $\rho_j = G_j(\varsigma_x, \varsigma_y)G_u(\varsigma)L(r_j)$, where r_j is the link length between the interfering node j of type i and the typical user, and $\mathbf{n_0}$ is the $N_u \times 1$ vector of thermal noise elements which comprises i.i.d Gaussian random elements with variance equal to σ_0^2.

6.3 File Popularity and Size-aware Caching scheme

The discussion of the PSA caching scheme and its associated algorithms is provided in Chapter 5 of this thesis and is omitted in this chapter. The dynamic programming with backtracking algorithm is adopted for the file popularity and size-aware caching scheme in the subsequent analysis.

6.4 Performance Analysis

6.4.1 Analysis of Cache Hit Probability

The cache hit probability of a random file f out of the N available files is the probability that at least one node type i within the network area $\mathcal{B}$ stores the file f. The expressions for the cache hit probability under BS and D2D communication modes are respectively given by:

$$c_{b,f} = 1 - e^{-\pi\lambda_b q_{b,f} R_l^2}, \tag{6.10a}$$

$$c_{d,f} = 1 - e^{-\pi\mu\lambda_u q_{u,f} R_d^2}, \tag{6.10b}$$

where $c_{b,f}$ denotes the cellular (BS) cache hit probability for the file f and $c_{d,f}$ denotes the D2D cache hit probability for the file f. Additionally, the average cache hit probability in BS or D2D association modes is obtained by averaging over the requests for the N available files, i.e., $c_i = \sum_{f=1}^{N} p_f c_{i,f}$.

6.4.2 Analysis of Average Achievable Rate Per Unit Bandwidth

The expression for the signal-to-interference-plus-noise ratio (SINR) $\kappa_{i,f}$ at the typical user due to a node type i that transmits the file f using MRT is given based on the signal transmission model of (6.9):

$$\kappa_{i,f} = \frac{P_i ||\mathbf{H}_0 \mathbf{W}_0||^2 \rho_0}{\sum_{j \in \Phi'_{i,f}} P_i ||\mathbf{H}_j \mathbf{W}_j||^2 \rho_j + \sigma_0^2}. \tag{6.11}$$

The average achievable rate per unit bandwidth $\bar{\mathcal{A}}_{i,f}$ for receiving the file f from the node type i is given by:

$$\bar{\mathcal{A}}_{i,f} = \mathbb{E}\big[\log_2(1+\kappa_{i,f})\big], \tag{6.12}$$

where the expectation operator $\mathbb{E}(.)$ is applied over the distributions of the desired and interfering channel fading signals.

Theorem 6.1. *The expression for the average achievable rate per unit bandwidth $\bar{\mathcal{A}}_{b,f}$ when the typical user receives the file f from the desired BS is:*

$$\bar{\mathcal{A}}_{b,f} = \frac{1}{\ln(2)} \int_0^{R_L} \int_0^{\infty} \left(1 - \Big(\frac{1 + z P_b r^{-\alpha}}{\eta}\Big)^{-N_u \eta}\right) \Omega(z,r) e^{-z\sigma_0^2} g_{b,f}(r)\, dz\, dr, \tag{6.13}$$

where $\Omega(z,r)$ is the Laplace transform term due to the interfering BSs which is given by:

$$\Omega(z,r) = e^{-\frac{\pi q_{b,f} \lambda_b \nu^3}{4 d_x d_y d} \int_{\frac{-d_x}{\nu}}^{\frac{d_x}{\nu}} \int_{\frac{-d_y}{\nu}}^{\frac{d_y}{\nu}} \int_{\frac{-d}{\nu}}^{\frac{d}{\nu}} \left[\int_r^{R_L} \left(1 - \Big(\frac{1 + z r^{\alpha} G_b(\varsigma_x,\varsigma_y) G_u(\varsigma)}{\eta x^{\alpha}}\Big)^{-N_u \eta}\right) x\, dx \right] d\varsigma d\varsigma_x d\varsigma_y}. \tag{6.14}$$

Similar expression in (6.13) *applies to the average achievable rate per unit bandwidth for D2D communication mode with the subscripts for the node type $i = b$ being replaced by $i = u$.*

Proof. See Appendix D.1. □

Remark. *$\Omega(z,r)$ decreases with increasing N_u, i.e., the number of user antenna elements as seen in* (6.14),

which results in an increase in $\bar{\mathcal{A}}_{b,f}$ *as observed in* (6.13). *Also, increasing the BS density* λ_b *decreases* $\Omega(z,r)$ *which negatively impacts* $\bar{\mathcal{A}}_{b,f}$.

The average achievable rate per unit bandwidth for both BS and D2D communication modes is obtained by considering the conditional probabilities for BS and D2D association and averaging over the requests for files. Thus,

$$\bar{\mathcal{A}} = \sum_{i\in\{b,d\}} \sum_{f=1}^{N} p_f c_{i,f} \zeta_{i,f} \bar{\mathcal{A}}_{i,f}. \tag{6.15}$$

6.4.3 Analysis of Rate Coverage Probability and Successful Content Delivery Probability

The rate coverage probability due to transmissions of the file f from a node type i is defined as the probability that the rate per unit bandwidth $\mathcal{A}_{i,f} = \log_2(1+\kappa_{i,f})$ is greater than a predefined rate threshold ψ for decoding the file f [12], i.e,

$$\mathcal{R}_i(\psi, f) = \mathbb{P}(\mathcal{A}_{i,f} > \psi) \tag{6.16}$$

Theorem 6.2. *The expression for the rate coverage probability for BS communication mode* $\mathcal{R}_b(\psi,f)$ *when the typical user receives the file* f *from the desired BS is:*

$$\mathcal{R}_b(\psi,f) \approx \sum_{n=1}^{\eta N_u} (-1)^{n+1} \int_0^{R_L} \binom{\eta N_u}{n} \mathcal{L}_b\big(n\varrho r^\alpha, \gamma\big) \exp\Big(-n\varrho\gamma\sigma_0^2 r^\alpha\Big) g_{b,f}(r)\, dr, \tag{6.17}$$

where $\varrho = \eta(\eta!)^{-\frac{1}{\eta}}$, $\gamma = 2^\psi - 1$, *and* $\mathcal{L}_b\big(n\varrho r^\alpha,\gamma\big)$ *is the Laplace transform term due to the interference from other BSs that transmit the file* f *which is expressed as:*

$$\mathcal{L}_b\big(s,\gamma\big) = e^{-\frac{\pi q_{b,f}\lambda_b \nu^3}{4 d_x d_y d} \int_{\frac{-d_x}{\nu}}^{\frac{d_x}{\nu}} \int_{\frac{-d_y}{\nu}}^{\frac{d_y}{\nu}} \int_{\frac{-d}{\nu}}^{\frac{d}{\nu}} \left[\int_r^{R_L} \left(1-\left(\frac{1+ns\gamma G_b(\varsigma_x,\varsigma_y) G_u(\varsigma)}{\eta x^\alpha}\right)^{-N_u\eta}\right) x\, dx\right] d\varsigma d\varsigma_x d\varsigma_y}, \tag{6.18}$$

where $s = n\varrho r^\alpha$. *Similar expression in* (6.17) *applies to the rate coverage probability for D2D communication mode with the subscripts for the node type* $i = b$ *being replaced by* $i = u$.

Proof. See Appendix D.2. □

Remark. *Similar to* $\bar{\mathcal{A}}_{b,f}$, $\mathcal{R}_b(\psi,f)$ *is enhanced by increasing* N_u *at a fixed value of the rate coverage threshold,* ψ *because the Laplace transform term,* $\mathcal{L}_b\big(s,\gamma\big)$ *decreases with increasing* N_u.

The successful content delivery probability for both BS and D2D communication modes is obtained by considering the conditional probabilities for BS and D2D association and averaging over the file requests. Thus,

$$\mathcal{H}(\psi) = \sum_{i\in\{b,d\}} \sum_{f=1}^{N} p_f c_{i,f} \zeta_{i,f} \mathcal{R}_i(\psi, f) \tag{6.19}$$

6.5 Evaluation Methodology and Discussion of Numerical Results

6.5.1 Evaluation Methodology

In this section, the numerical results are computed in Mathematica and are presented to evaluate the performance of the PSA caching scheme and the impact of the device communication mode, device density, and the large-scale antenna design on the network performance metrics. Moreover, the numerical results are validated with the aid of Monte-Carlo simulations and benchmarked with the state-of-the-art probabilistic, SWP-based, and MPC caching schemes. The assumed parameter values which are valid for realistic outdoor mmWave networks are referenced from the existing works. The assumed values are listed in Table 6.2 and are used unless otherwise stated.

Table 6.2: Values of System Parameters.

Notations	Definition	Assumed Values
P_b, P_u	BS transmit power, user transmit power	30 dBm, 20 dBm [49]
λ_b, λ_u	BS density, user density	$1/(0.25^2\pi)$ km^2, $20/(0.25^2\pi)$km^2, [49]
f_c, c, ν	carrier frequency, speed of light, carrier wavelength	28 GHz, 3×10^8ms^{-1}, $\frac{c}{f_c}$ m [162]
α, η	Path loss exponent, Nakagami shape parameter	2.75, 3 [33, 49]
d_x, d_y, d, N_b, N_u	Rectangular array horizontal antenna spacing, rectangular array vertical spacing, uniform linear array spacing, number of BS antenna elements, number of user antenna elements	$\frac{\nu}{3}$, $\frac{\nu}{6}$, 256 ($=8\times32$), 16 [49, 169]
R, R_L, r_d	Network radius, LOS range, D2D communication range	1000 m, 200 m, 75 m [47]
M_b, M_u, N, δ, τ	Cache capacity of a BS, cache capacity of a user, number of files in file library, Zipf factor, Mandelbrot plateau factor	4 GB, 1 GB, 100, 0.4, 0 [46, 160, 163]
ξ, β, $\varkappa$, ϖ	Scale parameter of Pareto file size distribution, shape parameter of Pareto file size distribution, scale parameter of Gamma file size distribution, shape parameter of Gamma file size distribution	0.01 GB, 2.0, 0.01 GB, 2.0 [160]

6.5.2 Impact of the Device Density and Communication Mode on the Cache Hit Probability

In Figs. 6.2a and 6.2b, the cellular cache hit probability is plotted versus the BS density under the Pareto and Gamma file size distributions, respectively. As observed in the figures, the close match between the analytical results and the simulations validates the accuracy of the numerical analysis. Further, going by (6.10a), the cellular cache hit probability increases with the BS density for all the caching schemes because more BSs are available to store the files and the PSA caching scheme achieves the highest cellular cache hit probability under the Pareto file size distribution. On the other hand, the PSA scheme and the SWP-based scheme exhibit similar performance in the cellular cache hit probability under the Gamma file size distribution. The explanation of the behavior of the proposed and state-of-the-art schemes stems from the choice of the algorithms and the parameters of the file size distribution. The PSA scheme makes use of the dynamic programming with backtracking algorithm to determine the optimum aggregate popularity value that corresponds to the largest combination of files that can be stored in a BS. The SWP-based scheme uses the size-weighted-popularity metric as its objective function and relies on a greedy approach to store the files without considering whether or not the aggregate popularity of the stored files gives the optimum value. Moreover, when the variance in the file size distribution is large, as captured by $\beta = 2.0$ under the Pareto file size distribution, a few files dominate the aggregate file size and the dynamic programming with backtracking algorithm can exploit the wide variance to achieve a gain over the SWP-based scheme. On the other hand, the Gamma file size distribution gives a smaller variance in the file size. Thus, the PSA and SWP-based schemes achieve similar performance under the Gamma file size distribution. The probabilistic and MPC caching schemes give sub-optimal performance because both schemes do not jointly consider the impact of file size and file popularity in determining the set of stored files.

In Figs. 6.3a and 6.3b, the D2D cache hit probability is plotted versus the D2D partition factor under the Pareto file size distribution and Gamma file size distribution, respectively. Similar to Figs. 6.2a and 6.2b, the D2D cache hit probability is monotonic with the D2D partition factor μ because increasing the fraction of users that are potential D2D transmitters increases the number of users that can store a file. The PSA scheme also leverages the wide variance of the Pareto file size distribution to achieve up to 20% gain in the D2D cache hit probability compared to the probabilistic caching scheme which achieves the next best performance. On the other hand, the achievable gain under the Gamma file size distribution is minimal because of similar reasons explained under Fig. 6.2b.

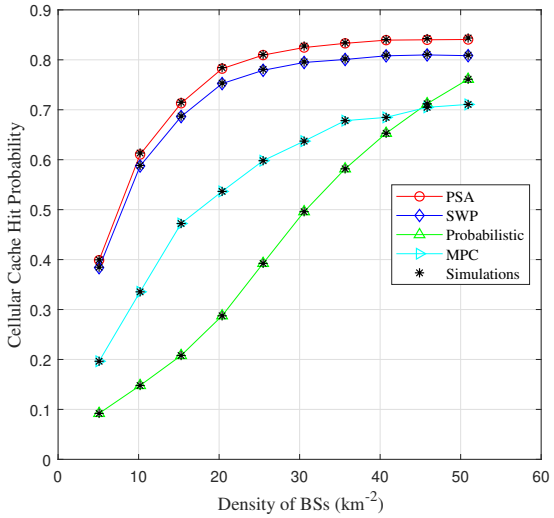

(a) Pareto file size distribution.

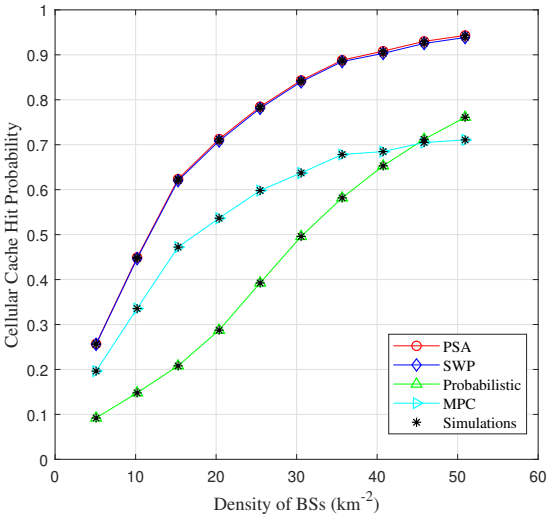

(b) Gamma file size distribution.

Figure 6.2: Cellular cache hit probability vs. density of BSs.

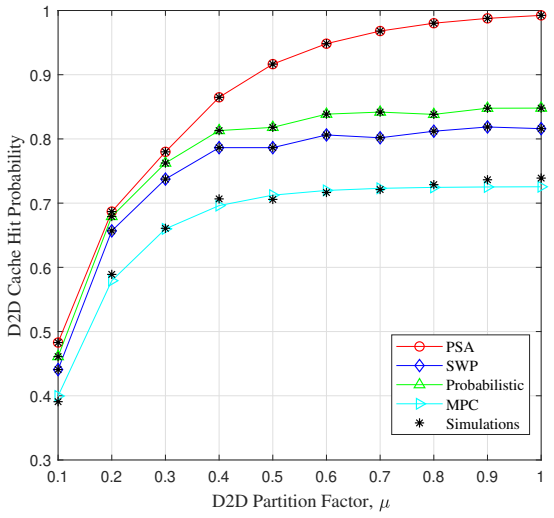

(a) Pareto file size distribution.

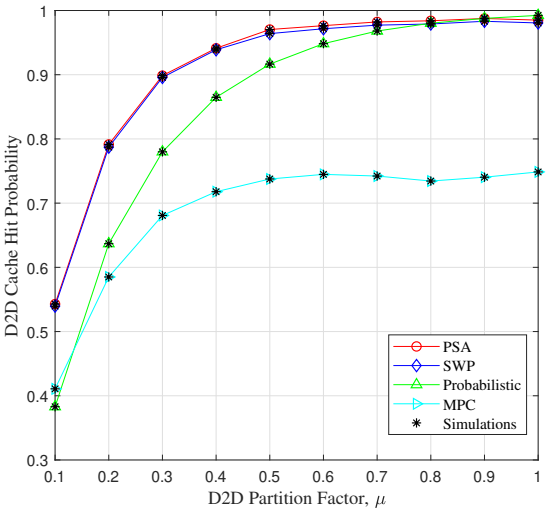

(b) Gamma file size distribution.

Figure 6.3: D2D cache hit probability vs. D2D partition factor.

6.5.3 Impact of the BS Transmit Power and Number of BS Antenna Elements on the Average Achievable Rate Per Unit Bandwidth

The impact of the BS transmit power and the number of BS antenna elements on the average achievable rate per unit bandwidth of the mmWave cellular network is studied in this section. Figs. 6.4a and 6.4b depict a linear monotonic behavior of the average achievable rate with the BS transmit power under the Pareto and Gamma file size distributions, respectively. The equal power allocation scheme and the MRT precoding technique ensures that the signals are coherently combined to maximize the transmitted symbol power. Thus, the received SINR and average achievable rate per unit bandwidth are enhanced. On the other hand, Figs. 6.5a and 6.5b show that the achievable rate per unit bandwidth increases logarithmically with the number of antenna elements. The logarithmic behavior stems from the fact that the BS transmit power is divided equally among the number of antenna elements, hence, the transmit power of each symbol stream reduces as the number of BS antenna elements increases.

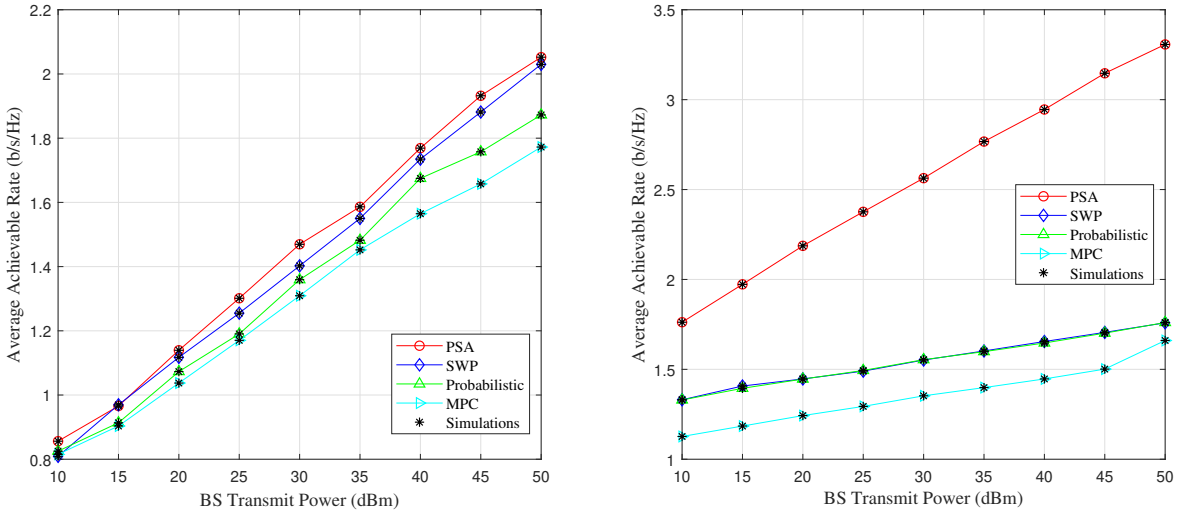

(a) Pareto file size distribution.

(b) Gamma file size distribution.

Figure 6.4: Average achievable rate per unit bandwidth vs. BS transmit power.

6.5.4 Impact of the Rate Threshold and BS Density on the Successful Content Delivery Probability

In Figs. 6.6a and 6.6b, the successful content delivery probability is plotted versus the rate threshold for the Pareto and Gamma file size distributions, respectively. The successful content delivery probability is controlled by the rate coverage probability as seen in (6.16). The fraction of users whose received rate is

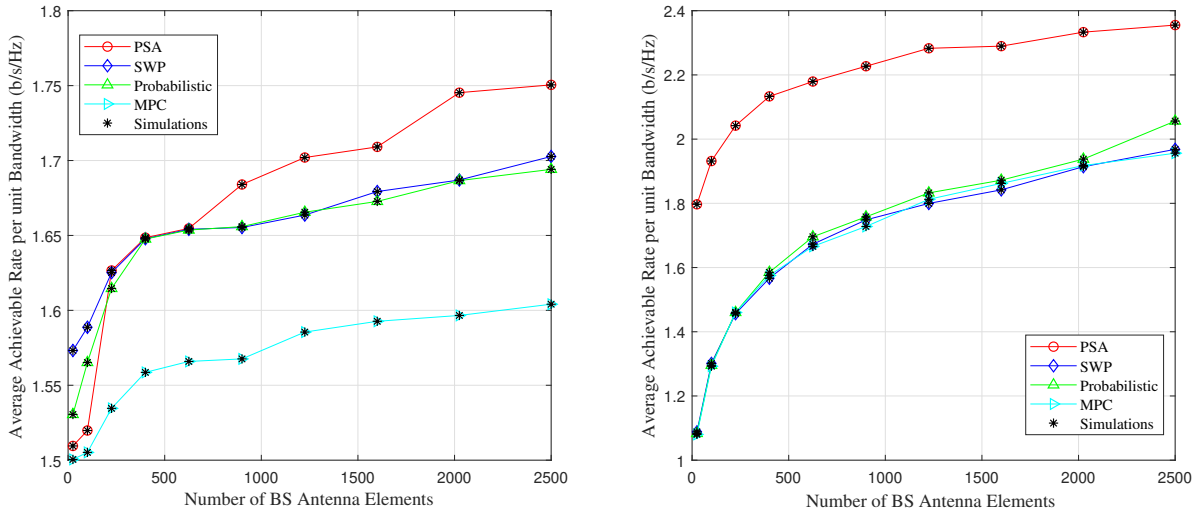

(a) Pareto file size distribution.

(b) Gamma file size distribution.

Figure 6.5: Average achievable rate per unit bandwidth vs. number of BS antenna elements for $P_b = 30$ dBm

greater than the rate threshold decreases as the rate threshold increases which also decreases the successful content delivery probability. On the other hand, Figs. 6.7a and 6.7b depict a concave behavior of the successful content delivery probability with the BS density. When the BS density is low ($< 25/\text{km}^2$), the availability of more BSs gives rise to a higher cache hit probability, thus, positively impacting the performance of the successful content delivery probability. In contrast, in the high BS density regime ($> 25/\text{km}^2$), the network becomes interference limited and the successful content delivery probability becomes negatively impacted.

6.6 Summary

This chapter presented the performance analysis of the file popularity and size-aware caching scheme in a cache-enabled mmWave cellular network with D2D communications and large-scale antenna arrays. The impacts of the system design parameters including file size distribution, transmit power, antenna design, and device communication modes on the system performance were studied. The findings in this chapter prove that a significant gain in the successful content delivery probability can be realized provided there is a wide variance in the file size distribution and a sparse distribution of transmitting nodes. In addition, linear precoding schemes such as MRT can exploit transmit diversity to achieve linear gains in the average achievable rate of a cache-enabled mmWave cellular network with D2D communication provided the number of transmit antenna elements is on the order of several hundreds.

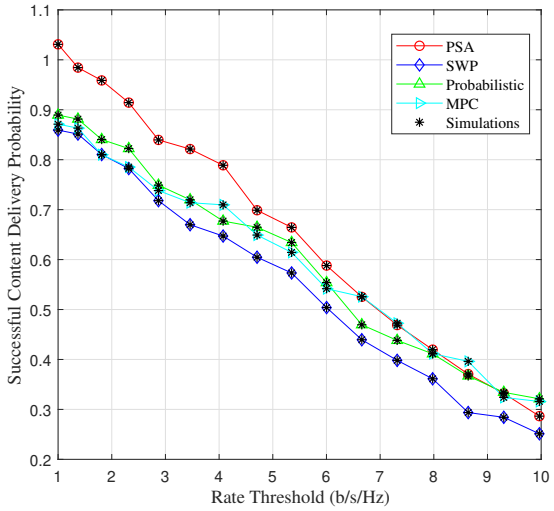

(a) Pareto file size distribution.

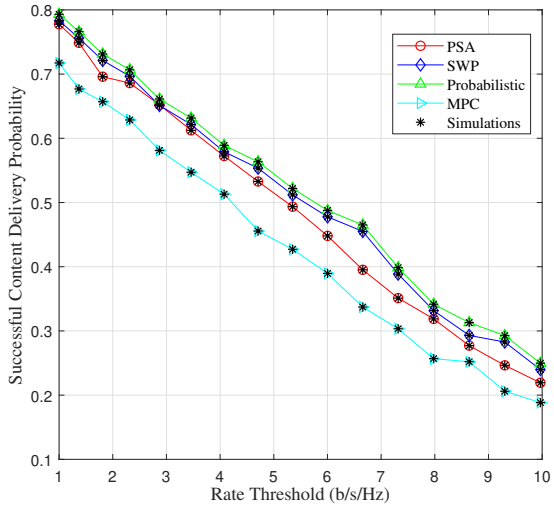

(b) Gamma file size distribution.

Figure 6.6: Successful content delivery probability vs. rate threshold.

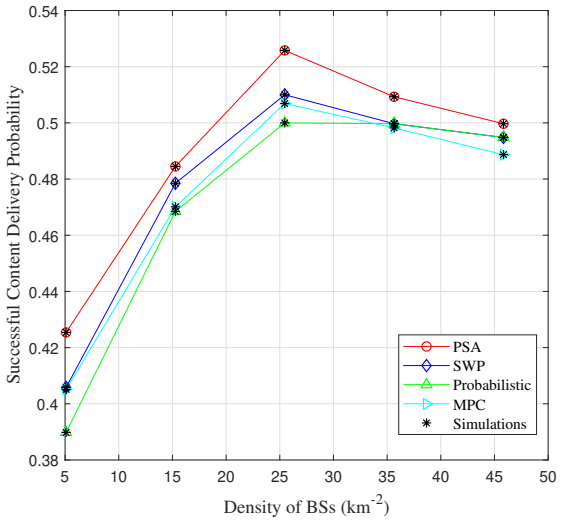

(a) Pareto file size distribution.

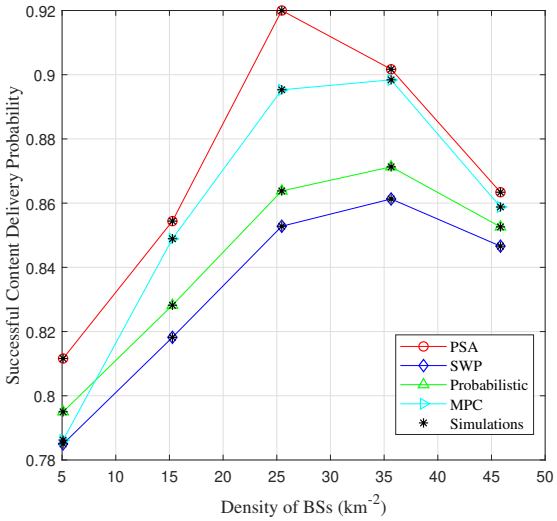

(b) Gamma file size distribution.

Figure 6.7: Successful content delivery probability vs. density of BSs.

Chapter 7

Conclusions

This chapter highlights the main conclusions that are derived from the findings in this thesis. In addition, the engineering significance of the findings and suggestions for future work are provided.

7.1 Major Research Findings

The primary objective of this thesis is the proposal of an association scheme and a caching scheme in a HetNet where file requests can be serviced by multiple BSs or neighboring users. The numerical results and simulations demonstrate the efficacy of the proposed schemes in enhancing the SE, EE, and successful delivery of files in a HetNet where users can request random files.

Specifically, the objectives of this thesis are realized by proposing an interference-aware, D2D distance threshold-based association scheme and a goal attainment algorithm. The numerical results show that the interference-aware, D2D distance threshold-based association scheme achieves up to 67% increase in area SE and EE of a D2D-enabled mmWave cellular network when compared to the state-of-the-art minimum path loss-based and maximum average received power-based association schemes. Further, in a HetNet with device clustering, employing a mixed FD/HD D2D strategy achieves up to 60% gain in the cluster average SE compared to FD-only and HD-only strategies.

Lastly, a PSA caching scheme is proposed and analyzed under a hybrid HetNet operating in the microwave and millimeter wave bands. By employing dynamic programming and branch and bound-based algorithms, the proposed PSA caching scheme achieves up to 17% gain in the average success probability compared to the state-of-the-art SWP-based, probabilistic, and MPC caching schemes. A cooperative transmission design with coded caching can realize up to 20% increase in the average success probability compared to a cooperative transmission design without coded caching. Besides, a deployment of BSs with several hundreds

of transmit antenna elements assures a linear gain in the average achievable rate of a HetNet with cellular and D2D transmissions.

Chapter 3 presents an analytical framework for studying the performance of a HetNet with D2D communications where user devices in a cluster are capable of caching popular content. Assuming spatially randomly distributed D2D users in the cluster where the users request for content according to the Zipf distribution, analytical expressions are derived for the device communication probability, coverage probability, cluster average SE, and content average download latency of the system. The system performance metrics are derived for the three user device operating modes of FD-only mode, HD-only mode, and mixed FD/HD mode. The numerical results show that the mixed FD/HD mode is the most appropriate communication mode for cache-enabled D2D networks to achieve the highest cluster average SE and low content average download latency.

In Chapter 4, the SE and EE performance of a mmWave HetNet is studied where a user device can associate with a BS or another user for D2D communication based on an interference-aware, D2D distance threshold. Using the tools of stochastic geometry, the mean interference, coverage probability, area SE, and network EE are derived under the proposed association scheme. Moreover, the performance of the proposed association scheme is compared with the performance of the minimum path loss-based and maximum received power-based association schemes. The proposed association scheme is shown to give the best coverage probability performance in noise-limited networks, while the three schemes converge in performance in interference-limited networks in the high coverage threshold regime. Further, the proposed scheme achieves up to 67% increase in the area SE and EE compared to the minimum path loss-based scheme that gives the next best performance. Besides, a goal attainment algorithm is proposed that achieves up to a seven-fold decrease in the mean deviation from a preset SE objective and 50% savings in EE, compared to the achievable performance under a constant transmit power and bandwidth allocation scheme.

Chapter 5 proposes and analyzes the performance of a PSA caching scheme in a hybrid HetNet. The HetNet comprises a microwave-based macro BS tier, a mmWave-based pico BS tier, and a user tier whose locations form independent HPPPs. Additionally, files available at a file server have sizes that are assumed to follow Pareto and lognormal distributions based on studies on the file size statistics in servers. During a caching session, the set of files that are stored in a BS is found as a solution to a 0-1 KP problem such that the largest set of popular files whose combined size does not exceed the BS cache capacity is stored. Dynamic programming and branch and bound-based algorithms are proposed to solve the 0-1 KP and the numerical results achieve up to 17% gain in the average success probability compared to the state-of-the-art SWP-based and popularity-based caching schemes. Also, cooperative transmission with coded caching is shown to provide up to 20% gain in the success probability of the pico BS tier when compared to a cooperative

transmission scheme without coded caching.

Chapter 6 investigates the performance of the PSA caching scheme in a cache-enabled mmWave cellular HetNet with D2D communication and large scale antenna arrays. The mmWave HetNet comprises a centralized file server, BSs, and users whose locations form independent FHPPPs. Moreover, the Gamma distribution is adopted as an additional file size distribution according to recent studies. The analytical expressions for the cache hit probability and successful content delivery probability are derived using the tools of stochastic geometry and verified with the aid of simulations. The results show that the PSA caching scheme can achieve up to 20% gain in the cache hit probability compared to the state-of-the-art schemes. By employing maximum-ratio-transmission, the numerical results display a significant gain in the successful content delivery probability when the density of BSs is small. Chapter 6 concludes with a study of the impact of the large scale antenna arrays on the average achievable rate of the HetNet.

7.2 Engineering Significance of Findings

The research topics of this thesis address the various design issues that pertain to the coordination of caching and delivery mechanisms in a HetNet with limited backhaul and storage capability. In this regard, the proposed research presents a holistic understanding of the impact of the physical layer parameters including path loss, fading, channel propagation, and directional beamforming in conjunction with the file request and file size distributions.

The co-existence between cellular and D2D communications is vital to leverage the wide bandwidth and highly directional characteristics of mmWave bands. Moreover, the densification of cells via small cells and device clustering in wireless hotspots require short-range D2D communication. Thus, the D2D communication mode, cluster size, and the number of cached files are important parameters to consider when maximizing the average SE and minimizing the delivery latency of user requests.

D2D communications that occur between proximate devices will be adversely affected if the interference between concurrent transmissions is not carefully managed. Thus, the selection of the maximum D2D range and the extent to which the physical propagation characteristics affect the D2D range is non-trivial in enhancing the SE and EE of a D2D-enabled HetNet. Besides, to cope with the system design variables that are changing and not within the control of the network designer, e.g., wireless channel, blockage, user mobility, etc., joint optimization of SE and EE via an algorithm that adapts the bandwidth fraction and transmit power to the system conditions is a necessity.

The exponential growth in the demand of content which is unmatched by the storage capability of HetNets requires the employment of caching schemes that are content-aware. Specifically, the problem of which files

to cache to maximize the average successful content delivery requires algorithms that jointly account for the file size and file popularity statistics. Moreover, joint transmission of files from multiple BSs can exploit the redundancy in cached content to improve the average achievable rate. Large scale antenna arrays can activate transmit diversity gains which can result in substantial performance gains of a HetNet.

The application of the proposed techniques and protocols in this thesis requires the reuse of existing protocols and enhancements to the LTE radio access network (RAN) and core network infrastructure. First, the coexistence between cellular and D2D communications is defined under LTE ProSe [173, 174]. LTE ProSe provides network-assisted discovery of users in close proximity and direct communication between users without network assistance. However, the adoption of ProSe among mobile phone manufacturers is not widespread because of the requirement to upgrade existing phone chipsets which comes at a cost, coupled with the high reliability of existing LTE cellular infrastructure which serves existing customer needs. Notwithstanding, LTE ProSe is a good candidate to leverage the availability of cheap device memory and to address the growth in ultra-low latency applications.

Second, the file PSA caching scheme of this thesis requires significant signaling overhead which is not feasible with the conventional LTE RAN and core network architectures. LTE employs a distributed control mechanism over the X2 interface between LTE eNodeBs, whereas the feasibility of the file PSA caching scheme requires knowledge of the global network parameters at a centralized server. Thus, the present LTE network will require an enhanced core network infrastructure that can support the processing of large-scale signaling data. Besides, ultra-high bandwidth links are necessary to facilitate high-speed data exchange over the S1 interface between the LTE RAN and core network elements.

7.3 Suggestions for Future Work

The present thesis has considered several physical layer and caching layer design variables that affect the SE and EE performance of a cache-enabled HetNet with D2D communications. However, some open problems and future research directions are suggested in the following:

- The current research assumes prior knowledge of the file size and file popularity distributions for the available files in a HetNet. The proposal of learning algorithms for HetNets without prior knowledge of the file size and file popularity is a proposed future research direction.

- The PSA caching scheme of this thesis determines the optimal set of files and stores the same set of files in all the BS caches. In this regard, the extension of the PSA caching scheme to allow the storage of non-overlapping sets of files to realize caching diversity gains is suggested as a future research direction.

- Lastly, the combination of coded caching with cooperative transmission design to exploit multicasting opportunities under a PSA scheme with non-overlapping file storage has not been addressed and is suggested as a future research direction.

Bibliography

[1] G. M. D. T. Forecast, "Cisco visual networking index: global mobile data traffic forecast update, 2017–2022," *Update*, vol. 2017, p. 2022, 2019.

[2] R. Li, K. Matsuzono, H. Asaeda, and X. Fu, "Achieving High Throughput for Heterogeneous Networks with Consecutive Caching and Adaptive Retrieval," *IEEE Transactions on Network Science and Engineering*, 2020.

[3] Q. Fan and N. Ansari, "Towards throughput aware and energy aware traffic load balancing in heterogeneous networks with hybrid power supplies," *IEEE Transactions on Green Communications and Networking*, vol. 2, no. 4, pp. 890–898, 2018.

[4] K. Zhang, Y. Mao, S. Leng, Q. Zhao, L. Li, X. Peng, L. Pan, S. Maharjan, and Y. Zhang, "Energy-efficient offloading for mobile edge computing in 5G heterogeneous networks," *IEEE access*, vol. 4, pp. 5896–5907, 2016.

[5] A. Damnjanovic, J. Montojo, Y. Wei, T. Ji, T. Luo, M. Vajapeyam, T. Yoo, O. Song, and D. Malladi, "A survey on 3GPP heterogeneous networks," *IEEE Wireless communications*, vol. 18, no. 3, pp. 10–21, 2011.

[6] G. Nigam, P. Minero, and M. Haenggi, "Coordinated multipoint joint transmission in heterogeneous networks," *IEEE Transactions on Communications*, vol. 62, no. 11, pp. 4134–4146, 2014.

[7] W. Nie, F.-C. Zheng, X. Wang, W. Zhang, and S. Jin, "User-centric cross-tier base station clustering and cooperation in heterogeneous networks: Rate improvement and energy saving," *IEEE Journal on Selected Areas in Communications*, vol. 34, no. 5, pp. 1192–1206, 2016.

[8] G. R. A. N. W. Group *et al.*, "Study on channel model for frequencies from 0.5 to 100 GHz (release 15)," 3GPP TR 38.901, Tech. Rep., 2018.

[9] S. Rangan, T. S. Rappaport, and E. Erkip, "Millimeter wave cellular wireless networks: Potentials and challenges," *Proceedings of the IEEE*, vol. 102, pp. 366–385, 2014.

[10] S. Sun, T. S. Rappaport, M. Shafi, P. Tang, J. Zhang, and P. J. Smith, "Propagation models and performance evaluation for 5G millimeter-wave bands," *IEEE Transactions on Vehicular Technology*, vol. 67, no. 9, pp. 8422–8439, 2018.

[11] T. Bai, R. Vaze, and R. W. Heath, "Analysis of blockage effects on urban cellular networks," *IEEE Transactions on Wireless Communications*, vol. 13, no. 9, pp. 5070–5083, 2014.

[12] J. G. Andrews, T. Bai, M. N. Kulkarni, A. Alkhateeb, A. K. Gupta, and R. W. Heath, "Modeling and analyzing millimeter wave cellular systems," *IEEE Transactions on Communications*, vol. 65, no. 1, pp. 403–430, 2016.

[13] A. Asadi, Q. Wang, and V. Mancuso, "A survey on device-to-device communication in cellular networks," *IEEE Communications Surveys & Tutorials*, vol. 16, no. 4, pp. 1801–1819, 2014.

[14] Z. Guizani and N. Hamdi, "mmwave E-Band D2D communications for 5G-underlay networks: Effect of power allocation on D2D and cellular users throughputs," in *2016 IEEE Symposium on Computers and Communication (ISCC)*. IEEE, 2016, pp. 114–118.

[15] E. Turgut and M. C. Gursoy, "Uplink performance analysis in D2D-enabled mmwave cellular networks," in *2017 IEEE 86th Vehicular Technology Conference (VTC-Fall)*. IEEE, 2017, pp. 1–5.

[16] M. A. Abana, M. Peng, Z. Zhao, and L. A. Olawoyin, "Coverage and rate analysis in heterogeneous cloud radio access networks with device-to-device communication," *IEEE Access*, vol. 4, pp. 2357–2370, 2016.

[17] D. Malak, M. Al-Shalash, and J. G. Andrews, "Spatially correlated content caching for device-to-device communications," *IEEE Transactions on Wireless Communications*, vol. 17, no. 1, pp. 56–70, 2017.

[18] M. Afshang, H. S. Dhillon, and P. H. J. Chong, "Modeling and performance analysis of clustered device-to-device networks," *IEEE Transactions on Wireless Communications*, vol. 15, no. 7, pp. 4957–4972, 2016.

[19] ——, "Fundamentals of cluster-centric content placement in cache-enabled device-to-device networks," *IEEE Transactions on Communications*, vol. 64, no. 6, pp. 2511–2526, 2016.

[20] X. Song, Y. Geng, X. Meng, J. Liu, W. Lei, and Y. Wen, "Cache-enabled device to device networks with contention-based multimedia delivery," *IEEE Access*, vol. 5, pp. 3228–3239, 2017.

[21] C. Yang, Y. Yao, Z. Chen, and B. Xia, "Analysis on cache-enabled wireless heterogeneous networks," *IEEE Transactions on Wireless Communications*, vol. 15, no. 1, pp. 131–145, 2015.

[22] N. Golrezaei, A. G. Dimakis, and A. F. Molisch, "Scaling behavior for device-to-device communications with distributed caching," *IEEE Transactions on information Theory*, vol. 60, no. 7, pp. 4286–4298, 2014.

[23] A. Papazafeiropoulos and T. Ratnarajah, "Modeling and performance of uplink cache-enabled massive MIMO heterogeneous networks," *IEEE Transactions on Wireless Communications*, vol. 17, no. 12, pp. 8136–8149, 2018.

[24] X. Wei, L. Xiang, L. Cottatellucci, T. Jiang, and R. Schober, "Cache-Aided Massive MIMO: Linear Precoding Design and Performance Analysis," in *ICC 2019-2019 IEEE International Conference on Communications (ICC)*. IEEE, 2019, pp. 1–7.

[25] J. G. Andrews, A. K. Gupta, and H. S. Dhillon, "A primer on cellular network analysis using stochastic geometry," *arXiv preprint arXiv:1604.03183*, 2016.

[26] M. Haenggi, *Stochastic geometry for wireless networks*. Cambridge University Press, 2012.

[27] M. Haenggi, J. G. Andrews, F. Baccelli, O. Dousse, and M. Franceschetti, "Stochastic geometry and random graphs for the analysis and design of wireless networks," *IEEE Journal on Selected Areas in Communications*, vol. 27, no. 7, pp. 1029–1046, 2009.

[28] N. Deng, W. Zhou, and M. Haenggi, "The ginibre point process as a model for wireless networks with repulsion," *IEEE Transactions on Wireless Communications*, vol. 14, no. 1, pp. 107–121, 2014.

[29] M. Afshang, C. Saha, and H. S. Dhillon, "Nearest-neighbor and contact distance distributions for thomas cluster process," *IEEE Wireless Communications Letters*, vol. 6, no. 1, pp. 130–133, 2016.

[30] M. Afshang and H. S. Dhillon, "Fundamentals of modeling finite wireless networks using binomial point process," *IEEE Transactions on Wireless Communications*, vol. 16, no. 5, pp. 3355–3370, 2017.

[31] ——, "Spatial modeling of device-to-device networks: Poisson cluster process meets poisson hole process," in *2015 49th Asilomar Conference on Signals, Systems and Computers*. IEEE, 2015, pp. 317–321.

[32] T. Bai and R. W. Heath, "Coverage in dense millimeter wave cellular networks," in *2013 Asilomar Conference on Signals, Systems and Computers*. IEEE, 2013, pp. 2062–2066.

[33] ——, "Coverage and rate analysis for millimeter-wave cellular networks," *IEEE Transactions on Wireless Communications*, vol. 14, no. 2, pp. 1100–1114, 2015.

[34] S. Niknam, B. Natarajan, and R. Barazideh, "Interference analysis for finite-area 5g mmwave networks considering blockage effect," *IEEE Access*, vol. 6, pp. 23 470–23 479, 2018.

[35] S. Niknam, R. Barazideh, and B. Natarajan, "Cross-layer interference modeling for 5g mmwave networks in the presence of blockage," in *2018 IEEE 88th Vehicular Technology Conference (VTC-Fall)*. IEEE, 2018, pp. 1–5.

[36] M. Naslcheraghi, S. A. Ghorashi, and M. Shikh-Bahaei, "FD device-to-device communication for wireless video distribution," *Iet Communications*, vol. 11, no. 7, pp. 1074–1081, 2017.

[37] ——, "Full-duplex device-to-device collaboration for low-latency wireless video distribution," in *2017 24th International conference on telecommunications (ICT)*. IEEE, 2017, pp. 1–5.

[38] ——, "Performance analysis of inband FD-D2D communications with imperfect si cancellation for wireless video distribution," in *2017 8th international conference on the network of the future (NOF)*. IEEE, 2017, pp. 176–181.

[39] E. Turgut and M. C. Gursoy, "Coverage in heterogeneous downlink millimeter wave cellular networks," *IEEE Transactions on Communications*, vol. 65, no. 10, pp. 4463–4477, 2017.

[40] S. Kusaladharma and C. Tellambura, "Interference and outage in random d2d networks under millimeter wave channels," in *2017 IEEE International Conference on Communications (ICC)*. IEEE, 2017, pp. 1–7.

[41] S. Kusaladharma, Z. Zhang, and C. Tellambura, "Interference and outage analysis of random D2D networks underlaying millimeter-wave cellular networks," *IEEE Transactions on Communications*, vol. 67, no. 1, pp. 778–790, 2018.

[42] H.-S. Jo, Y. J. Sang, P. Xia, and J. G. Andrews, "Heterogeneous cellular networks with flexible cell association: A comprehensive downlink SINR analysis," *IEEE Transactions on Wireless Communications*, vol. 11, no. 10, pp. 3484–3495, 2012.

[43] T. Bai and R. W. Heath, "Coverage and rate analysis for millimeter-wave cellular networks," *IEEE Transactions on Wireless Communications*, vol. 14, no. 2, pp. 1100–1114, 2014.

[44] S. Singh, M. N. Kulkarni, A. Ghosh, and J. G. Andrews, "Tractable model for rate in self-backhauled millimeter wave cellular networks," *IEEE Journal on Selected Areas in Communications*, vol. 33, no. 10, pp. 2196–2211, 2015.

[45] J. G. Andrews, T. Bai, M. N. Kulkarni, A. Alkhateeb, A. K. Gupta, and R. W. Heath, "Modeling and analyzing millimeter wave cellular systems," *IEEE Transactions on Communications*, vol. 65, no. 1, pp. 403–430, 2017.

[46] Q. Li, W. Shi, Y. Xiao, X. Ge, and A. Pandharipande, "Content size-aware edge caching: A size-weighted popularity-based approach," in *2018 IEEE Global Communications Conference (GLOBECOM)*. IEEE, 2018, pp. 206–212.

[47] Z. Chen, N. Pappas, and M. Kountouris, "Probabilistic caching in wireless D2D networks: Cache hit optimal versus throughput optimal," *IEEE Communications Letters*, vol. 21, no. 3, pp. 584–587, 2016.

[48] B. Blaszczyszyn and A. Giovanidis, "Optimal geographic caching in cellular networks," in *2015 IEEE international conference on communications (ICC)*. IEEE, 2015, pp. 3358–3363.

[49] W. Yi, Y. Liu, and A. Nallanathan, "Cache-enabled hetnets with millimeter wave small cells," *IEEE Transactions on Communications*, vol. 66, no. 11, pp. 5497–5511, 2018.

[50] K. T. Hemachandra, O. Ochia, and A. O. Fapojuwo, "Performance study on cache enabled full-duplex device-to-device networks," in *2018 IEEE Wireless Communications and Networking Conference (WCNC)*. IEEE, 2018, pp. 1–6.

[51] O. E. Ochia and A. O. Fapojuwo, "Energy and spectral efficiency analysis for a device-to-device-enabled millimeter-wave OFDMA cellular network," *IEEE Transactions on Communications*, vol. 67, no. 11, pp. 8097–8111, 2019.

[52] S. Antipolis, "3rd generation partnership project; Technical specification group SA; Feasibility study for Proximity Services (ProSe)(Release 12)," *3GPP TR 22.803 V1. 0.0*, 2012.

[53] Z. Liu, T. Peng, H. Chen, and W. Wang, "Optimal D2D user allocation over multi-bands under heterogeneous networks," in *2012 IEEE global communications conference (GLOBECOM)*. IEEE, 2012, pp. 1339–1344.

[54] X. Lin, J. G. Andrews, and A. Ghosh, "A comprehensive framework for device-to-device communications in cellular networks," *CoRR, vol. abs/1305.4219*, 2013.

[55] Y. Chen, B. Ai, Y. Niu, R. He, Z. Zhong, and Z. Han, "Resource allocation for device-to-device communications in multi-cell multi-band heterogeneous cellular networks," *IEEE Transactions on Vehicular Technology*, vol. 68, no. 5, pp. 4760–4773, 2019.

[56] J. Bukhari and W. Yoon, "Simulated view of SDN based multicasting over D2D enabled heterogeneous cellular networks," in *2019 16th International Bhurban Conference on Applied Sciences and Technology (IBCAST)*. IEEE, 2019, pp. 926–929.

[57] M. Chen, L. Wang, J. Chen, Y. Liu, and L. Zhou, "Analysis and scheduling for cooperative content delivery in 5G heterogeneous networks," in *2018 IEEE International Conference on Communications Workshops (ICC Workshops)*. IEEE, 2018, pp. 1–6.

[58] S. Zeng, C. Wang, C. Qin, and W. Wang, "Interference alignment assisted by D2D communication for the downlink of MIMO heterogeneous networks," *IEEE Access*, vol. 6, pp. 24 757–24 766, 2018.

[59] F. Jiang, Y. Liu, B. Wang, and X. Wang, "A relay-aided device-to-device-based load balancing scheme for multitier heterogeneous networks," *IEEE Internet of Things Journal*, vol. 4, no. 5, pp. 1537–1551, 2017.

[60] J. Liu, G. Wu, S. Xiao, X. Zhou, G. Y. Li, S. Guo, and S. Li, "Joint power allocation and user scheduling for device-to-device-enabled heterogeneous networks with non-orthogonal multiple access," *IEEE Access*, vol. 7, pp. 62 657–62 671, 2019.

[61] X. Wu and Z. Ma, "Modeling and performance analysis of cellular and device-to-device heterogeneous networks," in *2017 IEEE Globecom Workshops (GC Wkshps)*. IEEE, 2017, pp. 1–6.

[62] I. O. Sanusi, K. M. Nasr, and K. Moessner, "Channel assignment and power control for D2D-enabled cellular networks," in *2019 International Conference on Computing, Electronics & Communications Engineering (iCCECE)*. IEEE, 2019, pp. 225–228.

[63] M. Kamruzzaman, N. I. Sarkar, J. Gutierrez, and S. K. Ray, "A mode selection algorithm for mitigating interference in D2D enabled next-generation heterogeneous cellular networks," in *2019 International Conference on Information Networking (ICOIN)*. IEEE, 2019, pp. 131–135.

[64] A. Galanopoulos, F. Foukalas, and T. Khattab, "Energy efficient spectrum allocation and mode selection for D2D communications in heterogeneous networks," *IEEE Transactions on Signal and Information Processing over Networks*, vol. 6, pp. 382–393, 2020.

[65] Y. Niu, L. Yu, Y. Li, Z. Zhong, and B. Ai, "Device-to-device communications enabled multicast scheduling for mmwave small cells using multi-level codebooks," *IEEE Transactions on Vehicular Technology*, vol. 68, no. 3, pp. 2724–2738, 2018.

[66] H. Elshaer, M. N. Kulkarni, F. Boccardi, J. G. Andrews, and M. Dohler, "Downlink and uplink cell association with traditional macrocells and millimeter wave small cells," *IEEE Transactions on Wireless Communications*, vol. 15, no. 9, pp. 6244–6258, 2016.

[67] E. Bastug, M. Bennis, and M. Debbah, "Living on the edge: The role of proactive caching in 5G wireless networks," *IEEE Communications Magazine*, vol. 52, no. 8, pp. 82–89, 2014.

[68] D. Liu and C. Yang, "Cache-enabled heterogeneous cellular networks: Comparison and tradeoffs," in *2016 IEEE International Conference on Communications (ICC)*. IEEE, 2016, pp. 1–6.

[69] G. Quer, I. Pappalardo, B. D. Rao, and M. Zorzi, "Proactive caching strategies in heterogeneous networks with device-to-device communications," *IEEE Transactions on Wireless Communications*, vol. 17, no. 8, pp. 5270–5281, 2018.

[70] J. Elias and B. Błaszczyszyn, "Optimal geographic caching in cellular networks with linear content coding," in *2017 15th International Symposium on Modeling and Optimization in Mobile, Ad Hoc, and Wireless Networks (WiOpt)*. IEEE, 2017, pp. 1–6.

[71] G. Shan and Q. Zhu, "Sociality and mobility-based caching strategy for device-to-device communications underlying heterogeneous networks," *IEEE Access*, vol. 7, pp. 53 777–53 791, 2019.

[72] P. Xu, S. Cai, and H. Zhu, "Collaborative hierarchical caching strategy in D2D-enabled heterogeneous networks," in *2018 IEEE/CIC International Conference on Communications in China (ICCC)*. IEEE, 2018, pp. 578–582.

[73] M. S. H. Abad, E. Ozfatura, O. Ercetin, and D. Gündüz, "Dynamic content updates in heterogeneous wireless networks," in *2019 15th Annual Conference on Wireless On-demand Network Systems and Services (WONS)*. IEEE, 2019, pp. 107–110.

[74] X. Zhang, T. Lv, Y. Ren, W. Ni, N. C. Beaulieu, and Y. J. Guo, "Economical caching for scalable videos in cache-enabled heterogeneous networks," *IEEE Journal on Selected Areas in Communications*, vol. 37, no. 7, pp. 1608–1621, 2019.

[75] C. Fan, T. Zhang, Y. Liu, and Z. Zeng, "Backhaul aware analysis of cache-enabled heterogeneous networks," in *2019 IEEE 30th Annual International Symposium on Personal, Indoor and Mobile Radio Communications (PIMRC)*. IEEE, 2019, pp. 1–7.

[76] J. Yang, C. Ma, B. Jiang, G. Ding, G. Zheng, and H. Wang, "Joint optimization in cached-enabled heterogeneous network for efficient industrial iot," *IEEE Journal on Selected Areas in Communications*, vol. 38, no. 5, pp. 831–844, 2020.

[77] S. Krishnendu, B. Bharath, and V. Bhatia, "Cache enabled cellular network: Algorithm for cache placement and guarantees," *IEEE Wireless Communications Letters*, vol. 8, no. 6, pp. 1550–1554, 2019.

[78] R. Chai, Y. Li, and Q. Chen, "Joint cache partitioning, content placement, and user association for D2D-enabled heterogeneous cellular networks," *IEEE Access*, vol. 7, pp. 56 642–56 655, 2019.

[79] M. Liu, Y. Teng, K. Cheng, Y. Man, and B. Zhang, "Joint content caching and delivery policy for heterogeneous cellular networks," in *2018 IEEE 29th Annual International Symposium on Personal, Indoor and Mobile Radio Communications (PIMRC)*. IEEE, 2018, pp. 1–5.

[80] F. Chiu, T.-Y. Kuo, F.-T. Chien, W.-J. Huang, and M.-K. Chang, "Joint user clustering and content caching with heterogeneous user content preferences," in *2019 53rd Asilomar Conference on Signals, Systems, and Computers*. IEEE, 2019, pp. 1314–1317.

[81] E. Ozfatura and D. Gündüz, "Mobility and popularity-aware coded small-cell caching," *IEEE Communications Letters*, vol. 22, no. 2, pp. 288–291, 2017.

[82] B. Hu, Y. Chen, Z. Huang, N. A. Mehta, and J. Pan, "Intelligent caching algorithms in heterogeneous wireless networks with uncertainty," in *2019 IEEE 39th International Conference on Distributed Computing Systems (ICDCS)*. IEEE, 2019, pp. 1549–1558.

[83] T. Nie, J. Luo, L. Gao, F.-C. Zheng, and L. Yu, "Cooperative edge caching in small cell networks with heterogeneous channel qualities," in *2020 IEEE 91st Vehicular Technology Conference (VTC2020-Spring)*. IEEE, 2020, pp. 1–6.

[84] M. Ma and V. W. Wong, "Age of information driven cache content update scheduling for dynamic contents in heterogeneous networks," *IEEE Transactions on Wireless Communications*, 2020.

[85] D. Liu, B. Chen, C. Yang, and A. F. Molisch, "Caching at the wireless edge: design aspects, challenges, and future directions," *IEEE Communications Magazine*, vol. 54, no. 9, pp. 22–28, 2016.

[86] D. Liu and C. Yang, "Caching policy toward maximal success probability and area spectral efficiency of cache-enabled hetnets," *IEEE Transactions on Communications*, vol. 65, no. 6, pp. 2699–2714, 2017.

[87] Y. Zhu, G. Zheng, L. Wang, K.-K. Wong, and L. Zhao, "Content placement in cache-enabled sub-6 GHz and millimeter-wave multi-antenna dense small cell networks," *IEEE Transactions on Wireless Communications*, vol. 17, no. 5, pp. 2843–2856, 2018.

[88] Y. Zhu, G. Zheng, K.-K. Wong, S. Jin, and S. Lambotharan, "Performance analysis of cache-enabled millimeter wave small cell networks," *IEEE Transactions on Vehicular Technology*, vol. 67, no. 7, pp. 6695–6699, 2018.

[89] D. G. Feitelson, *Workload modeling for computer systems performance evaluation*. Cambridge University Press, 2015.

[90] C. Gros, G. Kaczor, and D. Marković, "Neuropsychological constraints to human data production on a global scale," *The European Physical Journal B*, vol. 85, no. 1, p. 28, 2012.

[91] Q. Cui, H. Wang, P. Hu, X. Tao, P. Zhang, J. Hamalainen, and L. Xia, "Evolution of limited-feedback CoMP systems from 4G to 5G: CoMP features and limited-feedback approaches," *IEEE vehicular technology magazine*, vol. 9, no. 3, pp. 94–103, 2014.

[92] R. Tanbourgi, S. Singh, J. G. Andrews, and F. K. Jondral, "A tractable model for noncoherent joint-transmission base station cooperation," *IEEE Transactions on Wireless Communications*, vol. 13, no. 9, pp. 4959–4973, 2014.

[93] N. Lee, D. Morales-Jimenez, A. Lozano, and R. W. Heath, "Spectral efficiency of dynamic coordinated beamforming: A stochastic geometry approach," *IEEE Transactions on Wireless Communications*, vol. 14, no. 1, pp. 230–241, 2014.

[94] N. Lee, R. W. Heath, D. Morales-Jimenez, and A. Lozano, "Coordinated beamforming with dynamic clustering: A stochastic geometry approach," in *2014 IEEE International Conference on Communications (ICC)*. IEEE, 2014, pp. 2165–2170.

[95] W. Wen, Y. Cui, F. Zheng, S. Jin, and Y. Jiang, "Random caching based cooperative transmission in heterogeneous wireless networks," *IEEE Transactions on Communications*, vol. 66, no. 7, pp. 2809–2825, 2018.

[96] W. Wen, Y. Cui, F.-C. Zheng, S. Jin, and Y. Jiang, "Random caching based cooperative transmission in heterogeneous wireless networks," *IEEE Transactions on Communications*, vol. 66, no. 7, pp. 2809–2825, 2018.

[97] L. Hu, F.-C. Zheng, J. Luo, and L. Yang, "Random caching based cooperative transmission in hetnets in the presence of popularity prediction errors," in *2019 IEEE 89th Vehicular Technology Conference (VTC2019-Spring)*. IEEE, 2019, pp. 1–6.

[98] S. Kuang and N. Liu, "Cache-enabled base station cooperation for heterogeneous cellular network with dependence," in *2017 IEEE Wireless Communications and Networking Conference (WCNC)*. IEEE, 2017, pp. 1–6.

[99] Z. Chen, J. Lee, T. Q. Quek, and M. Kountouris, "Cooperative caching and transmission design in cluster-centric small cell networks," *IEEE Transactions on Wireless Communications*, vol. 16, no. 5, pp. 3401–3415, 2017.

[100] H. Wu, N. Zhang, Z. Wei, S. Zhang, X. Tao, X. Shen, and P. Zhang, "Content-aware cooperative transmission in hetnets with consideration of base station height," *IEEE Transactions on Vehicular Technology*, vol. 67, no. 7, pp. 6048–6062, 2018.

[101] W. Jiang, G. Feng, and S. Qin, "Optimal cooperative content caching and delivery policy for heterogeneous cellular networks," *IEEE Transactions on Mobile Computing*, vol. 16, no. 5, pp. 1382–1393, 2016.

[102] H. Gao, S. Zhang, Y. Su, and M. Diao, "Joint resource allocation and power control algorithm for cooperative D2D heterogeneous networks," *IEEE Access*, vol. 7, pp. 20 632–20 643, 2019.

[103] S. Yang, K.-H. Ngo, and M. Kobayashi, "Content delivery with coded caching and massive MIMO in 5G," in *2016 9th International Symposium on Turbo Codes and Iterative Information Processing (ISTC)*. IEEE, 2016, pp. 370–374.

[104] L. Wang, K.-K. Wong, S. Lambotharan, A. Nallanathan, and M. Elkashlan, "Edge caching in dense heterogeneous cellular networks with massive MIMO-aided self-backhaul," *IEEE Transactions on Wireless Communications*, vol. 17, no. 9, pp. 6360–6372, 2018.

[105] H. Mei, Q. Zhao, and L. Peng, "Energy-efficiency in cache-enabled mmwave cellular networks," in *2019 International Conference on Networking and Network Applications (NaNA)*. IEEE, 2019, pp. 107–112.

[106] T. Zhang, S. Biswas, and T. Ratnarajah, "Performance analysis of cache aided hybrid mmwave & sub-6 GHz massive MIMO networks," in *2020 IEEE 21st International Workshop on Signal Processing Advances in Wireless Communications (SPAWC)*. IEEE, 2020, pp. 1–5.

[107] J. Guo, J. Yuan, and J. Zhang, "An achievable throughput scaling law of wireless device-to-device caching networks with distributed MIMO and hierarchical cooperations," *IEEE Transactions on Wireless Communications*, vol. 17, no. 1, pp. 492–505, 2017.

[108] J. Guo, J. Yuan, and J. A. Zhang, "Wireless device-to-device caching networks with distributed MIMO and hierarchical cooperations," in *GLOBECOM 2017-2017 IEEE Global Communications Conference*. IEEE, 2017, pp. 1–6.

[109] Y. Pan, C. Pan, Z. Yang, M. Chen, and J. Wang, "A caching strategy towards maximal D2D assisted offloading gain," *IEEE Transactions on Mobile Computing*, 2019.

[110] N. Giatsoglou, K. Ntontin, E. Kartsakli, A. Antonopoulos, and C. Verikoukis, "D2D-aware device caching in mmwave-cellular networks," *IEEE Journal on Selected Areas in Communications*, vol. 35, no. 9, pp. 2025–2037, 2017.

[111] Y. Cao, F. Xu, K. Liu, and M. Tao, "A storage-latency tradeoff study for cache-aided MIMO interference networks," in *2016 IEEE Global Communications Conference (GLOBECOM)*. IEEE, 2016, pp. 1–6.

[112] Y. Cao, M. Tao, F. Xu, and K. Liu, "Fundamental storage-latency tradeoff in cache-aided MIMO interference networks," *IEEE Transactions on Wireless Communications*, vol. 16, no. 8, pp. 5061–5076, 2017.

[113] K.-H. Ngo, S. Yang, and M. Kobayashi, "Scalable content delivery with coded caching in multi-antenna fading channels," *IEEE Transactions on Wireless Communications*, vol. 17, no. 1, pp. 548–562, 2017.

[114] S. A. R. Naqvi, H. Pervaiz, S. A. Hassan, L. Musavian, Q. Ni, M. A. Imran, X. Ge, and R. Tafazolli, "Energy-aware radio resource management in d2d-enabled multi-tier hetnets," *IEEE Access*, vol. 6, pp. 16 610–16 622, 2018.

[115] N. Golrezaei, A. F. Molisch, A. G. Dimakis, and G. Caire, "Femtocaching and device-to-device collaboration: A new architecture for wireless video distribution," *IEEE Communications Magazine*, vol. 51, no. 4, pp. 142–149, 2013.

[116] H. Gao, M. Wang, and T. Lv, "Energy efficiency and spectrum efficiency tradeoff in the D2D-enabled hetnet," *IEEE Transactions on Vehicular Technology*, vol. 66, no. 11, pp. 10 583–10 587, 2017.

[117] A. Bhardwaj and S. Agnihotri, "Energy-and spectral-efficiency trade-off for D2D-multicasts in underlay cellular networks," *IEEE Wireless Communications Letters*, vol. 7, no. 4, pp. 546–549, 2018.

[118] X. Lin, J. G. Andrews, and A. Ghosh, "Spectrum sharing for device-to-device communication in cellular networks," *IEEE Transactions on Wireless Communications*, vol. 13, no. 12, pp. 6727–6740, 2014.

[119] G. D. Swetha and G. R. Murthy, "Selective overlay mode operation for D2D communication in dense 5G cellular networks," in *2017 IEEE Symposium on Computers and Communications (ISCC)*. IEEE, 2017, pp. 704–709.

[120] D. J. Daley and D. V. Jones, *An Introduction to the Theory of Point Processes: Elementary Theory of Point Processes*. Springer, 2003.

[121] N. Golrezaei, P. Mansourifard, A. F. Molisch, and A. G. Dimakis, "Base-station assisted device-to-device communications for high-throughput wireless video networks," *IEEE Transactions on Wireless Communications*, vol. 13, no. 7, pp. 3665–3676, 2014.

[122] J. G. Andrews, F. Baccelli, and R. K. Ganti, "A tractable approach to coverage and rate in cellular networks," *IEEE Transactions on communications*, vol. 59, no. 11, pp. 3122–3134, 2011.

[123] K. S. Ali, H. ElSawy, and M.-S. Alouini, "Modeling cellular networks with full-duplex D2D communication: A stochastic geometry approach," *IEEE Transactions on Communications*, vol. 64, no. 10, pp. 4409–4424, 2016.

[124] M. Cha, H. Kwak, P. Rodriguez, Y.-Y. Ahn, and S. Moon, "I tube, you tube, everybody tubes: analyzing the world's largest user generated content video system," in *Proceedings of the 7th ACM SIGCOMM conference on Internet measurement*, 2007, pp. 1–14.

[125] L. Zhang, M. Xiao, G. Wu, and S. Li, "Efficient scheduling and power allocation for D2D-assisted wireless caching networks," *IEEE Transactions on Communications*, vol. 64, no. 6, pp. 2438–2452, 2016.

[126] P. D. Mankar, G. Das, and S. S. Pathak, "Modeling and coverage analysis of BS-centric clustered users in a random wireless network," *IEEE Wireless Communications Letters*, vol. 5, no. 2, pp. 208–211, 2016.

[127] M. Ahmed, H. Shi, X. Chen, Y. Li, M. Waqas, and D. Jin, "Socially aware secrecy-ensured resource allocation in d2d underlay communication: An overlapping coalitional game scheme," *IEEE Transactions on Wireless Communications*, vol. 17, no. 6, pp. 4118–4133, 2018.

[128] R. Fellers, "Millimeter waves and their applications," *Electrical Engineering*, vol. 75, no. 10, pp. 914–917, 1956.

[129] W. Roh, J.-Y. Seol, J. Park, B. Lee, J. Lee, Y. Kim, J. Cho, K. Cheun, and F. Aryanfar, "Millimeter-wave beamforming as an enabling technology for 5G cellular communications: Theoretical feasibility and prototype results," *IEEE communications magazine*, vol. 52, no. 2, pp. 106–113, 2014.

[130] R. Chevillon, G. Andrieux, R. Négrier, and J.-F. Diouris, "Spectral and energy efficiency analysis of mmwave communications with channel inversion in outband D2D network," *IEEE Access*, vol. 6, pp. 72 104–72 116, 2018.

[131] Z. Guizani and N. Hamdi, "Spectrum resource management and interference mitigation for D2D communications with awareness of BER constraint in mmwave 5G underlay network," in *2016 IEEE Symposium on Computers and Communication (ISCC)*. IEEE, 2016, pp. 855–860.

[132] G. T. 38.901, "Study on channel model for frequencies from 0.5 to 100 GHz," 2017.

[133] M. K. Simon and M.-S. Alouini, *Digital communication over fading channels*. John Wiley & Sons, 2005, vol. 95.

[134] E. Access, "Further advancements for E-UTRA physical layer aspects," *3GPP Technical Specification TR*, vol. 36, p. V2, 2010.

[135] G. R. MacCartney and T. S. Rappaport, "Study on 3GPP rural macrocell path loss models for millimeter wave wireless communications," in *2017 IEEE International Conference on Communications (ICC)*. IEEE, 2017, pp. 1–7.

[136] T. S. Rappaport, Y. Xing, G. R. MacCartney, A. F. Molisch, E. Mellios, and J. Zhang, "Overview of millimeter wave communications for fifth-generation (5G) wireless networks—with a focus on propagation models," *IEEE Transactions on Antennas and Propagation*, vol. 65, no. 12, pp. 6213–6230, 2017.

[137] N. Deng, M. Haenggi, and Y. Sun, "Millimeter-wave device-to-device networks with heterogeneous antenna arrays," *IEEE Transactions on Communications*, vol. 66, no. 9, pp. 4271–4285, 2018.

[138] A. Thornburg, T. Bai, and R. W. Heath, "Performance analysis of outdoor mmwave ad hoc networks," *IEEE Transactions on Signal Processing*, vol. 64, no. 15, pp. 4065–4079, 2016.

[139] J. Wildman, P. H. J. Nardelli, M. Latva-aho, and S. Weber, "On the joint impact of beamwidth and orientation error on throughput in directional wireless poisson networks," *IEEE Transactions on Wireless Communications*, vol. 13, no. 12, pp. 7072–7085, 2014.

[140] A. M. Mathai, *An introduction to geometrical probability: distributional aspects with applications*. CRC Press, 1999, vol. 1.

[141] S. Singh and J. G. Andrews, "Joint resource partitioning and offloading in heterogeneous cellular networks," *IEEE Transactions on Wireless Communications*, vol. 13, no. 2, pp. 888–901, 2013.

[142] R. K. Ganti and M. Haenggi, "Interference and outage in clustered wireless ad hoc networks," *IEEE Transactions on Information Theory*, vol. 55, no. 9, pp. 4067–4086, 2009.

[143] R. T. Marler and J. S. Arora, "Survey of multi-objective optimization methods for engineering," *Structural and multidisciplinary optimization*, vol. 26, no. 6, pp. 369–395, 2004.

[144] J. Jensen, "On the convex functions and inequalities between mean values," *Acta Math*, vol. 30, pp. 175–193, 1906.

[145] P. J. Fleming and A. Pashkevich, "Application of multi-objective optimisation to compensator design for SISO control systems," *Electronics Letters*, vol. 22, no. 5, pp. 258–259, 1986.

[146] M. Tao, D. Gündüz, F. Xu, and J. S. P. Roig, "Content caching and delivery in wireless radio access networks," *IEEE Transactions on Communications*, 2019.

[147] S. Tamoor-ul Hassan, M. Bennis, P. H. Nardelli, and M. Latva-Aho, "Caching in wireless small cell networks: A storage-bandwidth tradeoff," *IEEE Communications Letters*, vol. 20, no. 6, pp. 1175–1178, 2016.

[148] J. G. Andrews, S. Buzzi, W. Choi, S. V. Hanly, A. Lozano, A. C. Soong, and J. C. Zhang, "What will 5G be?" *IEEE Journal on selected areas in communications*, vol. 32, no. 6, pp. 1065–1082, 2014.

[149] T. S. Rappaport, S. Sun, R. Mayzus, H. Zhao, Y. Azar, K. Wang, G. N. Wong, J. K. Schulz, M. Samimi, and F. Gutierrez, "Millimeter wave mobile communications for 5G cellular: It will work!" *IEEE access*, vol. 1, pp. 335–349, 2013.

[150] Y.-H. Chiang and W. Liao, "mw-hierback: A cost-effective and robust millimeter wave hierarchical backhaul solution for hetnets," *IEEE Transactions on Mobile Computing*, vol. 16, no. 12, pp. 3445–3458, 2017.

[151] M.-C. Lee, M. Ji, A. F. Molisch, and N. Sastry, "Throughput–outage analysis and evaluation of cache-aided D2D networks with measured popularity distributions," *IEEE Transactions on Wireless Communications*, vol. 18, no. 11, pp. 5316–5332, 2019.

[152] D. G. Feitelson, "Workload modeling for performance evaluation," in *IFIP International Symposium on Computer Performance Modeling, Measurement and Evaluation*. Springer, 2002, pp. 114–141.

[153] D. Moltchanov, "Distance distributions in random networks," *Ad Hoc Networks*, vol. 10, no. 6, pp. 1146–1166, 2012.

[154] M. A. Maddah-Ali and U. Niesen, "Fundamental limits of caching," *IEEE Transactions on Information Theory*, vol. 60, no. 5, pp. 2856–2867, 2014.

[155] B. Serbetci and J. Goseling, "On optimal geographical caching in heterogeneous cellular networks," in *2017 IEEE Wireless Communications and Networking Conference (WCNC)*. IEEE, 2017, pp. 1–6.

[156] T. M. Ayenew, D. Xenakis, N. Passas, and L. Merakos, "Dynamic programming based content placement strategy for 5G and beyond cellular networks," in *2018 IEEE 23rd International Workshop on Computer Aided Modeling and Design of Communication Links and Networks (CAMAD)*. IEEE, 2018, pp. 1–6.

[157] G. L. Nemhauser and L. A. Wolsey, "Integer and combinatorial optimization john wiley & sons," *New York*, vol. 118, 1988.

[158] K. Fukunaga and P. M. Narendra, "A branch and bound algorithm for computing k-nearest neighbors," *IEEE transactions on computers*, vol. 100, no. 7, pp. 750–753, 1975.

[159] D. E. Kirk, *Optimal control theory: an introduction*. Courier Corporation, 2004.

[160] M. Mitzenmacher, "Dynamic models for file sizes and double Pareto distributions," *Internet Mathematics*, vol. 1, no. 3, pp. 305–333, 2004.

[161] M. Cha, H. Kwak, P. Rodriguez, Y.-Y. Ahn, and S. Moon, "Analyzing the video popularity characteristics of large-scale user generated content systems," *IEEE/ACM Transactions On Networking (Ton)*, vol. 17, no. 5, pp. 1357–1370, 2009.

[162] W. Yi, Y. Liu, and A. Nallanathan, "Modeling and analysis of mmwave communications in cache-enabled HetNets," *arXiv preprint arXiv:1801.08801*, 2018.

[163] J. Pääkkönen, P. Dharmawansa, R. Freij-Hollanti, C. Hollanti, and O. Tirkkonen, "File size distributions and caching for offloading," in *2019 IEEE 20th International Workshop on Signal Processing Advances in Wireless Communications (SPAWC)*. IEEE, 2019, pp. 1–5.

[164] S. M. Azimi-Abarghouyi, B. Makki, M. Haenggi, M. Nasiri-Kenari, and T. Svensson, "Coverage analysis of finite cellular networks: A stochastic geometry approach," in *2018 Iran Workshop on Communication and Information Theory (IWCIT)*. IEEE, 2018, pp. 1–5.

[165] E. G. Larsson, O. Edfors, F. Tufvesson, and T. L. Marzetta, "Massive MIMO for next generation wireless systems," *IEEE communications magazine*, vol. 52, no. 2, pp. 186–195, 2014.

[166] K. Yamazaki, K. Izui, K. Nakayasu, T. Okuyama, J. Mashino, S. Suyama, T. Sato, and Y. Okumura, "Field experimental DL MU-MIMO evaluations of low-SHF-band C-RAN Massive MIMO system with over 100 antenna elements for 5G," in *2018 IEEE 88th Vehicular Technology Conference (VTC-Fall)*. IEEE, 2018, pp. 1–5.

[167] T. A. Bressner, A. Farsaei, M. Fozooni, U. Johannsen, M. N. Johansson, and A. B. Smolders, "MIMO performance evaluation of isotropic, directional and highly-directional antenna systems for mm-wave communications," in *2019 13th European Conference on Antennas and Propagation (EuCAP)*. IEEE, 2019, pp. 1–5.

[168] C. A. Balanis, *Antenna theory: analysis and design*. John wiley & sons, 2016.

[169] X. Yu, J. Zhang, M. Haenggi, and K. B. Letaief, "Coverage analysis for millimeter wave networks: The impact of directional antenna arrays," *IEEE Journal on Selected Areas in Communications*, vol. 35, no. 7, pp. 1498–1512, 2017.

[170] G. R. MacCartney, J. Zhang, S. Nie, and T. S. Rappaport, "Path loss models for 5G millimeter wave propagation channels in urban microcells," in *2013 IEEE Global Communications Conference (GLOBECOM)*. IEEE, 2013, pp. 3948–3953.

[171] S. Atapattu, C. Tellambura, and H. Jiang, "A mixture gamma distribution to model the SNR of wireless channels," *IEEE transactions on wireless communications*, vol. 10, no. 12, pp. 4193–4203, 2011.

[172] S. Bazzi, G. Dietl, and W. Utschick, "Maximum ratio transmission for massive MIMO: non-asymptotic analysis with limited csir," in *SCC 2015; 10th International ITG Conference on Systems, Communications and Coding*. VDE, 2015, pp. 1–6.

[173] A. Prasad, A. Kunz, G. Velev, K. Samdanis, and J. Song, "Energy-efficient d2d discovery for proximity services in 3gpp lte-advanced networks: Prose discovery mechanisms," *IEEE vehicular technology magazine*, vol. 9, no. 4, pp. 40–50, 2014.

[174] X. Lin, J. G. Andrews, A. Ghosh, and R. Ratasuk, "An overview of 3gpp device-to-device proximity services," *IEEE Communications Magazine*, vol. 52, no. 4, pp. 40–48, 2014.

[175] K. A. Hamdi, "Capacity of MRC on correlated rician fading channels," *IEEE Transactions on Communications*, vol. 56, no. 5, pp. 708–711, 2008.

Appendix A

A.1 Proof of $\Psi_{rx,d2d}$ in Eqn. (3.3)

Let the random variables R_u and R_f denote the labels for the requesting user and requested file, respectively. Assume a deterministic caching strategy such that the user device u_i caches the i-th most popular file f_j. Define event A as $\{u_i$ receives file f_j from another user in the cluster$\}$. Event A represents a D2D communication event between u_i and the user that stores f_j in its cache since f_j is not stored in the cache of u_i. The probability of event A conditioned on the events $\{R_u = u_i\}$ and $\{R_f = f_j\}$ is given by

$$Pr\{A|R_u = u_i, R_f = f_j\} = \sum_{k=1}^{N_c} \Psi_{f_k} - \Psi_{f_j}, \tag{A.1}$$

where the term $\sum_{k=1}^{N_c} \Psi_{f_k}$ is the probability that the requested file is in the cluster and Ψ_{f_j} is subtracted from $\sum_{k=1}^{N_c} \Psi_{f_k}$ to exclude the self-request of u_i. Assume that f_j is equally likely to be requested among the $|\mathcal{F}_c| = N_c$ cached files in the cluster, such that $Pr\{R_f = f_j\} = \frac{1}{N_c}$. Similarly, assume that the requesting user u_i is equally likely among the $|\mathcal{N}_c| = N_c$ users in the cluster, such that $Pr\{R_u = u_i\} = \frac{1}{N_c}$. By averaging over the files f_j in the cluster and averaging over all the users u_i in the cluster, (A.1) becomes

$$Pr\{A\} = \Psi_{rx,d2d} = \sum_{\forall u_i \in \mathcal{N}_c} \Big(\sum_{\forall f_j \in \mathcal{F}_c} \Big(\sum_{k=1}^{N_c} \Psi_{f_k} - \Psi_{f_j} \Big) \times \frac{1}{N_c} \Big) \Big) \times \frac{1}{N_c}, \tag{A.2}$$

where $\Psi_{rx,d2d}$ is the probability that any user in the set $\mathcal{N}_c$, i.e, any user inside the cluster receives a file f_j from another user in the cluster. The proof is complete.

A.2 Proof of $\mathcal{L}_{intra}(s)$ in Eqn. (3.16)

Starting from (3.11), the Laplace transform of I_{intra} is given by

$$\mathcal{L}_{intra}(s) = \mathbb{E}_{N_I}\left[\mathbb{E}_{h_j,r_j}\left[\exp\Big(-s\sum_{j=1}^{N_I} P_d h_j r_j^{-\alpha}\Big)\right]\right] \tag{A.3}$$

$$\stackrel{(a)}{=} \mathbb{E}_{N_I}\left[\prod_j \exp\Big(-sP_d h_j r_j^{-\alpha}\Big)\right]$$

$$\stackrel{(b)}{=} \mathbb{E}_{N_I}\left[\Big(\int_{y=0}^{\infty} \frac{y^{-\alpha}}{y^{-\alpha}+sP_d} g_Y(y)\,dy\Big)^{N_I}\right]$$

$$\stackrel{(c)}{=} \sum_{k=0}^{N_a-1}\Big(\int_{y=0}^{\infty} \frac{y^{-\alpha}}{y^{-\alpha}+sP_t} g_Y(y)\,dy\Big)^{k} \times Pr\{N_I = k | N_I < (N_a-1)\}, \tag{A.4}$$

where (a) follows from $\exp\big(\sum_i x_i\big) = \prod_i \exp\big(x_i\big)$, (b) follows by first interchanging the order of $\mathbb{E}_{h_j,r_j}$ and $\prod_j$, then averaging over the distribution of the fading channels (assumed to be independent and exponential with unity mean), and also averaging over the distribution of the intra-cluster distances (assumed to be independent with identical probability distribution $g_Y(y)$ where Y is the generic random variable for the r_j's), and (c) follows by averaging over the number of interferers of the desired D2D transmitter in the cluster. Since each device transmits with probability Ψ_{tx}, the number of interferers in the cluster is a binomial random variable with parameters (N_a-1) and Ψ_{tx}, conditioned on the total being less than (N_a-1). Hence, the conditioned probability $Pr\{N_I | N_I < (N_a-1)\}$ is given by

$$Pr\{N_I | N_I < (N_a-1)\} = \binom{N_a-1}{k}\Psi_{tx}^k\big(1-\Psi_{tx}\big)^{N_a-1-k}\zeta^{-1}, \tag{A.5}$$

where $\zeta = \sum_{j=0}^{N_a-1}\binom{N_a-1}{j}\Psi_{tx}^j\big(1-\Psi_{tx}\big)^{N_a-1-j}$. Substituting (A.5) into (A.4) and making the approximation that $(N_a-1) >> (N_a-1)\Psi_{tx}$, (A.4) becomes

$$\mathcal{L}_{intra}(s) \approx \exp\Big(-(N_a-1)\Psi_{tx}\int_{y=0}^{\infty}\frac{sP_d}{y^{\alpha}+sP_d} g_Y(y)\,dy\Big). \tag{A.6}$$

The proof is complete.

Appendix B

B.1 Proof of the Mean Interference Terms in Eqns. (4.13) and (4.14)

The mean interference under the blockage model-A and the ULA pattern is derived as follows:

$$\begin{aligned}
\bar{I}_{dd} &\overset{(a)}{=} \mathbb{E}\sum_{x\in\Phi_{2\mathrm{L}}} \epsilon_L P_2 G_i h_x \max\{d_o,x\}^{-\alpha_L} + \mathbb{E}\sum_{x'\in\Phi_{2\mathrm{N}}} \epsilon_N P_2 G_i h'_x \max\{d_o,x'\}^{-\alpha_N} \\
&\overset{(b)}{=} P_2\Big(\mathbb{E}_{G,h,\Phi}\sum_{x\in\Phi_{2\mathrm{L}}} \epsilon_L G_i h_x \max\{d_o,x\}^{-\alpha_L} + \mathbb{E}_{G,h,\Phi}\sum_{x'\in\Phi_{2\mathrm{N}}} \epsilon_N G_i h'_x \max\{d_o,x'\}^{-\alpha_N}\Big) \\
&\overset{(c)}{=} 2\pi\lambda_2 P_2 \sum_{u=1}^{4} \xi_u \phi_{i,u}\Big(\int_0^{r_{net}} \epsilon_L \max\{d_o,x\}^{-\alpha_L} x\cdot e^{-\frac{x}{C}}\,dx \\
&\quad + \int_0^{r_{net}} \epsilon_N \max\{d_o,x'\}^{-\alpha_N} x'\cdot\big(1-e^{-\frac{x'}{C}}\big)\,dx'\Big),
\end{aligned} \tag{B.1}$$

where (a) follows from substitution, (b) follows from the independence of the random channel fading power gains, antenna gains, and the locations of the LOS and NLOS interferers. The label (c) follows from applying Campbell's theorem for the expectation of a sum over a PPP and applying the LOS probability function to the density of the baseline PPP. Lastly, (4.13) follows from integrating the two integral terms on the right hand side of (c). The proof of (4.14) follows a similar approach to (4.13) and is omitted.

B.2 Proof of SINR coverage probability in Eqn. (4.18)

$$\begin{aligned}
\Upsilon_{cov,c}(\gamma) &\overset{(a)}{=} \int_{r_d}^{r_{net}} \mathbb{E}_{I_{cc}}\Big\{Pr\big(h_{l,o} > \frac{\gamma x^{\alpha_L}(I_{cc}+N_0)}{P_1 G_{c,o}\epsilon_L}\big)\Big\} g_X(x)\,dx \\
&\overset{(b)}{=} \int_{r_d}^{r_{net}} \mathbb{E}_{I_{cc}} \sum_{j=0}^{m_L-1} \frac{1}{j!}\Big(\frac{\gamma x^{\alpha_L}(I_{cc}+N_0)}{P_1 G_{c,o}\epsilon_L}\Big)^j e^{-\frac{\gamma x^{\alpha_L}(I_{cc}+N_0)}{P_1 G_{c,o}\epsilon_L}} g_X(x)\,dx \\
&\overset{(c)}{=} \int_{r_d}^{r_{net}} \sum_{j=0}^{m_L-1} \frac{1}{j!}\Big(\frac{\gamma x^{\alpha_L}}{P_1 G_{c,o}\epsilon_L}\Big)^j \sum_{q=0}^{j}\binom{j}{q}\mathbb{E}_{I_{cc}}\big[I_{cc}^q\big] N_0^{j-q} \\
&\quad \mathcal{L}_{I_{cc}}(s)\Big|_{s=\frac{\gamma x_L^{\alpha}}{P_1 G_{c,o}\epsilon_L}} \Big(e^{-\frac{\gamma x^{\alpha_L} N_0}{P_1 G_{c,o}\epsilon_L}}\Big) g_X(x)\,dx,
\end{aligned} \tag{B.2}$$

where (a) follows from substituting and rearranging terms, (b) follows from taking the expectation of the Gamma distributed channel power gain $h_{c,o}$, and (c) follows from the Binomial expansion of the sum of the noise and interference terms and using the Laplace transform equation: $\mathcal{L}_X(s) = \mathbb{E}[e^{-sX}]$, while $\mathbb{E}_{I_{cc}}\big[I_{cc}^q\big] = (-1)^q \frac{d^q \mathcal{L}_{I_{cc}}(s)}{ds^q}\Big|_{s=0}$ is the q^{th} moment of I_{cc}.

B.3 Proof of the Laplace Transforms in Eqn. (4.19)

$$\begin{aligned}
\mathcal{L}_{I_{cc}}(s) &\overset{(a)}{=} \mathbb{E}\Big[e^{-sI_{cc,l}}\Big]\cdot\mathbb{E}\Big[e^{-s' I_{cc,n}}\Big] \\
&\overset{(b)}{=} \mathbb{E}_h\mathbb{E}_G\Big[e^{-\int_{r_d}^{\infty} 2\pi\lambda_1\left(1-e^{-sP_1 G\epsilon_L h x^{-\alpha_L}}\right)x\,dx}\Big]\cdot\mathbb{E}_h\mathbb{E}_G\big[e^{-\int_{r_d}^{\infty} 2\pi\lambda_1\left(1-e^{-sP_1 G\epsilon_N h x^{-\alpha_N}}\right)x\,dx}\big] \\
&\overset{(c)}{=} \prod_{u=1}^{4} e^{-2\pi\lambda_1\xi_u\int_{r_d}^{\infty}\frac{\sum_{j=1}^{M_L}\binom{M_L}{j}(sP_1\phi_{i,u}\epsilon_L\sigma_L x^{-\alpha_L})^j}{(sP_1\phi_{i,u}\epsilon_L\sigma_L x^{-\alpha_L}+1)^{M_L}}\times x P_L(x)\,dx} \times \prod_{u=1}^{4} e^{-2\pi\lambda_1\xi_u\int_{r_d}^{\infty}\frac{\sum_{j=1}^{M_N}\binom{M_N}{j}(sP_1\phi_{i,u}\epsilon_N\sigma_N x^{-\alpha_N})^j}{(sP_1\phi_{i,u}\epsilon_N\sigma_N x^{-\alpha_N}+1)^{M_N}}\times x P_N(x)\,dx}
\end{aligned} \tag{B.3}$$

where the Laplace transform parameters are $s = \frac{\gamma r^{\alpha_l}}{P_1 G_{o,c}\epsilon_L}$ and $s' = \frac{\gamma r^{\alpha_n}}{P_1 G_{o,c}\epsilon_N}$ for LOS and NLOS terms, respectively. In addition, (a) and (b) follow from the independence of the LOS and NLOS PPPs of the interferer locations, and (c) stems from applying the probability generating functional theorem to the LOS and NLOS PPPs with h and G as dummy variables, taking the expectation of the discrete random interference link directivity gain G_i, the gamma distributed channel power gains h_j, h_m, and simplifying using the Binomial theorem.

B.4 Proof of the Non-Convexity of Eqn. (4.28)

The proof of the non-convexity of (4.28) follows from Jensen's inequality, i.e, if $0 < \Xi_1, \cdots, \Xi_n$ such that $\sum_{k=1}^{n} \Xi_k = 1, n \geq 2$, and $f(x)$ is a real continuous function that is convex, then

$$f\big(\sum_{k=1}^{n} \Xi_k x_k\big) \leq \sum_{k=1}^{n} \Xi_k f(x_k), \tag{B.4}$$

otherwise, the inequality sign is reversed if $f(x)$ is non-convex (concave). It is sufficient to prove that either $\mathcal{A}_c$ or $\mathcal{A}_d$ in (4.28) is non-convex because both terms are functions of the same set of decision variables. Setting $n = 2$ and extending over the decision set, the LHS of $\mathcal{A}_c$ in (4.28) becomes:

$$\mathcal{A}_c\big(\sum_{k=1}^{2} \Xi_k\big) = (\Xi_1\kappa_1 + \Xi_2\kappa_2)\left(\omega - \frac{\beta(\omega-\beta)}{\Xi_1\big(\sum_{i=1}^{\mathcal{N}_c} P_{1,1j} + \sum_{j=1}^{\mathcal{N}_d} P_{2,1j}\big) + \Xi_2\big(\sum_{i=1}^{\mathcal{N}_c} P_{1,2i} + \sum_{j=1}^{\mathcal{N}_d} P_{2,2j}\big)}\right) \tag{B.5a}$$

$$= (\Xi_1\kappa_1 + \Xi_2\kappa_2)\omega - \beta(\omega-\beta)\left(\frac{\Xi_1\kappa_1 + \Xi_2\kappa_2}{\Xi_1\big(\sum_{i=1}^{\mathcal{N}_c} P_{1,1j} + \sum_{j=1}^{\mathcal{N}_d} P_{2,1j}\big) + \Xi_2\big(\sum_{i=1}^{\mathcal{N}_c} P_{1,2i} + \sum_{j=1}^{\mathcal{N}_d} P_{2,2j}\big)}\right). \tag{B.5b}$$

Similarly, the RHS of $\mathcal{A}_c$ in (4.28) becomes:

$$\sum_{k=1}^{2} \Xi_k\mathcal{A}_c = \Xi_1\kappa_1\left(\omega - \frac{\beta(\omega-\beta)}{\Xi_1\big(\sum_{i=1}^{\mathcal{N}_c} P_{1,1i} + \sum_{j=1}^{\mathcal{N}_d} P_{2,1j}\big)}\right) + \Xi_2\kappa_2\left(\omega - \frac{\beta(\omega-\beta)}{\Xi_2\big(\sum_{i=1}^{\mathcal{N}_c} P_{1,2i} + \sum_{j=1}^{\mathcal{N}_d} P_{2,2j}\big)}\right) \tag{B.6a}$$

$$= (\Xi_1\kappa_1 + \Xi_2\kappa_2)\omega - \beta(\omega-\beta)\left(\frac{\Xi_1\kappa_1}{\Xi_1\big(\sum_{i=1}^{\mathcal{N}_c} P_{1,1i} + \sum_{j=1}^{\mathcal{N}_d} P_{2,1j}\big)} + \frac{\Xi_2\kappa_2}{\Xi_2\big(\sum_{i=1}^{\mathcal{N}_c} P_{1,2i} + \sum_{j=1}^{\mathcal{N}_d} P_{2,2j}\big)}\right). \tag{B.6b}$$

A comparison between (B.5b) and (B.6b) reveals that (B.5b) $>$ (B.6b) because $0 < \Xi_1, \Xi_2, \kappa_1, \kappa_2 < 1$, therefore, $\frac{\Xi_1\kappa_1+\Xi_2\kappa_2}{\Xi_1\big(\sum_{i=1}^{\mathcal{N}_c} P_{1,1j}+\sum_{j=1}^{\mathcal{N}_d} P_{2,1j}\big)+\Xi_2\big(\sum_{i=1}^{\mathcal{N}_c} P_{1,2i}+\sum_{j=1}^{\mathcal{N}_d} P_{2,2j}\big)} < \frac{\Xi_1\kappa_1}{\Xi_1\big(\sum_{i=1}^{\mathcal{N}_c} P_{1,1i}+\sum_{j=1}^{\mathcal{N}_d} P_{2,1j}\big)} + \frac{\Xi_2\kappa_2}{\Xi_2\big(\sum_{i=1}^{\mathcal{N}_c} P_{1,2i}+\sum_{j=1}^{\mathcal{N}_d} P_{2,2j}\big)}$. The proof is complete.

Appendix C

C.1 Proof of the SINR Coverage Probability Expression in the Pico BS Tier — Theorem 5.1

Starting from (5.14) and applying the Cauchy-Schwarz inequality to the numerator, an upper bound expression for $P_{cov,2}(\gamma, f)$ can be derived as follows:

$$P_{cov,2}(\gamma,f) \overset{(a)}{\leq} \mathbb{E}_{\mathbf{y}}\Bigg\{\mathbb{P}\Big(\sum_{j=1}^{K}|h_{j,o}|^2 > \frac{\gamma\big(N_o+\sum_{i\in\Phi_{2,f}}P_2G_{2,i}y_i^{-\alpha_2}|h_{2,i}|^2+\sum_{i\in\Phi_{2,f'}}P_2G_{2,i}y_i^{-\alpha_2}|h_{2,i}|^2\big)}{P_2G_2\sum_{j=1}^{K}y_j^{-\alpha_2}}\Big)\Bigg\}, \tag{C.1a}$$

$$\begin{aligned}
&\overset{(b)}{\approx} \sum_{n=1}^{K\eta_l}(-1)^{n+1}\binom{K\eta_l}{n}\exp\Big(-\frac{n\eta_l\gamma N_o}{P_2G_2\sum_{j=1}^{K}y_j^{-\alpha_2}}\Big)\\
&\times\mathbb{E}_{\Phi_2}\Big[\exp\Big(-\frac{n\eta_l\sum_{i\in\Phi_{2,f}}P_2G_{2,i}y_i^{-\alpha_2}|h_{2,i}|^2}{P_2G_2}\Big)\Big]\\
&\times\mathbb{E}_{\Phi_2}\Big[\exp\Big(-\frac{n\eta_l\sum_{i\in\Phi_{2,f'}}P_2G_{2,i}y_i^{-\alpha_2}|h_{2,i}|^2}{P_2G_2}\Big)\Big],
\end{aligned} \tag{C.1b}$$

$$\begin{aligned}
&\overset{(c)}{\approx} \int\limits_{0<y_1<\cdots<y_K<R}\sum_{n=1}^{\rho}(-1)^{n+1}\binom{K\eta_l}{n}\exp\Big(-\frac{\eta_l((K\eta_l)!)^{-\frac{1}{K\eta_l}}\gamma N_o}{C_2G_2\sum_{j=1}^{K}y_j^{-\alpha_2}}\Big)\\
&\times\exp\Bigg\{-\Big(2\pi\Lambda_{2f}\sum_{a=1}^{4}\zeta_a\int_{y_k}^{\infty}\Big[1-\frac{1}{\big(1+\frac{n\overline{\phi}_{i,a}(K\eta_l)!((K\eta_l)!)^{-\frac{1}{K\eta_l}}\gamma}{K\eta_l w^{\alpha_2}\sum_{j=1}^{K}y_j^{-\alpha_2}}\big)^{K\eta_l}}\Big]\cdot w\mathbf{U}(R_l-w)\,\mathrm{d}w\Big)\Bigg\}\\
&\times\exp\Bigg\{-\Big(2\pi\big(\lambda_2-\Lambda_{2f}\big)\\
&\sum_{a=1}^{4}\zeta_a\int_{0}^{\infty}\Big[1-\frac{1}{\big(1+\frac{n\overline{\phi}_{i,a}(K\eta_l)!((K\eta_l)!)^{-\frac{1}{K\eta_l}}\gamma}{K\eta_l w'^{\alpha_2}\sum_{j=1}^{K}y_j^{-\alpha_2}}\big)^{K\eta_l}}\Big]\cdot w'\mathbf{U}(R_l-w')\,\mathrm{d}w'\Big)\Bigg\}\\
&\times g_{2,f}(\mathbf{y})\,\mathrm{d}y_1\cdots\mathrm{d}y_K,
\end{aligned} \tag{C.1c}$$

where (a) follows from substitution and rearrangement of terms in (5.17), (b) follows from the complementary cumulative distribution function of the sum of the K independent gamma random variables $\sum_{j=1}^{K}|h_{k,o}|^2$ with scaled parameter $K\eta_l$ and applying Alzer's lemma [33], while (c) follows from applying the sum-product rule for exponential functions, the probability generating functional theorem for a PPP, and integrating over the joint pdf of $\mathbf{y}$.

C.2 Proof of Lemma 1

Starting from (5.30a),

$$\max_{\mathcal{F}\subseteq\mathcal{N}}\sum_{f=1}^{N}\frac{p_f q_{k,f}\lambda_k P_k^{\frac{2}{\alpha_k}}\left(1-e^{-\pi q_{k,f}\lambda_k R^2}\right)}{q_{k,f}\lambda_k P_k^{\frac{2}{\alpha_k}}+q_{j,f}\lambda_j P_j^{\frac{2}{\alpha_j}}}\overset{(a)}{\leq}\max_{\mathcal{F}\subseteq\mathcal{N}}\sum_{f=1}^{N}\left(1-e^{-\pi q_{k,f}\lambda_k R^2}\right)\overset{(b)}{\equiv}-\max_{\mathcal{F}\subseteq\mathcal{N}}\sum_{f=1}^{N}e^{-\pi q_{k,f}\lambda_k R^2}$$
$$\overset{(c)}{\equiv}\min_{\mathcal{F}\subseteq\mathcal{N}}\sum_{f=1}^{N}e^{-\pi q_{k,f}\lambda_k R^2}\overset{(d)}{\equiv}\max_{\mathcal{F}\subseteq\mathcal{N}}\sum_{f=1}^{N}q_{k,f}, \tag{C.2}$$

where (a) is valid because the k-th tier association probability, conditioned on requesting for the file f, i.e., $\frac{p_f q_{k,f}\lambda_k P_k^{\frac{2}{\alpha_k}}}{q_{k,f}\lambda_k P_k^{\frac{2}{\alpha_k}}+q_{j,f}\lambda_j P_j^{\frac{2}{\alpha_j}}}\in(0,1)$. Further, (b) results from expanding (a), (c) results from the max-min relationship, and (d) follows from the fact that for a constant F, $e^{-Fx}\to 0$ as $x\to\infty$.

C.3 Proof of (5.35)

Substituting the expression for $\Upsilon_{cov,1}(\gamma,f)$ in (5.23) into (5.33a), the objective function can be expanded as:

$$\bar{S}_2(\varrho_{2,f},q^*_{2,f})+\sum_{f=1}^{N}p_f q_{1,f}\lambda_1 P_1^{\frac{2}{\alpha_1}}(1-e^{-\pi q_{1,f}\lambda_1 R^2})\cdot\exp\left[\frac{\left(\pi q_{1,f}\lambda_1(\frac{P_2G_2C_{2,LOS}}{P_1G_1C_1})q_{2,f}\lambda_2\right)^2}{4\frac{\gamma N_o}{C_1G_1}}\right]$$
$$\times\,\pi^{\frac{3}{2}}\frac{q_{1,f}\lambda_1\,\mathrm{erfc}\left[\frac{\pi(q_{1,f}\lambda_1+q_{2,f}\lambda_2\frac{P_2G_2C_{2,LOS}}{P_1C_1G_1})}{2\sqrt{\frac{\gamma N_o}{C_1G_1}}}\right]}{2\varrho_{2,f}\sqrt{\frac{\gamma N_o}{C_1G_1}}}, \tag{C.3}$$

where $\bar{S}_2(\varrho_{2,f},q^*_{2,f})$ denotes the average success probability in the pico BS tier which is obtained by substituting $\varrho_{2,f}$ and $q^*_{2,f}$ into (5.33a). (5.34) is obtained by differentiating (C.3) with respect to $q_{1,f}$ and setting the result to zero.

Appendix D

D.1 Proof of Average Achievable Rate Per Unit Bandwidth — Theorem 6.1

Starting from (6.12), the expression for the average achievable rate per unit bandwidth is expanded as follows:

$$\bar{\mathcal{A}}_{b,f} \overset{(a)}{=} \mathbb{E}\left[\frac{1}{\ln(2)}\int_0^\infty \frac{1}{z}(1-e^{-z\kappa_{b,f}})e^{-z}dz\right], \tag{D.1a}$$

$$\overset{(b)}{=} \frac{1}{\ln(2)}\mathbb{E}\left[\int_0^\infty \frac{1}{z}(1-e^{-zP_b||\mathbf{H}_0\mathbf{W}_0||^2\rho_0})e^{-z(P_b||\mathbf{H}_j\mathbf{W}_j||^2\rho_j+\sigma_0^2)}dz\right], \tag{D.1b}$$

$$\overset{(c)}{=} \frac{1}{\ln(2)}\int_0^\infty \frac{1}{z}(1-\mathbb{E}_{||\mathbf{H}_0||^2\mathbf{W}_0}e^{-zP_b||\mathbf{H}_0\mathbf{W}_0||^2\rho_0})\mathbb{E}_{||\mathbf{H}_j||^2\mathbf{W}_j,G}\left[e^{-z(P_b||\mathbf{H}_j\mathbf{W}_j||^2\rho_j)}\right]e^{-z\sigma_0^2}dz\Bigg]. \tag{D.1c}$$

where (a) follows from applying the transformation in Lemma 1 of [175], (b) follows from substitution of the desired signal and interference terms, and (c) follows from the linearity of the expectation operator, resulting in the Laplace transform of the desired signal and interfering terms. Finally, (6.16) results from taking the expectation with respect to the distributions of the $N_u\eta$-dimensional multivariate Gamma distributed random variables, the link length, and the array gain functions.

D.2 Proof of Rate Coverage Probability — Theorem 6.2

Starting from (6.16), substituting the expression for $\mathcal{A}_{i,f}$, and re-arranging terms, the expression for the rate coverage probability is expanded as follows:

$$\mathcal{R}_b(\Psi, f) = \mathbb{P}(\kappa_{i,f} > 2^{\Psi} - 1) \tag{D.2a}$$

$$\overset{(a)}{=}\mathbb{P}\bigg(\frac{P_b||\mathbf{H}_0\mathbf{W}_0||^2\rho_0}{\sum_{j\in\Phi'_{b,f}} P_b||\mathbf{H}_j\mathbf{W}_j||^2\rho_j + \sigma_0^2} > 2^{\Psi} - 1\bigg), \tag{D.2b}$$

$$\overset{(b)}{=}\mathbb{P}\bigg(\sum_{k=1}^{N_u}\Lambda_k^2 > \frac{\sum_{j\in\Phi'_{b,f}} P_b\sum_{k=1}^{N_u}\Psi_k^2\rho_j + \sigma_0^2}{\rho_0} \times \Big(\frac{2^{\Psi}-1}{P_b}\Big)\bigg), \tag{D.2c}$$

$$\overset{(c)}{\approx}\mathbb{E}_{\mathbf{r}}\bigg\{1 - \mathbb{E}_{\Phi_{b,f}}\bigg(1 - \exp\Big(\frac{(2^{\Psi}-1)\big(\sum_{j\in\Phi'_{i,f}} P_b\sum_{k=1}^{N_u}\Psi_k^2 G_j(\varsigma_x,\varsigma_y)G_u(\varsigma)r_j^{-\alpha} + \sigma_0^2\big)}{G_b(\varsigma_x,\varsigma_y)G_u(\varsigma)r_0^{-\alpha}}\Big)\bigg)^{N_u\eta}\bigg\}, \tag{D.2d}$$

$$\begin{aligned}\overset{(d)}{=}&\mathbb{E}_{\mathbf{r}}\bigg\{\sum_{n=1}^{N_u\eta}(-1)^{n+1}\binom{N_u\eta}{n}\exp\Big(-n\eta(2^{\Psi}-1)\sigma_0^2 r_0^{\alpha}\Big)\\ &\times\mathbb{E}_{\Phi_{b,f}}\Big[\exp\Big(-\frac{n\eta\sum_{j\in\Phi_{b,f}}P_b G_j(\varsigma_x,\varsigma_y)G_u(\varsigma)r_j^{-\alpha}\sum_{k=1}^{N_u}\Psi_k^2}{P_b G_b(\varsigma_x,\varsigma_y)G_u(\varsigma)}\Big)\Big]\bigg\}\\ &\int_0^{R_l}\sum_{n=1}^{N_u\eta}(-1)^{n+1}\binom{N_u\eta}{n}\exp\Big(-n\eta(2^{\Psi}-1)\sigma_0^2 r^{\alpha}\Big)\\ &\times\exp\bigg(-2\pi\lambda_b q_{b,f}\int_r^{R_l}1 - \Big(\frac{1+n\eta(\eta!)^{-\frac{1}{\eta}}\mathbb{E}_G\{G_j(\varsigma_x,\varsigma_y)G_u(\varsigma)\}}{\eta x^{\alpha}}\Big)^{-N_u\eta}x\,dx\bigg)g_{b,f}(r)dr,\end{aligned} \tag{D.2e}$$

where (a) and (b) result from substitution and rearrangement of terms. Moreover, $\{\Lambda_k\}_{k=1}^{N_u}$ denote the N_u eigenvalues of $\mathbf{H}_0\mathbf{W}_0$ and $\{\Psi_k^2\}_{k=1}^{N_u}$ denote the N_u eigenvalues of $\mathbf{H}_j\mathbf{W}_j$. (c) follows from the complementary cumulative distribution function of the sum of the N_u eigenvalues with scaled parameter $N_u\eta$ and (c) follows from Alzer's lemma [33]. Lastly, (d) follows from applying the sum-product rule for exponential functions, the probability generating functional theorem for a PPP, and integrating over the random array gain functions and the pdf of r to get the result in (6.17).